Local Monitoring and Modeling of the Spatio-temporal Spread of Ca^{2+} Signals Initiated by Single or Multiple Action Potentials in Frog and Rat Sympathetic Ganglion Neurons

PhD dissertation

Author: Zoltán Cseresnyés

Supervisor: Prof. Dr. Gáspár Bánfalvi

DEBRECENI EGYETEM
Természettudományi Doktori Tanács
Juhász-Nagy Pál Doktori Iskola, Biológia Doktori Program
Debrecen, 2009

Ezen értekezést a Debreceni Egyetem Természettudományi Doktori Tanács Juhász-Nagy Pál Doktori Iskola, Biologia programja keretében készítettem a Debreceni Egyetem természettudományi doktori (PhD) fokozatának elnyerése céljából.

Debrecen, 2009. december 15.

.....
Cseresnyés Zoltán

Tanúsítom, hogy Cseresnyés Zoltán doktorjelölt 2007-2009 között a fent megnevezett Doktori Iskola Biológia programjának keretében irányításommal végezte munkáját. Az értekezésben foglalt eredményekhez a jelölt önálló alkotó tevékenységével meghatározóan hozzájárult. Az értekezés elfogadását javaslom.

Debrecen, 2009. december 15.

.....
Dr. Bánfalvi Gáspár

Local Monitoring and Modeling of the Spatio-temporal Spread of Ca^{2+} Signals Initiated by Single or Multiple Action Potentials in Frog and Rat Sympathetic Ganglion Neurons

Értekezés a doktori (Ph.D.) fokozat megszerzése érdekében
a BIOLÓGIA tudományágban

Írta: Cseresnyés Zoltán okleveles fizikus

Készült a Debreceni Egyetem Juhász-Nagy Pál doktori iskolája
(Bioreguláció Molekuláris és Fiziológiai szerveződése és
Biotechnológiai vonatkozásai programja) keretében

Témavezető: Dr. Bánfalvi Gáspár

A doktori szigorlati bizottság:

elnök: Dr. .....
tagok: Dr. .....
Dr. .....
A doktori szigorlat időpontja: 200… . …… … …
Az értekezés bírálói:
Dr. .....
Dr. .....
Dr. .....
A bírálóbizottság:
elnök: Dr. .....
tagok: Dr. .....
Dr. .....
Dr. .....
Dr. .....
Az értekezés védésének időpontja: 20… . …… … .

Table of Contents

1. ABSTRACT

Global Ca^{2+} signals have been extensively studied in mammalian sympathetic neurons. However, relatively little is known about the details of local, subcellular Ca^{2+} signals. In addition to robust Ca^{2+} influx via voltage- and ligand gated Ca^{2+} channels of the plasma membrane, Ca^{2+} release from the endoplasmic reticulum (ER) has also been shown to contribute to Ca^{2+} transients in frog sympathetic ganglion neurons. Here we use video rate confocal fluo-4 fluorescence imaging to show that single action potentials (APs) reproducibly trigger rapidly rising Ca^{2+} transients at 1 - 3 local "hot spots" within the peripheral ER-rich layer in intact neurons in fresh ganglia, and in the majority (74 %) of cultured neurons. Hot spots were located near the nucleus or the axon hillock region. Other regions exhibited either slower and smaller signals or no response. Ca^{2+} signals spread into the cell at constant velocity across the ER in non-nuclear regions, indicating active propagation, but spread with a $(time)^{1/2}$ dependence within the nucleus, consistent with diffusion. 26 % of cultured cells exhibited uniform Ca^{2+} signals around the periphery, but hot spots were produced by loading the cytosol with EGTA or by bathing the cells in low-Ca^{2+} Ringer's solution. Peripheral hot spots for Ca^{2+} release within the perinuclear and axon hillock regions provide a mechanism for preferential initiation of nuclear

and axonal Ca^{2+} signals by action potentials in sympathetic ganglion neurons.

In addition to describing the spatio-temporal properties of Ca^{2+} signals initiated by action potentials, we also establish a model that accounts for these properties. Our results show that after single action potentials, localized Ca^{2+} responses in sympathetic neurons are spatially heterogeneous. In the absence of CICR in rat SCG neurons, the amplification of Ca^{2+} signals relies mostly on repetitive firing. Our simple but fully generalized model successfully simulates the Ca^{2+} fluxes between six subcellular domains, as well as estimates the relative importance of Ca^{2+} signaling mechanisms assigned to the plasma membrane, the endoplasmic reticulum and the mitochondria in each of these domains. The domains correspond to the six functionally and/or morphologically distinct sub-areas of a typical sympathetic ganglion neuron, but could easily be translated to fit other cell types. In addition, our model proves very useful in separating mixed Ca^{2+} signals that were detected from in-focus and out-of-focus domains. Due to the flexibility of the model, it allows the estimation of the above parameters in any cell geometry, including cells with peripherally or centrally located nuclei.

2. INTRODUCTION

Cytosolic Ca^{2+} regulates a wide range of functions within an individual cell. In neurons, Ca^{2+} levels govern many processes, including neurotransmitter secretion, regulation of membrane excitability, and induction of gene expression (Kennedy, 1989; Ghosh and Greenberg, 1995; Clapham, 1995). Spatio-temporal differences in $[Ca^{2+}]$ within a given cell, as well as spatial organization of the Ca^{2+}-receptive proteins that bind and respond to Ca^{2+}, may provide a partial explanation for how the single messenger Ca^{2+} is able to selectively modulate multiple cellular functions (Linden, 1999; Akita and Kuba, 2000; Marchant and Parker, 2000; Pozzo-Miller et al, 2000; Koopman et al., 2001; Young et al., 2001). The experimental characterization of local Ca^{2+} signals is thus of major interest for understanding Ca^{2+} signaling.

We also used video rate laser scanning confocal microscopy to investigate local Ca^{2+} signals at the periphery of the cell body of cultured frog sympathetic ganglion neurons (McDonough et al, 2000). We found that application of caffeine, a pharmacological agent that sensitizes ryanodine receptor (RyR) Ca^{2+} release channels in the endoplasmic reticulum (ER) membrane to activation by Ca^{2+}-induced Ca^{2+} release (CICR), reproducibly initiated Ca^{2+} release at one or more distinct localized sites around the periphery of the neuron (McDonough et al, 2000). Here we investigate elevations of Ca^{2+} at the cell periphery in response to single action potentials, which are also

initiated by CICR in frog sympathetic ganglion neurons (Akita and Kuba, 2000). Using video rate confocal imaging, we now find that the Ca^{2+} transient in response to a single action potential differs appreciably in different sub areas of the same neuron. In neurons in freshly dissected ganglia, as well as in a large majority of cultured neurons, $[Ca^{2+}]$ rises rapidly at a few local hot spots around the periphery of the cell, and rises more slowly and much less or not at all in other peripheral regions and in deeper areas of the cell. Our previous (McDonough et al, 2000) and present Ca^{2+} imaging results thus indicate local functional differences in CICR activation around the cell periphery.

We found that the peripheral perinuclear region, located between the plasma membrane and the peripherally positioned nucleus, almost always exhibits a hot spot for Ca^{2+} release in response to a single action potential, indicating a functional specialization of the perinuclear periphery to reliably respond to AP stimuli. A second, independent hot spot is frequently located across the cell body from the peripheral perinuclear site, near the actual or previous axon hillock region, in either intact or cultured, axotomized neurons, respectively. Even in those cultured neurons that exhibited a uniform peripheral Ca^{2+} transient in response to a single action potential under control conditions, addition of intracellular EGTA or lowering extracellular $[Ca^{2+}]$ reveals latent peripheral hot spots for initiation of Ca^{2+} release in the perinuclear and axon hillock regions. Frog sympathetic ganglion neurons thus appear to be functionally specialized to preferentially generate local Ca^{2+} signals at the peripheral

perinuclear and axon hillock regions in response to single neuronal action potentials.

In many cell types, including neurons, the concentration of free intracellular calcium ions $[Ca^{2+}]_i$ regulates a great variety of cellular processes. These include muscle contraction, hormone and transmitter release, ionic channel permeability, enzymatic activity and gene transcription (Berridge, 1998; Augustine et al., 2003; Carafoli 2005). In autonomic sympathetic neurons, spatio-temporal variations of free $[Ca^{2+}]_i$ regulate Ca^{2+}-dependent ionic conductances (Akita and Kuba, 2000; Martinez-Pinna et al., 2000), control transmitter release at nerve terminals (Cong et al., 2004), and influence transcription factor activation (Wheeler et al., 2006; Hernandez-Ochoa, 2006), which might be involved in the fine tuning of sympato-effector coupling (Boehm and Kubista, 2002). In a recent study we found that trains of action potentials at 10 Hz or induction of spike frequency facilitation by inhibition of M-channels, lead to increased NFATc1 activation via summation of cytosolic Ca^{2+} signals in sympathetic ganglion neurons (Hernandez-Ochoa, et al., 2006). These results confirm the concept of a link between frequency-dependent electrical signals, intracellular Ca^{2+} signals and transcription factor activation.

Many aspects of intracellular global Ca^{2+} signals (e.g. those mediated by nicotinic receptor activation, membrane depolarizations or caffeine application) as well as the mechanisms involved in the maintenance of basal cytosolic $[Ca^{2+}]$ have been extensively evaluated in rat sympathetic

neurons (Thayer et al., 1988; Trouslard et al., 1993; Hernández-Cruz et al., 1997; Wanaverbecq et al., 2003; for a review see Marsh et al., 2000). However, in these neurons relatively little is known about the details of local intracellular Ca^{2+} signals. One of the aims of this work is to conduct a detailed local recording of the spatio-temporal spread of Ca^{2+} signals initiated by single or multiple action potentials in mammalian sympathetic neurons, as well as to establish a model that accounts for these properties. Our results show that during and after single action potentials, local Ca^{2+} responses in sympathetic neurons are spatially heterogeneous. The amplification of Ca^{2+} signals relies mostly on the intrinsic plasma membrane properties, especially on repetitive firing. We also simulated the observed Ca^{2+} distribution using a multi-compartment model, which takes into account six different subcellular domains based on the spatial and functional distribution of different Ca^{2+} signaling components obtained by immuno-cytochemical, electrophysiological and Ca^{2+} imaging studies. Our multi-compartment model allows the estimation of Ca^{2+} fluxes between the six domains, as well as the relative importance of various Ca^{2+} signaling mechanism assigned to the plasma membrane (PM), the endoplasmic reticulum (ER) and the mitochondria. In addition, due to the flexibility of the model it allows the estimation of the above parameters in any cell geometry including cells with peripherally or centrally located nuclei.

3. MATERIALS AND METHODS

3.1. Ganglion dissection and cell culture

Frogs (*Rana pipiens*) were chilled in ice for 30 minutes and then sacrificed by decapitation and pithing, according to guidelines issued by the Institutional Animal Care and Use Committee, University of Maryland Baltimore (Baltimore, MD). The two chains of sympathetic ganglia were isolated, desheathed and placed into a Ca^{2+}-free Ringer's solution containing 3.3 mg/mL collagenase (SIGMA Type IA, C-9891, for 30 to 35 minutes at 35 C).

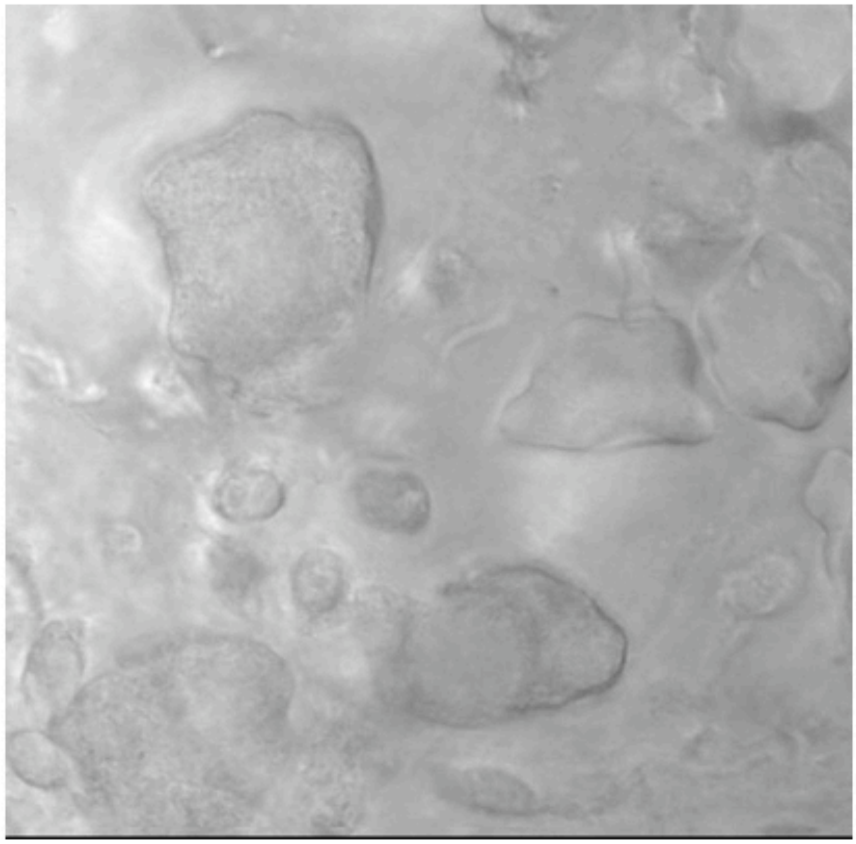

Figure 1. Intact ganglionic neurons of frog sympathetic ganglia. An intact, but partially digested (see Methods) frog sympathetic ganglion was imaged via scattered light confocal microscopy. Five individual neurons are identifiable as large "islands" in the smoother grey "sea" of connective tissue.

For studying cells within freshly isolated ganglia (see Fig.1.), the chains of ganglia were then washed gently in 2 mM Ca^{2+} Ringer's solution three times in order to remove collagenase completely. For Ca^{2+} indicator dye loading, ganglia were placed in 2 mM Ca^{2+} Ringer's solution containing 200 μM neostigmine (a cholinesterase inhibitor) and 20 μM fluo-4 AM for 1 hour at

room temperature, after which the ganglia were washed with dye- and neostigmine-free Ringer's solution and placed in a cover glass-bottom chamber for confocal experiments.

In order to isolate neurons for culture, the two chains of sympathetic ganglia were prepared and collagenase-digested as described above. The enzymatic dissociation was completed in a trypsin solution (2 mg/mL, Sigma Type I, T-8003, for 10 min at 35 C), after which individual cells were isolated from the digested tissue by trituration. The cells were then plated in cover glass-bottom Petri dishes coated with poly-L-lysine, and cultured for 2-7 days at 22-24 C in a 1:1 mixture of Leibovitz's L-15 solution and of our neuron culture medium containing 2 mM Ca^{2+}. Prior to experiments, cultured cells were washed 3 times in 2 mM Ca^{2+} Ringer's solution. For calcium experiments, cultured cells were loaded with 2 μM fluo-4AM in 2 mM Ca^{2+} Ringer's at room temperate for 20 minutes and then washed with dye-free Ringer's solution (for composition of all solutions, see Cseresnyés et al., 1997; McDonough et al., 2000).

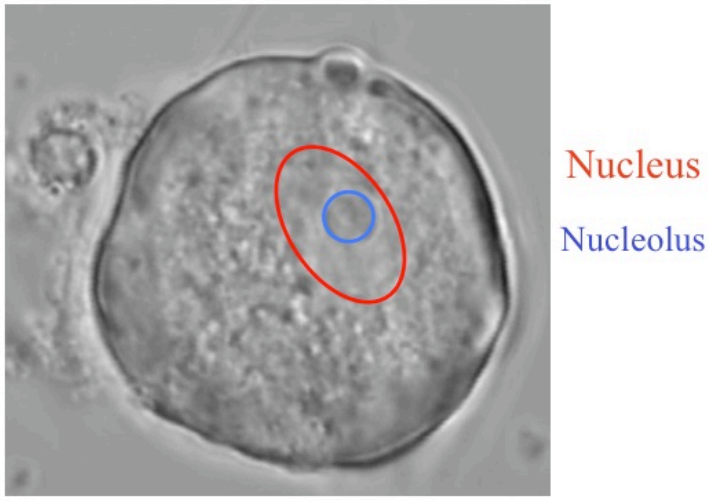

Figure 2. Cultured frog SGN after 24 h in culture at room temperature. Scattered light image acquired on a confocal system from an SGN, after 24 hours in culture at room temperature. The locations of the nucleus and the nucleolus are highlighted by red and blue outlines, respectively, in order to help the reader identifying them.

A few cultured cells (see Fig.2. for typical cell appearance in 24 hour culture at room temperature, with the outline of the nucleus and the nucleolus marked with color lines) were loaded with fluo-4 and imaged during plasma membrane permeabilization by 0.1% saponin in internal solution (in mM: 80 Cs glutamate, 2 trizma maleate, 20 Na creatine phosphate, 7 ATP, 6 $MgCl_2$, 1 DTT, 0.1 EGTA; pH=7.0).

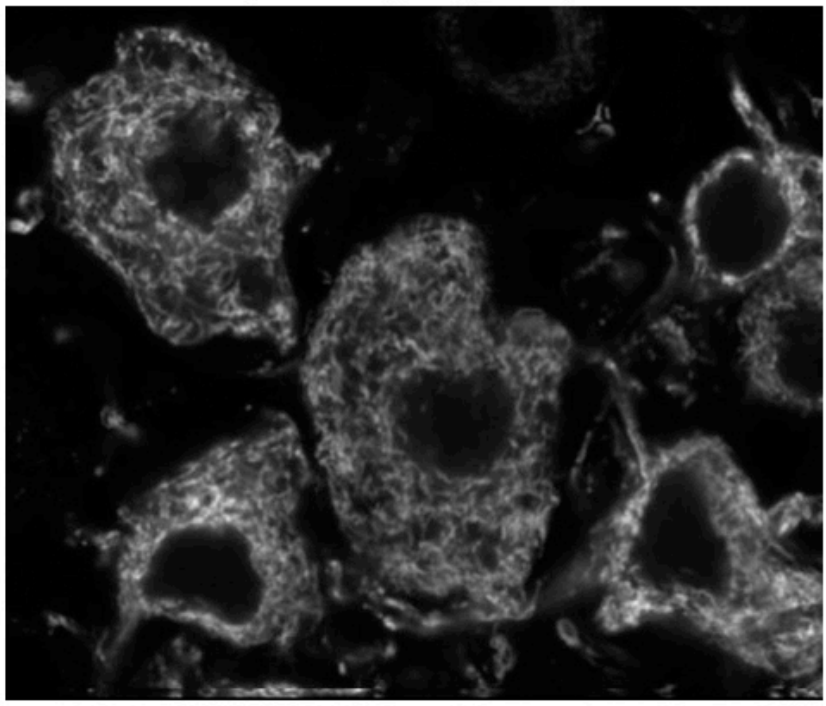

Figure 3. Frog SGNs loaded with TMRE (tetra-methyl rhodamine ethyl) in intact ganglion. Intact ganglion after partial enxymatic digestion (see Methods) was loaded with TMRE that labels functional mitochondria in live cells. The fluorescence pattern we observe here clearly indicates that the mitochondria stayed active and that they are separated into sausage-like structures.

After fluo-4 calcium measurements, some cultured neurons were loaded with TMRE (see Fig.3. and Fig.4. for typical mitochondria distribution patterns within intact ganglionic and cultured SGNs, revealed after loading the cells with tetra-methyl rhodamine ethyl, TMRE) for monitoring the spatial distribution of mitochondria within the cell. In such cases, cells were exposed to 1-2 μM TMRE for 1 to 5 minutes, and then to 100 nM TMRE for the rest of the experiment. Some cells (not

fluo-4 loaded) were stained with 100mM BODIPY-FL Ryanodine for 10-15 min, and then subsequently loaded with TMRE as above.

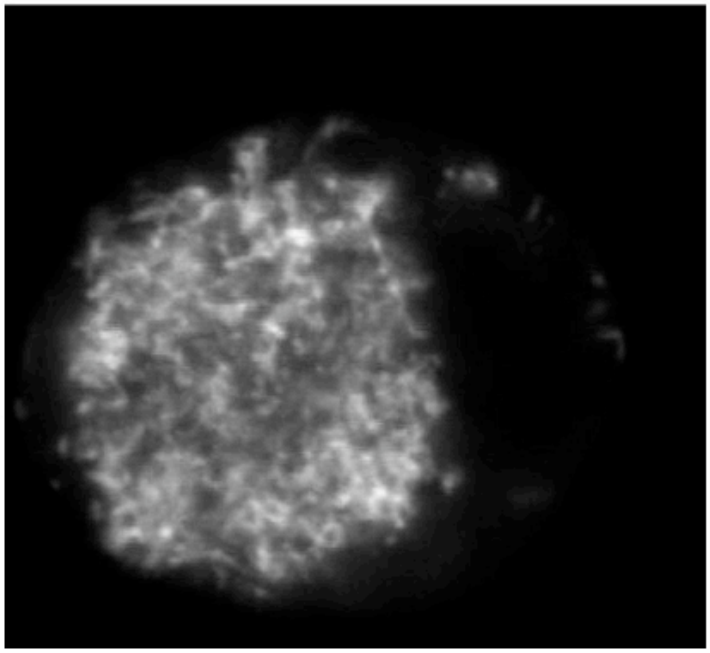

Figure 4. A frog SGN loaded with TMRE in culture. The neuron was kept in culture for 24 hours and loaded with TMRE, which labels functional mitochondria in live cells.

For studies on *mammalian cells*, superior cervical ganglion (SCG) neurons were enzymatically dissociated from 5-week-old male Wistar rats as described elsewhere [Garcia-Ferreiro et al., 2001].

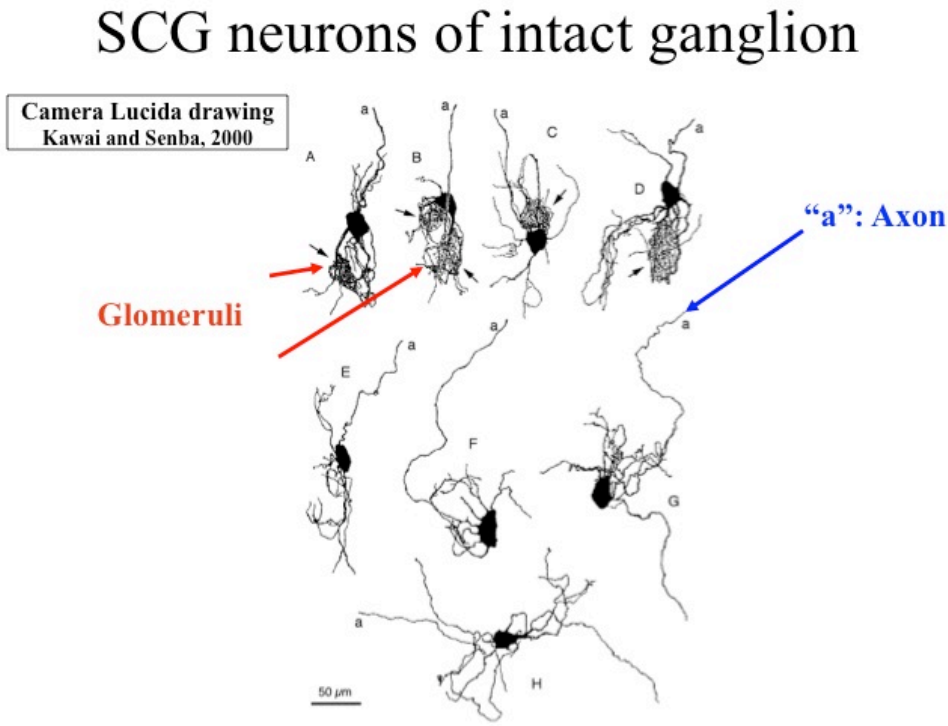

Figure 5. Typical appearances of SCG neurons in intact ganglia. Camera lucida drawings taken from Kawai and Senba, 2000. Appearances of axons (blue arrow) and dendritic glumeruli (red arrows) are clearly shown.

Rats were placed in a container and exposed to rising concentrations of CO_2. The animals were sacrificed according to authorized procedures of the Institutional Animal Care and Use Committee, University of Maryland Baltimore (Baltimore, MD). After dissection the ganglia were desheathed, cut into eight to ten small pieces and enzymatically dissociated with papain for 20 min and then with collagenase type I and dispase II for 40 min. Individual neurons were released by trituration and then plated on poly-L-lysine coated glass coverslips in culture dishes and

stored in a humidified atmosphere of 95% air 5% CO_2 at 37°C in Dulbecco's modified Eagle's medium (DMEM) supplemented with fetal bovine serum and penicillin-streptomycin. Neurons were studied 1 to 3 days after plating.

3.2. Confocal imaging

Studies of frog neurons were carried out via confocal imaging experiments using a Nikon RCM-8000 video-rate system, based on a Nikon Diaphot 300 inverted microscope. Cells were imaged with a Nikon 60X NA 1.2 water-immersion objective lens (for further details about the confocal system, see McDonough et al., 2000). Rat SCG neurons were studied via confocal imaging experiments on a Zeiss LSM 5 Live system, based on an Axiovert 200M inverted microscope. Cells were imaged with a 63X NA 1.2 water immersion objective lens. Excitation for fluo-4 was provided by the 488 nm line of a 100 mW diode laser, and emitted light was collected at > 510 nm.

To evaluate temporal properties of Ca^{2+} signals in rat SCG neurons, cells were loaded with 2 μM fluo-4AM in a mammalian Ringer's solution (containing mM: 160 NaCl, 3 KCl, 2 CaCl2, 10 HEPES, 8 glucose, 1 MgCl2, 0.1 EGTA; pH 7.4 with NaOH) at room temperate for 20 minutes and then washed three times with 2 mL of dye-free Ringers's solution. Principal rat SCG neurons were selected for Ca^{2+} experiments based on their size (> 15 μM in diameter). Brief electrical field stimuli were applied via two parallel platinum wires, positioned at the bottom of the dish, ~5 mm apart.

In frog cell cultures, the larger cells ("B" cells) were selected for all experiments. In most cases cells were also selected to exhibit a noticeable change of fluorescence (ΔF) in response to a test field stimulus. Sequences of successive images of fluo-4 loaded cells were acquired at video-rate without on-line averaging. In order to improve the signal-to-noise ratio of the images in these sequences of high time-resolution images, off-line signal averaging was generally applied. In such cases, a given neuron was repeatedly activated (3 to 6 times in most experiments), with the same field stimulus and stimulus timing and synchronization with the imaging system. The images corresponding to a given elapsed time in each series were averaged off-line using custom-written image analysis software in the IDL programming language. This signal averaging resulted in a sequence of averaged video rate confocal images that were much smoother, with a theoretical improvement of signal to noise proportional to $\sqrt{n}$, where n is the number of repeats. Keeping the number of repeats in the 3-6 range in most experiments allowed us to perform multi-step experiments without significant photobleaching. We will refer to the sequence of signal averaged video rate images as an "averaged sequence". Thus, members of an averaged sequence will be improved signal-to-noise images, which still correspond to video-rate acquisition. Cells respond very reproducibly to single APs, justifying the signal averaging procedure (see Fig.8. and 10).

In order to characterize local calcium signaling in our cells, we calculated the time course of spatially averaged

fluorescence within multiple user-specified areas of interest (AOIs) within each neuron using our custom-written software. First, the AOIs were specified. Then the pixel values within each AOI were corrected for background fluorescence, recorded from a cell-free area of each image, and the corrected values within the AOI were arithmetically averaged. The spatially averaged fluorescence values were calculated either from the original images or from the averaged sequence, providing video-rate time resolution in either case. The AOIs selected around the cell periphery were of identical size and shape in a given neuron, and at equal distances from the plasma membrane so as to avoid artificial differences of the local Ca^{2+} signals due to varied sizes or to radial locations of the AOIs. The AOI areas ranged from 14 to 33 μm^2 in different cells.

3.3. Field stimulation and stimulus synchronization with confocal imaging

Brief (0.5, 1 or 2 ms) field stimuli were used to generate single action potentials (APs) in isolated frog neurons or within neurons in freshly dissected ganglia. The field electrodes were custom-made, using high purity platinum wires. One electrode was shaped into a loop, with a diameter of about 3 mm. The cell to be tested was positioned approximately in the center of the loop electrode. The other electrode was a straight wire that was placed directly above the center of the loop electrode. The field stimulus was initiated by the image acquisition system that provided a TTL pulse to the signal generator at the instant of the

start of the image sequence. The timing and the duration of the field stimulus were set by a custom-made system, which consisted of a digital signal generator and an amplifier. The field stimulus was applied either 100 or 200 ms after the start of the image sequence, thus providing either 3 or 6 control images prior to stimulation at the start of each sequence. These control images were used to determine the steady-state fluorescence level (F_0) within each specified AOI, which was then applied to calculate the relative fluorescence values ($\Delta F/F_0$, where $\Delta F=F-F_0$).

At video rate, one line of pixels is scanned in 63 μs, resulting in acquisition of a full-frame image in 30 ms (480 horizontal lines per image; scanning from bottom to top of image as shown here). Return of the laser beam to its starting position and start of the next image required an additional 3 ms, thus providing us with a 33 ms/image acquisition rate when obtaining image sequences. In all but one figure, the end of the stimulation pulse was below the position of the lower edge of the cell at the bottom of the image. Thus, the fluorescent pattern inside the cell in the image in which the stimulus was applied represents the cell at a time after stimulus application. It should be noted, however, that the bottom of each acquired image (either original or of the averaged sequence) corresponds to a moment of time 30 ms earlier than the top of that same image due to the 30 ms acquisition time for each image, with successive lines being acquired from bottom to top of the image.

3.4. Optical signals arising from above or below the plane of focus

The fluorescence signal detected by the PMT in a confocal microscope is determined by the dimensions of the light cone that is positioned symmetrically to the focal point. Consequently, even under ideal confocal conditions (i.e., setting the pinhole small, usually between 1 and 3 Airy disk units), the detected optical signal will contain information that has arisen from intracellular domain(s) located above and/or below the current focal plane of observation. In order to characterize the depth of field from which we can expect such mixing of optical signals we imaged sub-resolution (d=0.2 μm) fluorescent beads in successive axial planes over a 10 μm vertical range using our LSM 5 LIVE system and found that the observed optical signal will contain information not only from the focal plane but also from planes up to approximately 2 μm above or below the focal plane as well (data not shown).

3.5. Electrophysiology

Membrane potential measurements were performed in the whole-cell configuration of the patch-clamp technique (Hamill et al., 1981) using an EPC-10 amplifier (HEKA Instruments Inc., Germany). Current-clamp experiments were carried out using Ringer's solution and an intracellular pipette solution containing (in mM): 150 KCl, 7 NaCl, 4 MgCl2, 5 Na2ATP, 14 phosphocreatine-Na2, 0.3 Na2GTP, 10 HEPES. (pH 7.2). For Ca^{2+} channel-current measurements bath solution contained (in

mM): 162.5 TEA-Cl, 2 CaCl2, 10 HEPES, 8 glucose, 1 MgCl2, 0.001 TTX, pH adjusted to 7.4 with TEA-OH. The pipette solution (internal solution) contained (in mM): 140 CsCl, 10 HEPES, 1 CaCl2, 5 MgCl2, 5 Na2ATP, 0.3 Na2GTP and 0.1 leupeptin, pH adjusted to 7.2 with CsOH. The sampling frequency was 10 kHz (filtered at 3 kHz). Data were acquired, stored, analyzed and plotted using Patchmaster, Fitmaster (HEKA Instruments Inc.) and Origin 7.5 software (OriginLab Corporation, Northampton, MA, USA).

3.6. Immunocytochemistry

In order to collect information about the spatial distribution and localization of Ca^{2+} release channels, internal membranes and organelles, in particular ER and mitochondria, cultured SCG neurons were incubated with the following primary antibodies: 1) Ryanodine receptor mouse antibody (anti-RyRs; Affinity Bioreagents, Golden, CO), 2) Cytochrome c oxidase (COX), complex IV subunit Vb, mouse antibody (anti-COX; Invitrogen, Carlsbag, CA, USA) and 3) Inositol-1, 4, 5-triphosphate receptor subtypes 1, 2 and 3 rabbit antibodies (anti-IP3RsI-III; Sigma Chemical, St. Louis, MO). The secondary antibodies used here were Cy5-conjugated donkey anti-mouse IgG and Cy3-conjugated donkey anti-rabbit IgG (Jackson Immunoresearch Laboratories, West Grove, PA). First, the neurons were fixed in phosphate-buffered saline (PBS, pH 7.4) containing 4% (w/v) of paraformaldehyde for 10 minutes and then permeabilized in PBS containing 0.1 % (v/v) Triton X 100 (SIGMA) for 10 minutes.

The neurons were exposed to PBS containing 8% (v/v) of donkey serum for 1 hour at 4 °C to block non-specific labeling. Primary and secondary antibodies were diluted in PBS containing 2% (v/v) of donkey serum. Neurons were incubated with either anti-RyRs (1:200 dilution), anti-COX (1:20) or anti-IP3RsI-III (1:100) for 2 hours at room temperature and then incubated with the appropriate secondary antibody (1:200 dilution) for 2 hours at room temperature. Dishes were washed thoroughly after each step in PBS containing 2% (v/v) of donkey serum. For each primary antibody-treated dish, another dish of SCG neurons was treated with the neutralizing peptide, when available, or with secondary antibody only, and used as control.

Antibody-labeled neurons were imaged on an Olympus FluoView 500 confocal system, built on an Olympus IX71 inverted microscope. Neurons were viewed with a UPlan Apo 60X NA 1.20 water-immersion objective lens using 633 nm excitation (He/Ne Red laser) for Cy 5, and 543 nm excitation (He/Ne Green laser) for Cy 3, with emission detected with 660 nm long-pass filter or 560-600 nm band-pass filter, respectively. Photobleaching and photodamage was reduced by operating the lasers at the lowest possible power that still provided images with satisfactory signal to noise ratio. Confocal images were viewed, processed and converted to TIFF using the FluoView software, as well as our custom-written software in IDL (RSI, Boulder, CO), and Adobe Photoshop.

3.7. Drugs and Chemicals

All drugs and chemicals used for Ca^{2+} imaging were purchased from Sigma, except fluo-4-AM and DAPI (Molecular Probes, Eugene, OR); thapsigargin (TG), ryanodine (Ry), cyclopiazonic acid (CPA) and 2,5-di-(*t*-Butyl)-1,4-hydroquinone (Calbiochem, EMD Biosciences, La Jolla, CA, USA).

All the experiments were conducted at room temperature (20-24° C).

3.8. Data analysis

Average intensity of fluorescence within selected small (generally 5-10 μm^2) areas of interest (AOIs) was measured using software custom-written in the IDL programming language (Research Systems, Inc.). Images in XY mode (frame sizes: 512 x 200 pixels; scan speeds: 108 f/s or 60 f/s) were background corrected by subtracting an average value recorded outside the cell. The average fluorescence value before electrical stimulation (F_0) was used to convert Ca^{2+} signals to a $\Delta F/F_0$ scale. The averages are provided as mean ± SEM and statistical significance was assessed using the Student's t-test at a P level of 0.05.

3.9. Computer model for simulating local Ca^{2+} signals

The computer model of an SCG neuron consists of six domains that are functionally distinct and morphologically separated (see cartoon in Fig.22A, bottom panel, for a map of the six domains).

In a dissociated and cultured mammalian neuron with peripherally located nucleus, these domains correspond to IP_3R-rich outer shells, one each in the nuclear (Domain 2) and non-nuclear (D 1) sub-PM periphery; a RyR-rich zone (D 3) bordering the non-nuclear IP_3R-rich area from the inside; a mitochondria-rich core zone (D 5) of the cytosol; the nucleus (D 4); and the central perinuclear area (D 6) that is immuno-stained mainly with IP_3R antibodies (see Results 4.2), predominantly type I (not shown).

A custom written FORTRAN computer program performed the numeric simulations of sub-cellular Ca^{2+} responses. The main components of Ca^{2+} signaling included in the model were plasma membrane Ca^{2+} entry (plasma membrane voltage-gated and leak Ca^{2+} channels), Ca^{2+} release from the ER via RyRs and IP_3Rs, Ca^{2+} accumulation and release by the mitochondria, and removal of cytosolic Ca^{2+} by ER and plasma membrane Ca^{2+} pumps. The relative concentrations of ER, mitochondria, PM, and of their main Ca^{2+} transport mechanisms could be set at various levels in each domain (D1-D6) of the model. The actual values used in the model calculations were first estimated by experimental data from antibody staining (see Fig.23A) and then adjusted slightly in order to improve the fit between the simulated and experimental data. The model system also included Ca^{2+} fluxes amongst the six domains, described via a set of symmetrically arranged flux coefficients ($F_{ij} = F_{ji}$, i, j =1 to 6, $i \neq j$, $i \neq 4$) in order to account for the spread of Ca^{2+} between the six domains.

4. RESULTS

4.1. Local monitoring of Ca^{2+} signals initiated by single or multiple action potentials

4.1.1. General structure of intact ganglion neurons.

Sympathetic ganglia were freshly isolated, enzymatically digested and loaded with fluo-4 AM in the presence of neostigmine, as described in Methods. The ganglia were imaged in the Biorad MRC 600 confocal system. In Fig.6A and B we show the scattered and fluo-4 fluorescence light images, respectively, of a selected area of a ganglion with three identifiable SGNs (one shown only in part, at the bottom of the image). The axons of the cells at the top and on the right are labeled with arrows (black arrows in A, white in B). The nuclei of these cells appear as dark, oval-shaped areas at the periphery of the cells (B, white stars). The bright areas of fluo-4 fluorescence (B) may correspond to presynaptic varicosities. The scalebar in (B) corresponds to 15 μm.

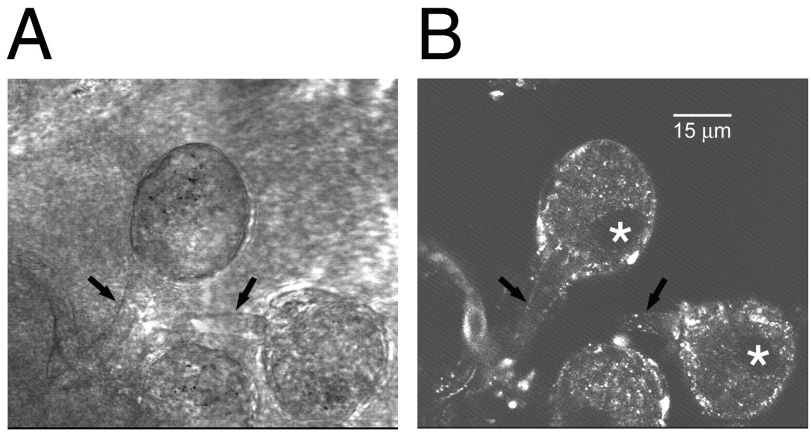

Figure 6. General structure of intact ganglion neurons. Frog SGNs are shown in a partially digested ganglion. A) Scattered light image; arrows point to axons. B) Fluorescence image of the same neurons as in A, loaded with fluo-4 for 60 min in the presence of 20 μM fluo-4 AM and 200 μM neostigmine.

As shown by these images, neurons in partially digested ganglia (see Methods) exhibited intact axons (Fig.6, arrows) and were successfully loaded with fluo-4 (Fig.6B) using 60 min exposure to fluo-4 AM (20 μM) in the presence of 200 μM neostigmine. After such loading treatments, relatively small bright round or oval structures were usually visualized on the surface of many SGNs within the ganglia (Fig.6B). In other images (not shown) these structures appeared connected by thinner fluorescent lines, indicating that they may be presynaptic varicosities located at synapses on the sympathetic ganglion neurons. Neuronal nuclei were visualized as darker oval or bean-shaped areas (Fig.6B, stars) near the cell periphery.

4.1.2. Local peripheral Ca^{2+} hot spots in neurons in intact sympathetic ganglia.

Fig.7 represents confocal images that were collected at video rate (33 ms/img) from a fluo-4 AM loaded frog neuron, located inside of a partially digested sympathetic ganglion, during APs induced by field-stimulation (see Methods). The APs were repeated 3 times, with a 2-minute break between each stimulus, and the corresponding images in each of the 3 series of images (53 images per series) were signal-averaged off-line to create an "averaged sequence". In panel A we show the first 8 images in sequence after averaging; the last panel corresponds to the 53rd image recorded after the two-minute break between AP applications. The field stimulus was applied 1 ms into the 2^{nd} image of Fig.7A, corresponding to $1/30^{th}$ of the vertical dimension of this image (see Methods). The fluorescence signal corresponds to ΔF ($=F-F_0$; see Methods) and is presented on a stretched look-up table (see below panel). The two white arrows indicate the two hot spots for Ca^{2+} release. The arrow at the direction of 7 o'clock points at the hot spot in the peripheral perinuclear area , whereas the arrow at 1 o'clock shows the non-nuclear hot spot, which is located near the axon hillock. Panel B is a confocal image of fluo-4 fluorescence of the same neuron, collected at the same focal plane as in (A) using on-line frame averaging of 16 frames of raw images, collected at video rate without stimulation, in order to improve image quality. The nucleus was always located at the periphery, a few microns

inside the PM, both in neurons in intact ganglia and in cultured cells.

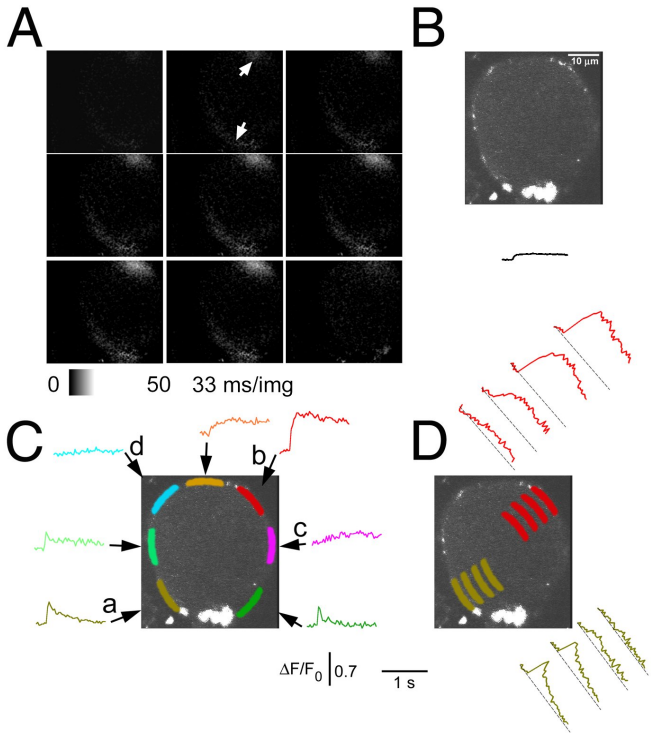

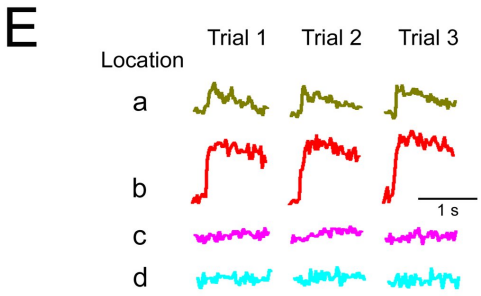

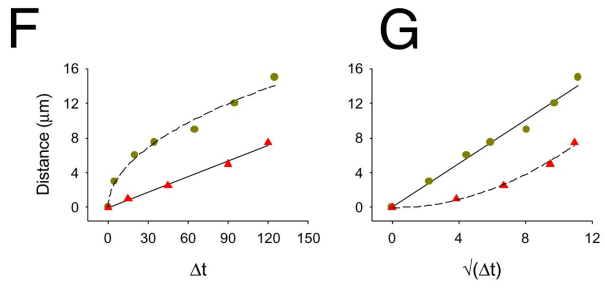

Figure 7. Non-uniform calcium responses of a frog neuron in <u>intact</u> sympathetic ganglion during individual action potentials. A) Video rate confocal images acquired from an SGN show two "hot spots", labeled with white arrow heads. B) shows the average of 16 fluorescence images of the same neuron. C) and D): average responses to single action potentials at seven peripheral locations (C) and at two locations during radial spread of the signal (D). E): the stability of the AP-induced fluorescence transient is shown by the similarity between three repeated responses to single APs (Trial 1 to 3). F) and G): Diffusion plot on linear time scale (F) and on square root time scale (G). The linearity of the olive curve on G) shows free diffusion, whereas the non-linear red curve in G) indicates assisted diffusion.

The bright area near six o'clock in (B) may be a presynaptic bouton of an axosomatic synapse. Similar bright fluorescent structures were found on the majority of intact ganglion neurons of this study. The solid line under the cell's image shows the $\Delta F/F_0$ response averaged over the entire cell, using the same time- and fluorescence scales as in (C) and (D). Panel C shows spatially averaged values of fluorescence that were calculated from the indicated color-highlighted areas of interest (AOIs) around the perimeter of the cell, using successive frames of the averaged sequences of images. The corresponding color-coded records give $\Delta F/F_0$ values, where F_0 was calculated as the mean of the fluorescence value in the AOI in the first five images in the average sequence, all recorded before the field stimulus. The AOIs that were plotted in shades of green (light, dark and olive) are at or near the peripheral perinuclear zone, whereas the red AOI is at the axon hillock. The location of the axon was observed directly by using transmitted light microscopy

before the AP experiments, but the axon was outside the confocal plane of focus after switching to fluorescence imaging. The orange and pink AOIs were close to the axon hillock. All of the colored AOIs were drawn inside the cell at a constant distance from the PM, and all were of the same width and length (33 μm^2). The non-uniform distribution of calcium signals around the periphery of the cell was detected in 7 out of 7 intact ganglion cells. Special care was taken when positioning the perinuclear AOI (olive green), while analyzing this and all other experiments, in order to avoid any overlap between this AOI and the intranuclear space. In panel D we plot the radial spread of the fluo-4 signal from two hot spots in the same neuron. The olive green (perinuclear) and red (axonal) AOIs were shifted to increasing radial distances from the periphery of the cell, in order to calculate the time course of $\Delta F/F_0$ at deeper zones of the cytosol (red) or nucleus (olive green). The position of each record within the two stacks of AOIs (red curves above the cell's image, olive green curves below and to the right of the image) corresponds to the position of the respective AOI inside the cell relative to the PM. Panel E shows the time course of un-averaged fluorescence during each of the individual 3 APs on a compressed time scale. The areas selected for presentation were from the peripheral perinuclear zone (a, olive green), the axon hillock area (b, red) and two of the quiescent peripheral non-nuclear regions (c, pink and d, cyan). The field stimuli were 2 ms long in all cases. Panel F plots the radial distance of the AOI from the PM as a function of the time to half-maximum rise

of $\Delta F/F_0$ at that AOI. In order to calculate these data, seven or five AOIs were selected in the nuclear and non-nuclear areas, respectively, arranged radially at gradually larger distances from the PM (similarly to the arrangement of AOIs in panel D). The distance between the AOIs and the PM was measured in micrometers using our custom-made IDL program, whereas the time to half peak at each AOI was calculated in milliseconds as the time interval between the arrival of the electric field stimulus and the half-maximum time of the resulting Ca^{2+} transient at that AOI. Panel G shows the same data as (F) but plotted as a function of the square root of the time to half peak. In both F and G, the rise time values were corrected for the time to half peak at the most peripherally located AOI, which was estimated for each data set by the x intercepts of the straight lines fit to the data for spread from non-nuclear (F, red triangle) or nuclear (G, olive circles) hot spots.

As indicated by these data, when we applied video-rate confocal microscopy to study local calcium signaling during APs in fluo-4 loaded SGNs and recorded three sequences of video rate images in precise synchrony with the electric field stimulus, we were able to average the corresponding images in each sequence digitally. The averaged sequence is shown in Fig.7A. The first video frame image in Fig.7A was recorded 33 ms before the field stimulus, the second image overlapped the time of stimulation, and the next 6 images were recorded sequentially after stimulation. These first 8 images correspond to sequential frames recorded at video rate (33 ms per image). The ninth image was

recorded after a 2 min recovery, during which no stimuli were applied and no images were collected. The images in Fig.7A demonstrate that the Ca^{2+}-dependent fluo-4 fluorescence change, the "Ca^{2+} signal" or "Ca^{2+} transient", first raises within two small areas or “hot spots” at the periphery of this cell (arrows). The spread of increased fluorescence away from the hot spots was rather restricted around the cell periphery, whereas the radial spread of the Ca^{2+} signal into the cell was somewhat less limited. Due to the small number, localized origin and limited spread of increased fluorescence at the hot spots, the fluorescence signal averaged over the whole cell image showed negligible fluorescence change as a result of the electrical stimulation (Fig.7B, record below image).

In order to characterize the spatio-temporal distribution of Ca^{2+} in the cell, small areas of interest (AOIs) were selected within the cell, as shown by the colored areas in the fluorescence images in Figs.7C and D. The fluorescence values within each of these colored areas were spatially averaged and used to calculate a $\Delta F/F_0$ time course in each AOI (Fig.7C and D).

All AOIs used in a given cell were of the same size and shape, and the AOIs around the periphery of a cell were all positioned to be at equal distances from the plasma membrane in order to avoid artificial differences in Ca^{2+} responses due simply to different sizes or different radial locations of the AOIs.

The time course of fluorescence in each of the AOIs positioned around the cell periphery in Fig.7C clearly demonstrate that this neuron exhibited two local peripheral hot

spots for initiation of Ca^{2+} release. One hot spot was located in the peripheral perinuclear area (a, olive green). This location exhibited a very rapidly rising local Ca^{2+} transient, going from rest to peak signal within the 33ms time interval from acquisition of data at a given location in one image and the next image, and a relatively rapid decay phase ($t_{1/2}$ = 240 ms). The other hot spot, at the cell periphery roughly opposite the nucleus (b, red), had a calcium transient with a similarly rapid onset but a slower decay ($t_{1/2}$ > 1 s) that was too long to be determined with the sampling interval used here. Other peripheral areas that were about mid-way between these two sites remained quiescent (c, violet and d, blue).

Local peripheral hot spots for initiation of Ca^{2+} release were observed in every neuron examined in this study in a partially dissociated ganglion (7 out of 7 cells). All neurons exhibited a hot spot in the peripheral perinuclear region and 5 out of 7 had one or more hot spots roughly opposite the nucleus in the axon hillock region. Thus, local peripheral hot spots for Ca^{2+} release in the perinuclear and axon hillock region are a consistent feature of neurons in freshly isolated ganglia.

All hot spots in both the perinuclear and the non-nuclear regions exhibited a very rapid rising phase, which was generally completed from one 33 ms image to the next. The half-time of decay of the local peripheral Ca^{2+} signals at the perinuclear hot spots was always relatively fast (180-300 ms; 260 ± 20 ms, N=7). In contrast, at some non-nuclear hot spots the half time of decay (240 ± 26 ms, N=3) was similar to that at the perinuclear hot

spots, whereas other non-nuclear hot spots (N=4) exhibited decay half-times greater than 1 s. In principle, the time course of rise and fall of Ca^{2+} at the release site will be determined by the balance between the rate of Ca^{2+} release and the rates of Ca^{2+} "removal" by Ca^{2+} binding and transport or by Ca^{2+} diffusion out of the release region. The more rapid decline of the Ca^{2+} signal observed in the peripheral perinuclear region compared to some of the non-nuclear peripheral release sites might thus indicate either more effective removal of Ca^{2+} in the perinuclear periphery or prolonged release in the non-nuclear release site.

The hot spots for Ca^{2+} release were temporally and spatially stable throughout an experiment. Fig.7E presents fluorescence records for individual (i.e., unaveraged) responses to single APs from both of the two hot spots (a: olive green peripheral perinuclear location; b: red peripheral non-nuclear location) and from two quiescent peripheral areas (c: violet; d: blue Fig.7C). These records demonstrate that the active areas gave reproducible Ca^{2+} transients in response to each electrical stimulus, and thus reliably and repeatedly functioned as hot spots for Ca^{2+} release, whereas the quiescent zones were reproducibly non-responsive throughout the experiment. These findings indicate that the hot spots are structurally determined, not random. Moreover, activation at the hot spots was always temporally synchronized to the time of the AP, thus excluding the possibility that these sites were stochastic or appeared spontaneously. Finally, the hot spots cannot be attributed to

localized depolarization, since the plasma membrane should form an isopotential surface over the entire cell body of these neurons.

In the cell in Fig.7 the intact axon was observed in lower power views (not shown) to be located at the top of the fluorescence images in Fig.7. The non-nuclear hot spot was thus in close proximity to the axon hillock, which may indicate a functional relationship between this site and the origination site of the axonal Ca^{2+} transients. However, the occurrence of non-nuclear peripheral hot spots in individual cultured axotomized frog SGNs (below) indicates that the continued presence of the axon is not required for maintenance or function of this non-nuclear Ca^{2+} release site.

Video rate confocal imaging not only allowed us to identify the peripheral hot spots for Ca^{2+} release, but also provided the means to characterize the spread of the Ca^{2+} signal away from the hot spots. The radial spread of the Ca^{2+} signal from the two hot spots in the neuron in Fig.7 is illustrated in Fig.7D. The $\Delta F/F_0$ signals calculated for each of the indicated sets of 4 AOIs positioned at increasing radial distance from the cell periphery (Fig.7D) indicate that the Ca^{2+} signal spreads with decrement and slowed time course both within the nucleus (a, olive, bottom) and in the non-nuclear (b, red, top) regions. Note that the records in Fig.7D are rotated so the baselines (dashed lines) are not horizontal but are roughly parallel to the central tangent to the corresponding circumferential AOIs.

4.1.3. Spread of the Ca^{2+} signal away from peripheral hot spots

The spread of Ca^{2+} away from the hot spots may be expected to occur via passive diffusion, with the spread retarded by Ca^{2+} binding and Ca^{2+} transport but possibly augmented by the active process of Ca^{2+} release from Ca^{2+} stores by CICR. However, since releasable Ca^{2+} stores are not present within the nucleus, radial spread of Ca^{2+} across the nucleus is expected to occur purely by Ca^{2+} diffusion and binding. The distance covered by passively diffusing Ca^{2+} is directly proportional to the square root of time (Crank, 1975), whereas release-assisted diffusion will exhibit a more constant velocity of spread. Ca^{2+}-binding would slow the diffusion. In Fig.7F we plot the distance (in micrometers, measured from the PM) as a function of the time to half-maximum rise of the $\Delta F/F_0$ signal recorded at that distance for the signals originating from the nuclear (olive green symbols) and non-nuclear (red symbols) hot spots. The difference between the mechanisms of spread in the nuclear and non-nuclear cytosolic areas is clearly shown by the different shapes of these two curves. The non-nuclear data (red triangles in Fig.7F) are closely approximated by a linear function (solid straight line) indicating a constant velocity of spread. In contrast, the nuclear signal (olive green) follows a non-linear time course. In order to determine whether the nuclear data followed a passive diffusion time course, the data from Fig.7F were re-plotted as a function of $(\text{time})^{1/2}$, i.e. on a "square-root time" scale in Fig.7G. The nuclear data were now well fit by a straight line in Fig.7G.

The fitted data values of the straight line in (G) were also transformed onto the linear time scale and re-plotted in Fig.7F (dashed curve), showing that the original nuclear data were well described by a square-root time function. The straight line fit to the non-nuclear data from (F) was also re-plotted on a square-root time scale in (G) (dashed line). These data suggest that Ca^{2+} spreads mainly via passive diffusion in the nuclear area, whereas the Ca^{2+} spread in the non-nuclear cytosolic areas is probably assisted by an active process such as Ca^{2+} release from the ER.

It is difficult to quantify the amplitude of the change in $[Ca^{2+}]$ from the fluorescence signals recorded with fluo-4, which is not a ratiometric indicator. Differences in fluorescence signals due to differences in local effective concentration of fluo-4 due to possible dye binding and/or dye exclusion from intracellular organelles can be partially compensated for by normalizing the fluorescence change observed in any AOI to the resting fluorescence in the same AOI (as done here), assuming that all dye is cytosolic and that resting cytosolic $[Ca^{2+}]$ is the same in all AOIs. This approach is not perfect since it is possible that some dye may be sequestered within organelles at relatively high $[Ca^{2+}]$, and thus contribute to the resting fluorescence but not to the cytosolic Ca^{2+} signal. However, our results (Fig.10, below) indicate that fluorescence due to sequestered dye may be minimal in these cells. Finally, it has also been shown that fluorescent Ca^{2+} sensitive dyes behave differently in the nucleus than in the cytosol (Thomas et al, 2000 and Fig.10, below). Nonetheless, despite these uncertainties in absolute calibration,

the very small or undetectable changes in fluorescence observed in the selected AOIs peripherally or radially displaced from the hot spots (Fig.7) would seem to correspond to very small or negligible rises in Ca^{2+} in response to a single action potential in these regions unless all dye contributing to resting fluorescence in these areas is totally unresponsive to elevated Ca^{2+}.

4.1.4. Peripheral Ca^{2+} hot spots in cultured SGNs

Neurons in freshly isolated intact ganglia have the advantage of maintained axons and synapses. However, the technical difficulties of manipulating and recording from neurons in intact ganglia make the use of this preparation rather time-inefficient and relatively impractical. Therefore, we also investigated AP-induced Ca^{2+} transients in individual cultured SGNs, which lack axons and synapses and may have undergone some possible cellular reorganization in culture. Despite these differences, the majority of cultured SGNs responded to single APs with local Ca^{2+} hot spots (Fig.8) similar to those observed in neurons in intact ganglia (Fig.7).

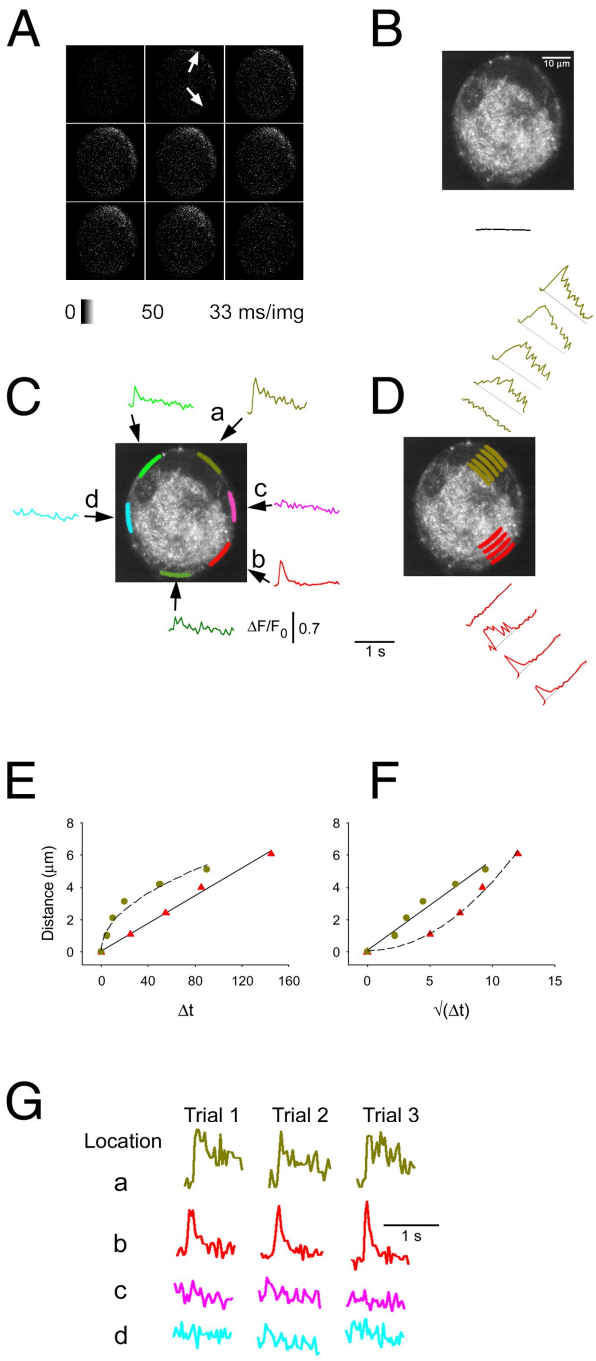

Figure 8. Non-uniform calcium responses of a cultured frog sympathetic ganglion neuron during individual action

potentials. A) Video rate confocal images acquired from a SGN cultured for 24 hours show two "hot spots", labeled with white arrow heads. B) shows the average of 16 fluorescence images of the same neuron. C) and D): average responses to single action potentials at seven peripheral locations (C) and at two locations during radial spread of the signal (D). E) and F): Diffusion plot on linear time scale (E) and on square root time scale (F). The linearity of the olive curve on F) shows free diffusion, whereas the non-linear red curve in F) indicates assisted diffusion. G): the stability of the AP-induced fluorescence transient is shown by the similarity between three repeated responses to single APs (Trial 1 to 3).

In these experiments, AP-induced Ca^{2+} transients were recorded in a cultured frog sympathetic ganglion neuron. The dye loading, fluorescence recording and off-lines analysis methods were largely similar to those applied in Fig.7. In panel A, the arrow at 1 o'clock points at the hot spot in the peripheral perinuclear area (compare with panel B), whereas the other arrow, at 5 o'clock, shows the non-nuclear hot spot. These images showed no small regions of constant high fluorescence, in accordance with the absence of synapses in cultured neurons (see Fig.6B). In panel B, the fluo-4 fluorescence of the same neuron is shown at the same focal plane, acquired using on-line image averaging at 16 frames/image. The higher spatial resolution of the averaged image provides a better view of the cell's structure. The solid curve under the image indicates the whole-cell average of the $\Delta F/F_0$ signal, generated by a single AP. Same scales apply as in (C) and (D.

Fig.8A presents video-rate confocal imaging data from such a neuron. Similar to the neurons from the intact ganglion in Fig.7,

this cultured SGN also exhibited local peripheral Ca^{2+} responses to a single AP. Two peripheral hot spots for Ca^{2+} release were identified in this neuron. As in the neurons in the intact ganglia, one of the hot spots was located in the perinuclear periphery (top), whereas the other was found at a peripheral location (bottom right) (Fig.8A, arrows). An average of 16 images of the resting cell (Fig.8B) shows the cell nucleus as a darker bean-shaped sub-plasma membrane region near the top of the cell. The fluorescence response averaged over the entire cell exhibited little change as a result of cell stimulation (Fig.8B, record below cell image).

Using the images in Fig.8A, we calculated the $\Delta F/F_0$ Ca^{2+} responses in the two peripheral hot spots, as well as in several other peripheral cytoplasmic AOIs. The selected AOIs and the corresponding $\Delta F/F_0$ records were color-coded (Fig.8C). Both the perinuclear and non-nuclear hot spots (a, olive green, top; b, red, bottom right, respectively) responded to a single-AP with a very rapidly rising and rapidly falling Ca^{2+} transient. In this cell, the $t_{1/2}$ for the decay of the $\Delta F/F_0$ signal was 360 ms or 130 ms at the perinuclear or non-nuclear hot spots, respectively. In 23 cultured cells with local peripheral Ca^{2+} hot spots, 17 exhibited a relatively rapid decay of $\Delta F/F_0$ at both perinuclear ($t_{1/2}$ = 330±60 ms) and non-nuclear ($t_{1/2}$ = 195±15 ms) hot spots, whereas 6 cells exhibited rapid decay at the nuclear hot spots ($t_{1/2}$ = 310±120 ms) but slower decay at the non-nuclear site ($t_{1/2}$ > 1 s). These 23 cells were from a “non-biased” sample (see below).

These experiments showed that Ca^{2+} transients also spread from the two hot spots towards the center of the neuron (Fig.8D). As the Ca^{2+} signal spreads toward more central locations, the local transients exhibited progressively smaller and slower Ca^{2+} responses. As in the intact neurons (Fig.7F and G), the radial spread of Ca^{2+} into the nucleus from the perinuclear hot spot was mainly via passive diffusion, whereas Ca^{2+} release significantly contributed to the radial spread of Ca^{2+} from the non-nuclear hot spot, as shown by the distance-time and distance-square root time graphs in panels (E) and (F), respectively. The two hot spots were also spatially and temporally stable (Fig.8G). Based on these results, the initiation sites in this cultured SGN and the spread of Ca^{2+} from these sites behaved similarly to those observed in intact ganglion neurons.

In order to estimate the fraction of all cultured neurons that exhibited local peripheral hot spots for Ca^{2+} release, we sampled a group of cells (n=31) that were selected solely by their shape and size prior to observing their fluorescence signals. Of the cells in this unbiased sample, 23 cells (74%) exhibited responses at a few local hot spots around the cell periphery. Thus a large majority of the B neurons in both intact ganglia and cell cultures exhibit localized peripheral Ca^{2+} hot spots in response to single action potentials. The other 8 (26%) cultured cells exhibited uniform Ca^{2+} signals around the cell periphery in response to a single AP (see below).

Non-nuclear hot spots in cultured neurons were usually located approximately across the cell from the nucleus, which

also corresponds to the most common location of the axon in an intact neuron. It thus appears likely that cultured cells with non-uniform peripheral Ca^{2+} signals preserved the structural elements in the axonal hillock region that give rise to preferential Ca^{2+} release, and thus still possess a hot spot for Ca^{2+} release in that area, even after several days in cell culture without the presence of the axon.

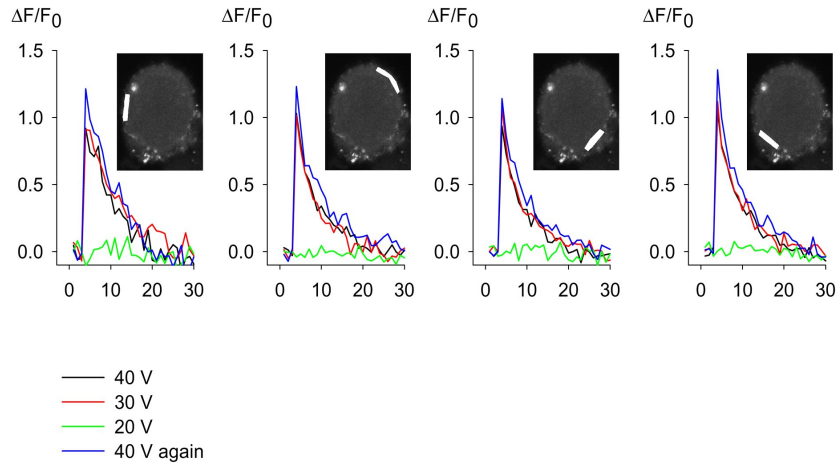

Figure 9. All-or-none behaviour of electric stimulus induced Ca^{2+} transients. A cultured frog SG neuron was exposed to 40V, 30V and 20V electrical pulses. The 40V and 30V pulses induced similar responses, whereas the 20V induced no responses, i.e. 20V was below the AP threshold. The 40V pulse was repeated at the end and resulted in the same response as before, indicating all-or-none behaviour, typical of action potentials.

In order to show that the field stimuli used here elicited APs, 3 cultured SGNs were exposed to 2 μM TTX, which completely eliminated the field-stimulus induced Ca^{2+} transient (data not shown). Moreover, the size and shape of the Ca^{2+} signal remained constant using electrical stimulus intensities above a

threshold level, but were zero when stimulated below that threshold (n=7), consistent with the Ca^{2+} responses being triggered by all or none APs, as shown in Fig.9.

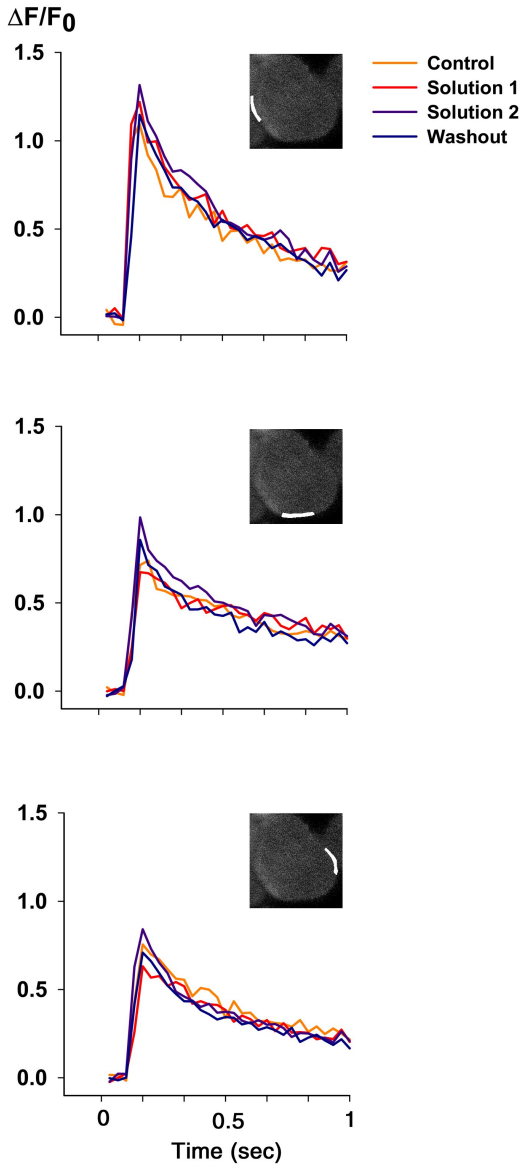

Figure 10. Stability of the Ca^{2+} response to single APs in an SCG neuron during trivial environmental changes. A cultured SGN was exposed to a suprathreshold electrical stimulus ("Control"). The bath solution was then replaced with a fresh

saline of the same composition and the stimulus was applied again (Solution 1"). The whole bath replacement procedure was repeated two more times ("Solution 2" and "Washout"). The similarity amongst all four fluorescence transients prove that the system was stable against rundown with time or during solution changes.

We have also shown that the Ca^{2+} responses for APs were stable to environmental changes, as shown in Fig.10. Here we changed the entire bath solution around the SCG neurons from a control solution to another with identical composition ("Solution 1"), and then repeated the process ("Solution 2"). The cells were then returned to the original control solution ("Washout"). The AP-induced Ca^{2+} transient didn't change at all during this process, proving the system's stability.

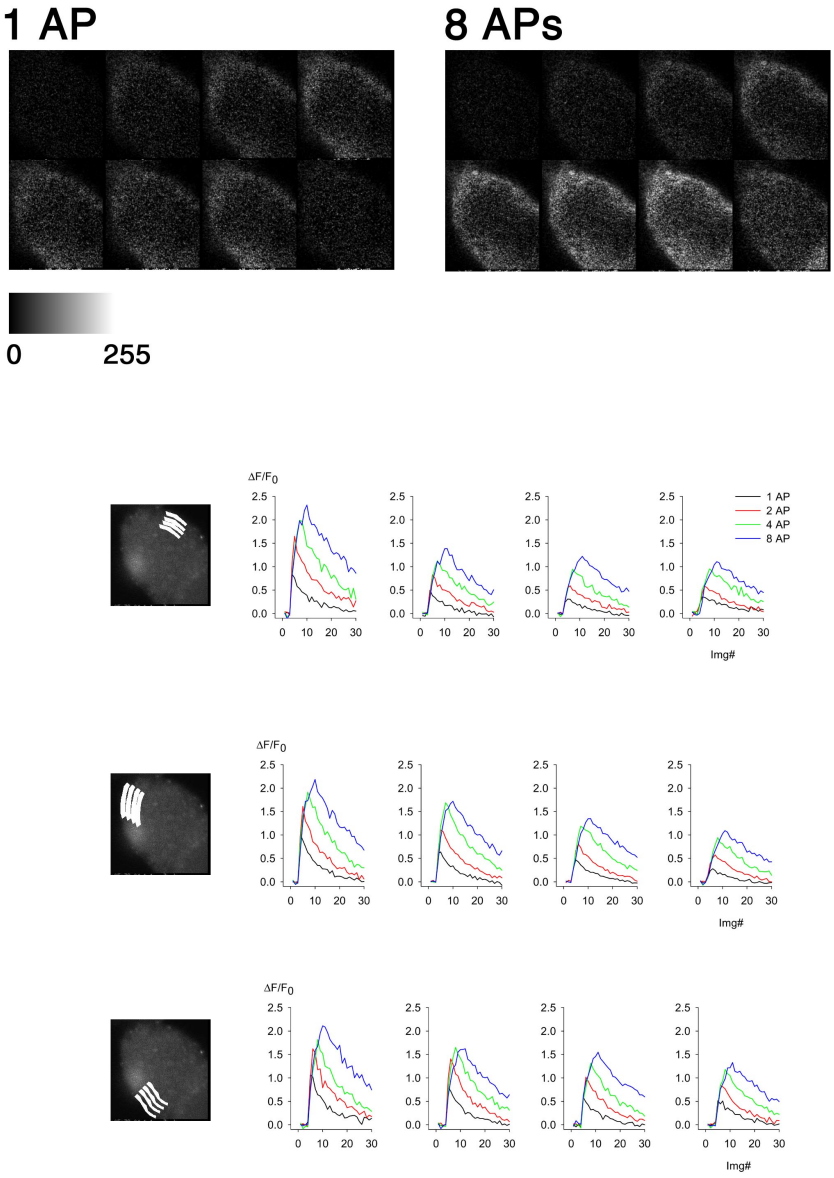

Figure 11. AP-induced Ca^{2+} transients scale linearly with the number of APs. A cultured frog SG neuron was exposed to 1, 2, 4 and finally 8 brief electric transients and the corresponding fluorescence transients were recorded at video rate. The top two panels show the first 7 video rate confocal images, followed by the last recorded image, which is the 8th image in the panel (recorded after a 30 sec recovery). The bottom panel shows the

time courses from three sub-plasma membrane (PM) areas (white crescents in the insets) as a function of time (X axes) and radial dislocation from the plasma membrane (left to right in each row corresponds to gradually larger distances from the PM).

As shown in Fig.11, AP-induced Ca^{2+} transients became proportionately larger and of slower decay when more than one AP was applied in quick sequence. Here we produced Ca^{2+} transients with 1, 2, 4 or 8 APs and the recoded Ca^{2+} responses are shown for 3 different hot spot areas (Fig.11, three rows of records). This finding indicates that the mechanisms behind the generation of these Ca^{2+} transients are able to either quickly recover between subsequent APs, or provide a robust supply of Ca^{2+} that isn't exhausted even with 8 APs arriving in quick success.

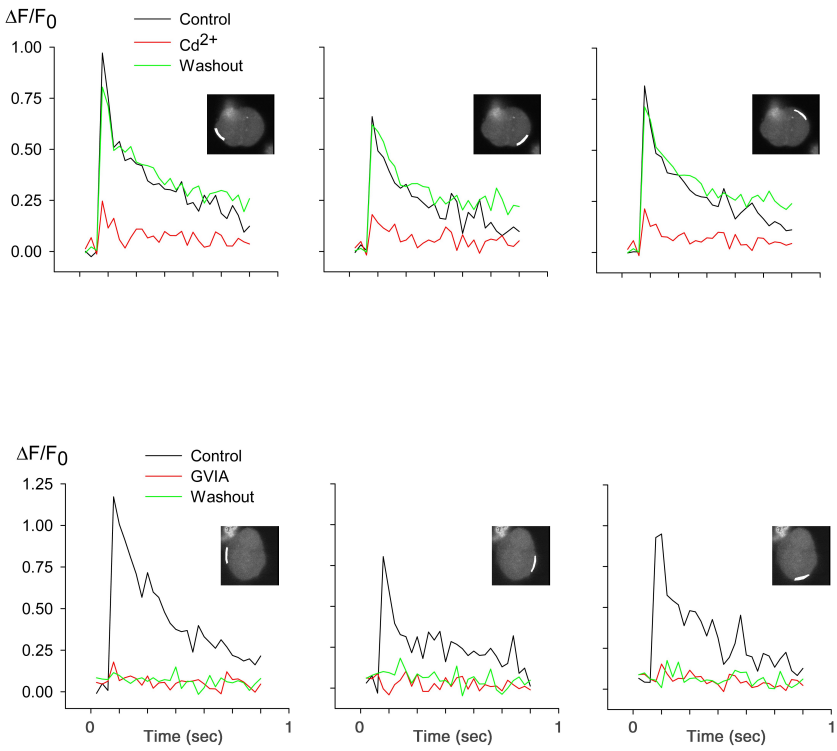

Figure 12. AP-induced Ca^{2+} transients are related to Ca^{2+} influx via the plasma membrane. Top row: the effect of the general calcium channel blocker cadmium on AP induced calcium transients in a cultured SGN. The inhibition was nearly complete and fully recoverable, indicating a significant role of calcium channels in the generation of these calcium transients. Bottom row: the effect of the N-type calcium channel specific inhibitor omega-conotoxin GVIA. The full inhibition of the transients specifies that N-type calcium channels are most likely to be behind these calcium responses.

Finally, we examined if the AP-induced Ca^{2+} transients were also related to Ca^{2+} influx via voltage gated Ca^{2+} channels. First, we applied the general calcium channel blocker cadmium to neurons that were previously tested under control conditions (Fig.12, top line of records). We observed that Cd^{2+} nearly completely

eliminated the Ca^{2+} transient, and that this effect was completely reversible (compare "Washout" curve with "Control").

Sympathetic ganglion neurons are known to have a significant population of N-type voltage gated calcium channels in their plasma membranes. In order to check whether our SGNs and SCG neurons are also populated by such channels, we applied the specific N-type calcium channels inhibitor omega-conotoxin GVIA to neurons that were previously tested with single APs. Here we found that this inhibitor indeed removed the entire AP-induced calcium transients (Fig.12, bottom row of records). Due to the very high affinity of GVIA to the N-type Ca^{2+} channels, washout is practically impossible, as confirmed by our "Washout" records when compared to the controls.

4.1.5. Ca^{2+} release from internal stores by CICR is critical for AP-induced local peripheral Ca^{2+} responses

Studies by Kuba and co-workers showed that Ca^{2+} release by CICR plays an important role in the initiation of AP-induced Ca^{2+} transients in bullfrog SGNs (Hua et al., 2000; Akita and Kuba, 2000), but those responses were probably not from highly localized hot spots as observed here. We thus examined the importance of CICR in AP-induced local peripheral Ca^{2+} signals in the grass frog neurons. These experiments are summed up in Fig.13.

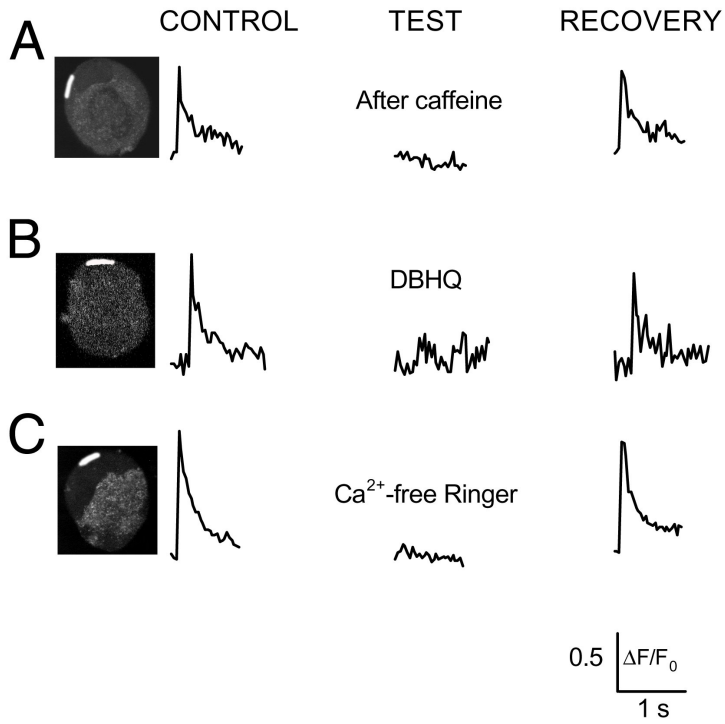

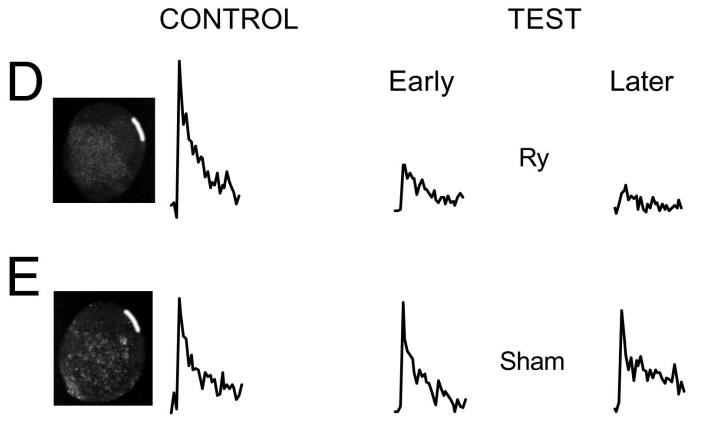

Figure 13. Calcium-induced Ca^{2+} release is essential for AP-induced Ca^{2+} transients. The effect of 10 mM caffeine (A), 30 μM DBHQ (B), calcium-free extracellular solution (C),

50 μM ryanodine (D), and solution exchange to identical saline (sham, E) on AP-induced calcium transients in cultured SGNs.

Here, spatially averaged values of relative fluorescence were calculated in several peripheral AOIs in five different neurons (A through E). Results from a single AOI in the peripheral perinuclear zone (white-highlighted areas in inset images of the neuron) are presented in each panel. The data correspond to $\Delta F/F_0$ values, calculated similarly to Figs.11 and 3. As shown in panel A, after the control measurements (left; average of 3 sequences), 10 mM caffeine was applied extracellularly for one minute in Ca^{2+} free Ringer's solution without recording images. The caffeine application was repeated two more times, one minute each, without recording images, with 3 minute washout periods between applications during which the cells were kept in caffeine- and Ca^{2+}-free Ringer's solution to deplete the ER of Ca^{2+}. Field stimuli were then applied 3 times and the average responses were recorded in each AOI (middle). Prior to each stimulus, 2 mM extracellular calcium was added back for 20-30 s to allow Ca^{2+} influx during APs. Between recording sequences, the extracellular solution was changed back to Ca^{2+}-free Ringer's. No increase of fluorescence was detected in any area of the cell under these experimental conditions. In an attempt to recover the cell's response to APs, the neuron was placed continuously in 2 mM Ca^{2+} Ringer's for 10 minutes and then 3 sequential field stimuli were applied. However, the AP-induced calcium response was still negligible (data not shown). To facilitate the recovery of calcium transients, the ER was then

re-loaded with Ca^{2+} by exposing the cell to 50 mM extracellular K^+ three times, for 30 s each (see Cseresnyés et al., 1997). The cell was placed in 2 mM K^+ solution for 5 minutes after each high-K^+ application. The high-K^+ exposures elevated the fluo-4 fluorescence in the entire cell (see Fig.14D, which shows data from the same cell as in Fig.13A). The field stimuli were then repeated 3 times and the average of the resulting records are shown in the right. In agreement with previous findings (Cseresnyés et al., 1997), three brief high-K^+ exposures were capable of completely reloading the ER with Ca^{2+}, as indicated by the full restoration of the Ca^{2+} responses (Fig.13A, right).

In order to examine the importance of SERCA pumps in AP-induced Ca^{2+} signaling, we recorded video-rate confocal images from another neuron that was stimulated by 0.5 ms duration electric field pulses under control conditions (left), in the presence of 30 μM DBHQ (middle) and after a 20 minute washout of DBHQ (right). DBHQ was applied for 10 minutes before recording the first AP-induced transient in the presence of the drug. Prior to the washout experiments, the cells were rinsed three times with DBHQ-free Ringer's, and then incubated in drug-free Ringer's for 20 minutes before recording. Averaged sequences for each experimental condition were calculated from 4 sequences of video-rate confocal images, with 2 min breaks between pulses (see Methods). Values of relative fluorescence from the averaged sequence were calculated within a peripheral perinuclear AOI in each panel (white-highlighted zone in the inset).

The role of Ca^{2+} influx via PM Ca^{2+} channels during AP-induced calcium signaling was studied as shown in panel C. Here the response of a neuron was first recorded under control conditions (left). The cell was then incubated in Ca^{2+}-free Ringer's solution for 3 minutes and excited by 2 ms field stimuli in the continued absence of extracellular calcium. No response was observed in the hot spot (middle), or any part of the neuron (not shown). The cell was then washed three times with 2 mM Ca^{2+} Ringer's solution. The cell's response to 3 consecutive field stimuli, separated by 2-minute recovery periods, was recorded after 6 minutes in 2 mM Ca^{2+} Ringer's. The averaged signal indicates complete recovery of the cell's response (right).

In order to characterize the effect of ryanodine receptors, AP-induced calcium transients were recorded from another neuron before and during exposure to ryanodine under conditions similar to those in panels B and C. After recording 3 control responses (left), the cell was exposed to 50 μM ryanodine (Ry), adding the drug directly to the recording chamber. After 1 minute in ryanodine, field stimuli were applied again in every 3 minutes and the video rate image sequences of the calcium transients were analyzed as described in A. "Early test" (middle) or "Late test" (right) data were calculated from the averaged sequence of the first three or the next three calcium responses, respectively, recorded in the presence of Ry. The difference between the early and late Ry data characterizes the use-dependent behavior of Ry. In order to validate our data with Ry in D, we tested if a significant rundown could be observed in

these neurons, under experimental conditions similar to those in panel (D). An example of these sham control data is shown in panel (E). This neuron was stimulated three times (left) before replacing the bath solution with fresh Ringer's solution, simulating the procedure of adding Ry to the recording chamber. The cell was then stimulated six times following a protocol similar to that in the presence of Ry in (D), and the first and last three Ca^{2+} responses were signal averaged and plotted in the middle and right panels, respectively. These data indicate that there was no significant rundown in this cell.

When we first used caffeine to deplete internal Ca^{2+} stores via three 1 min exposures to 10 mM caffeine in the absence of extracellular Ca^{2+} (2mM Mg^{2+} substituted for Ca^{2+} in Ringer's solution), we saw that this treatment completely abolished the local Ca^{2+} transient in response to a single AP (Fig.13A). Store refilling during two subsequent 30 s exposures to 50 mM K^+ Ringer's solution (by equimolar substitution of K^+ for Na^+ in normal Ringer's, 2 mM Ca^{2+}) largely restored the local Ca^{2+} signal at the original hot spot (Fig.13A). Interestingly, the depletion and refilling of the Ca^{2+} stores did not cause the appearance of local Ca^{2+} signals at any new peripheral locations that did not exhibit hot spots under control conditions (Fig.13A and 3 other cells in this protocol). Thus, the hot spot locations were specifically preserved during store depletion and refilling, indicating a conserved, store content-independent structural basis for the hot spots. In 5 hot spots from 4 neurons, store depletion by two or three 1 min exposures to caffeine in Ca^{2+}-free Ringer

decreased peak $\Delta F/F_0$ to 17±4% ($p<0.05$) of the control peak value, and store refilling during two or three 30 s exposures to 50 mM K^+ restored peak $\Delta F/F_0$ to 78±18% of control.

The AP-induced local Ca^{2+} transient was nearly completely eliminated by the SERCA inhibitor DBHQ (30 μM; Fig.13B; and by thapsigargin and cyclopiezonic acid, (data not shown), and largely recovered after 30 min washout in DBHQ-free solution (Fig.13B). In hot spots from 5 neurons, DBHQ (30 μM) decreased mean peak $\Delta F/F_0$ to 27±7% ($p<0.05$) of the pre-DBHQ control value, and 30 min washout of DBHQ restored the mean peak $\Delta F/F_0$ to 101±19% of control. Removal of Ca^{2+} from the external Ringer's solution (by equimolar substitution by Mg^{2+}) rapidly (4 min) and reversibly (1 min) eliminated the local peripheral Ca^{2+} transient in this (Fig.13C) and 3 other cells tested in this and 3 other neurons. Finally, the irreversible and use-dependent Ca^{2+} release channel blocker ryanodine (Ry; 10 μM) gradually decreased the amplitude of the local Ca^{2+} transients (Fig.13D). In hot spots in 5 neurons, the average peak $\Delta F/F_0$ of the first 3 responses in the presence of 10 μM Ry was 56±2% of the pre-Ry control, and the average of the subsequent 3 responses was 30±7% ($p<0.05$) of control. In parallel studies on three other neurons subjected to the same solution change protocol but in the absence of added Ry (Fig.13E), the peak $\Delta F/F_0$ of the first 3 "sham" responses was 90±13% of control and of the subsequent 3 responses was 79±3% of control, establishing lack of run down of the local Ca^{2+} signals in these neurons. These results indicate a major role of Ca^{2+} efflux via the ryanodine receptor Ca^{2+}

release channel in generating the local Ca^{2+} signals in frog SGNs. Thus, in both bullfrog (Hua et al., 2000; Akita and Kuba, 2000) and grass frog (Rana pipiens; present results) SGNs CICR may have a close functional coupling to the Ca^{2+} influx mechanism.. The structural basis for this strong functional coupling may arise from a concentrated sub-PM localization of the functional ER, as revealed by live-cell staining with BODIPY-Ryanodine in both grass frog (Fig.14E; McDonough et al, 2000) and bullfrog SGNs (Akita and Kuba, 2000).

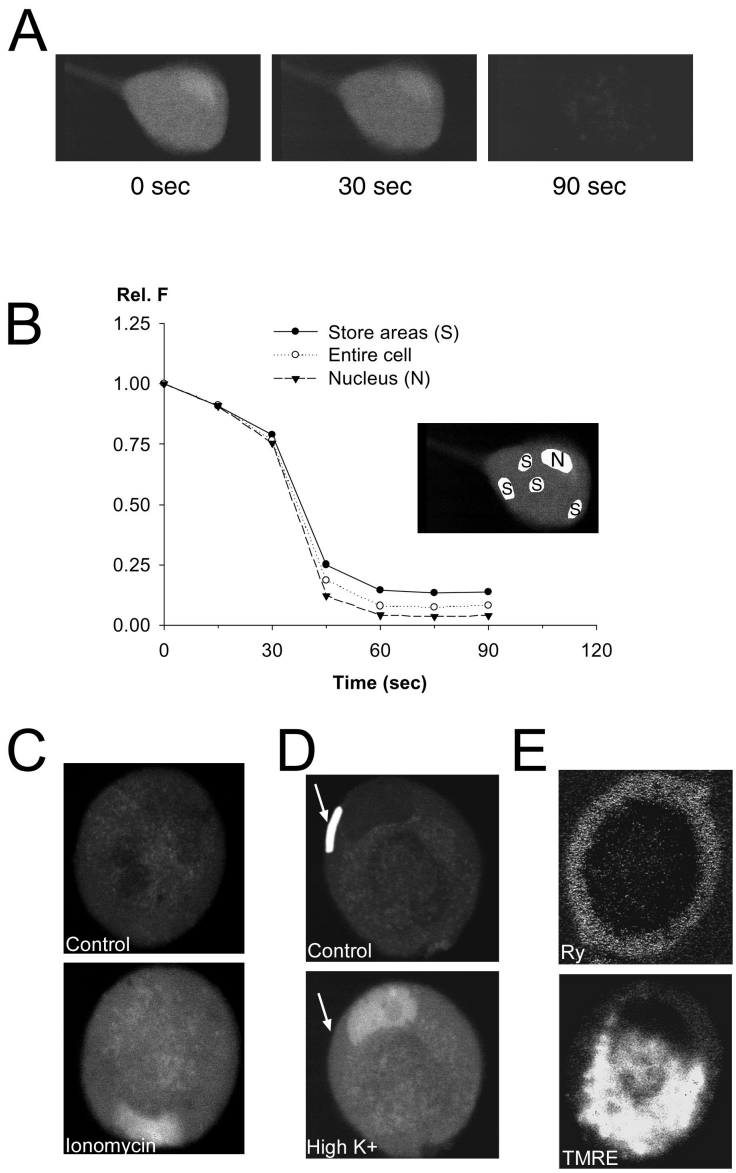

Figure 14. Distribution of Ca^{2+}-sensitive dye, and of intracellular Ca^{2+} compartments in cultured frog SGNs. A): The effect of 0.1% saponin, a mild detergent, on intracellular fluo-4 fluorescence after 30 sec and 90 sec exposure (saponin added directly to the bath solution). Saponin will open holes in lipid membranes that are large enough to let the fluo-4 molecules through, thus removing cytosolic dye, but not compartment-trapped molecules. B): The time course of fluorescence during

saponin exposure at store-like areas (averaged from four white regions labeled “S” in inset), at the nucleus (labeled “N” in inset), and the entire cell. C): The effect of ionomycin, a Ca^{2+} ionophor, on cytosolic fluo-4 fluorescence. D): The effect of robust cell depolarisation by 50 mM potassium chloride on the cytosolic fluo-4 fluorescence. E): The localization of functional ryanodine receptors (top panel, “Ry”) and mitochondria (bottom anel, “TMRE”). Ryanodine receptors were labeled with BODIPY-Ryanodine, whereas mitochondria were marked by TMRE.

In order to investigate if the local hot spots might be the result of non-cytosolic, store-accumulated dye, we measured the changes of fluo-4 fluorescence in a cell that was exposed to the membrane lipid detergent saponin, applied at 0.1% concentration in frog intracellular solution (see Fig.14). These three images show the fluo-4 fluorescence of an unstimulated cell at 0 s, 30 s and 90 s after adding saponin to the recording chamber. The images are the result of 16-frame on-line averaging, in order to improve the signal to noise ratio. In panel B, the average fluorescence was calculated over selected areas of the same cell (white-highlighted areas in insert), in order to quantify the saponin effect. The areas covered the nucleus (N in insert; triangles in graph), the entire cell (empty circles), and a few selected bright areas within the cell, probably corresponding to dye accumulation within Ca^{2+}-rich stores (S; filled circles). At the end of the experiment, only 5 to 10% of the original fluorescence was detectable, indicating that fluorescence signals originating from store-accumulated dye do not significantly affect our results. Panels C and D show that when other neurons, loaded with fluo-4 AM, were exposed to very large Ca^{2+} influx,

we were provided data about the uniformity of the distribution of Ca^{2+} sensitive dye in these cells. In panel C, the neuron was exposed to the Ca^{2+} ionophore ionomycin (2 μM) in 2 mM Ca^{2+} Ringer's solution for 5 min. Ca^{2+} influx resulted in a uniform increase of fluo-4 fluorescence in the cytoplasm and the nucleus (bean-shaped bright area near the bottom). In panel D, a cell was depolarized by 50mM K^{+} Ringer's solution, which resulted in a large and uniform increase of fluo-4 fluorescence in the cytosol, and a larger increase in nucleus. The cell in (D) is the same that was used in Fig.13A, and exhibited a local hot spot in response to a single action potential at the peripheral perinuclear AOI (white-highlighted area in the top image, pointed out by a white arrow in both the top and bottom images of D). In panel E, another cell was stained with 100 nM BODIPY Ry for 10 min, and 1 μM TMRE for 1 min, both in Ringer's solution. The cell was then kept in 100 nM TMRE Ringer's for the duration of the experiment, in order to avoid the leakage of the voltage-sensitive dye from the mitochondria. The cell was then imaged at 488 nm (BODIPY Ry, top) and at 550 nm (TMRE, bottom), averaging 16 frames on-line. The RyR Ca^{2+} release channels appear to be concentrated in a narrow shell at the periphery of the cell, and the mitochondria seem to occupy an interior zone.

The ready accessibility of cultured neurons to solution change provided the opportunity for controls of indicator localization and responsiveness, and for localization of intracellular organelles. The relatively low residual fluorescence after saponin permeabilization (Fig.14, A and B) is consistent

with minimal sequestration of dye into intracellular organelles and with relatively low cellular intrinsic fluorescence compared to the fluo-4 fluorescence in these resting cells. In another neuron, application of the Ca^{2+} ionophore ionomycin (2 μM for 5 min in Ringer's solution) caused a uniform increase in fluo-4 fluorescence throughout the peripheral cytoplasmic regions of the cell, and a larger and uniform increase in fluorescence throughout the nucleus (Fig.14 C). Cell depolarization by elevated (50mM) K^+ Ringer's solution also resulted in a uniform increase in cytoplasmic fluorescence and a larger increase in nuclear fluorescence (Fig.14D). Note that the AOI in white in Fig.14D (top) exhibited the same fluorescence increase as the rest of the cytoplasmic region (Fig.14D, bottom). This same AOI exhibited a local Ca^{2+} transient in response to a single action potential (Fig.13A). The results in Fig.14C and D indicate uniform, but different (Thomas et al, 2000) dye responsiveness to elevated Ca^{2+} throughout either the peripheral cytoplasm or throughout the nucleus. Thus, the local peripheral hot spots for Ca^{2+} release observed after action potentials are unlikely to be due to local peripheral pockets of highly responsive dye molecules. Cell staining with BODIPY Ry (100 nM for 10 min in Ringer's solution) and TMRE (1 μM for 1 min, followed by continuous exposure to 0.1 μM, both in Ringer's solution) revealed that the RyR release channels are located in an annulus at the periphery of the cell, and that the mitochondria are concentrated in a zone interior to the peripheral RyR-rich annulus (Fig.14E), in accordance with our earlier results (McDonough et al, 2000).

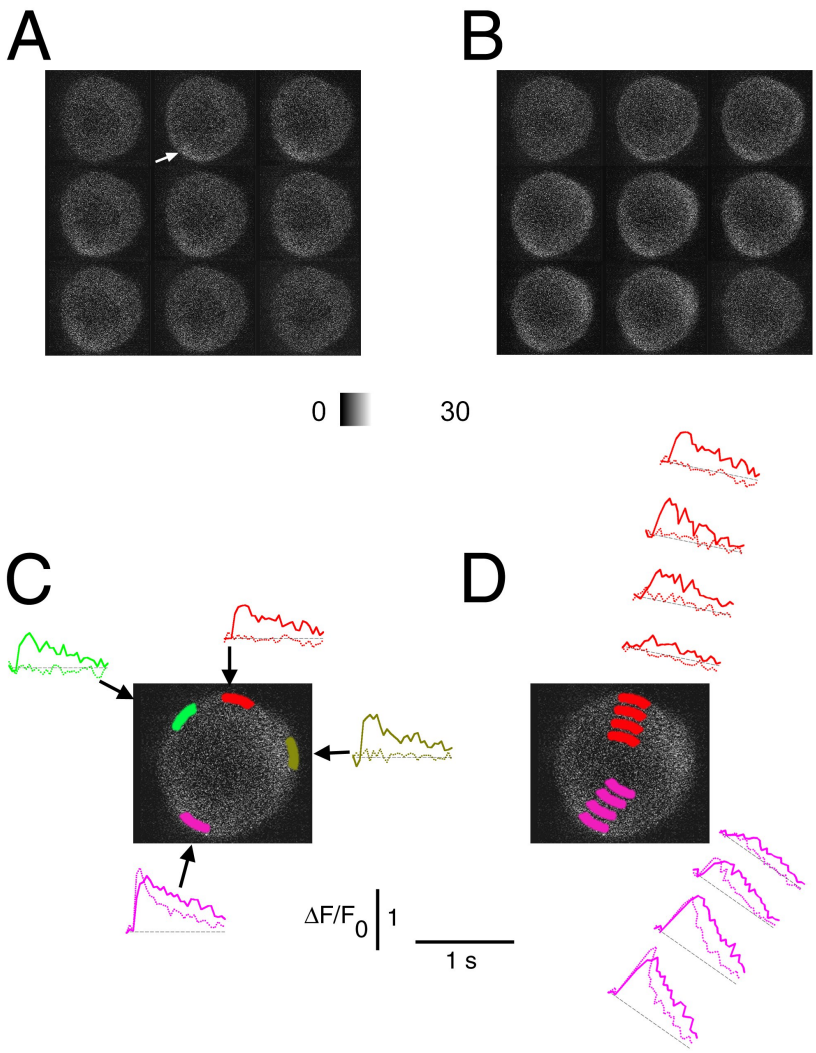

Figure 15. Non-uniform Ca^{2+} responses to single APs are not the result of uneven dye distribution. A): The effect of single electric stimulus on cytosolic fluo-4 fluorescence in a cultured SGN. Images acquired at video rate. White arrow marks the location of the "hot spot". B): The effect of 26 consecutive stimuli at 250 Hz on the same neuron. C): Fluorescence transients at 4 peripheral locations during single stimulus (thin lines) and during 26 fast repeated stimuli (thick lines). D): The radial spread of the calcium sensitive transient at two peripheral locations during single stimulus (thin line) and 26 stimuli (thick lines).

In order to further rule out the possibility of unresponsive dye in some regions in electrical stimulation experiments, AOIs that were non-responsive after a single action potential were shown to be capable of responding during a more massive and prolonged increase in total cytosolic Ca^{2+} produced by a train of stimuli. A neuron in which the response to a single AP was detected at a peripheral hot spot (Fig.15A, arrow) was subsequently stimulated using a train of 26 electric field stimuli (2 ms duration each) at 250 Hz (Fig.15B). The local response to the single AP is presented by the briefer duration (thin) record in the pair of superimposed records at the pink AOI in Fig.15C and D. The neuron exhibited a local peripheral site of Ca^{2+} release (pink) in response to a single AP (thin trace), with little or no change in fluorescence outside this hot spot (green, red and olive thin trace, Fig.15C). In contrast, the train of stimuli induced a longer and more slowly decaying change in fluorescence (thicker, more slowly decaying pink record in Fig.15C and D) at the hot spot for a single AP, and resulted in large signals in peripheral AOIs (green, red and olive thick trace, Fig.15C) that did not respond to the single stimulus. These results indicate that AOIs which did not respond after a single action potential did indeed contain responsive dye. In response to the train of action potentials, the fluorescence signal spread decrementally from the periphery into the cell from both the hot spot for a single AP (pink thick trace) and from the region that did not respond after a single AP (red thick trace). The smaller amplitude signal for the

train (thick pink) than for the single AP (thin pink) at the hot spot may be indicative of some run down of Ca^{2+} release over time (e.g. Fig.13E) in the cell.

4.1.6. Some cultured SGNs exhibit uniform peripheral Ca^{2+} responses

The majority (74%, above) of cultured SGNs behaved very similarly to intact ganglion cells (Fig.7) in exhibiting local peripheral hot spots for AP-induced Ca^{2+} release (Figs.11, 7, and 15). In contrast, other cultured SGNs responded to single APs with peripherally uniform Ca^{2+} transients, exhibiting no apparent hot spots.

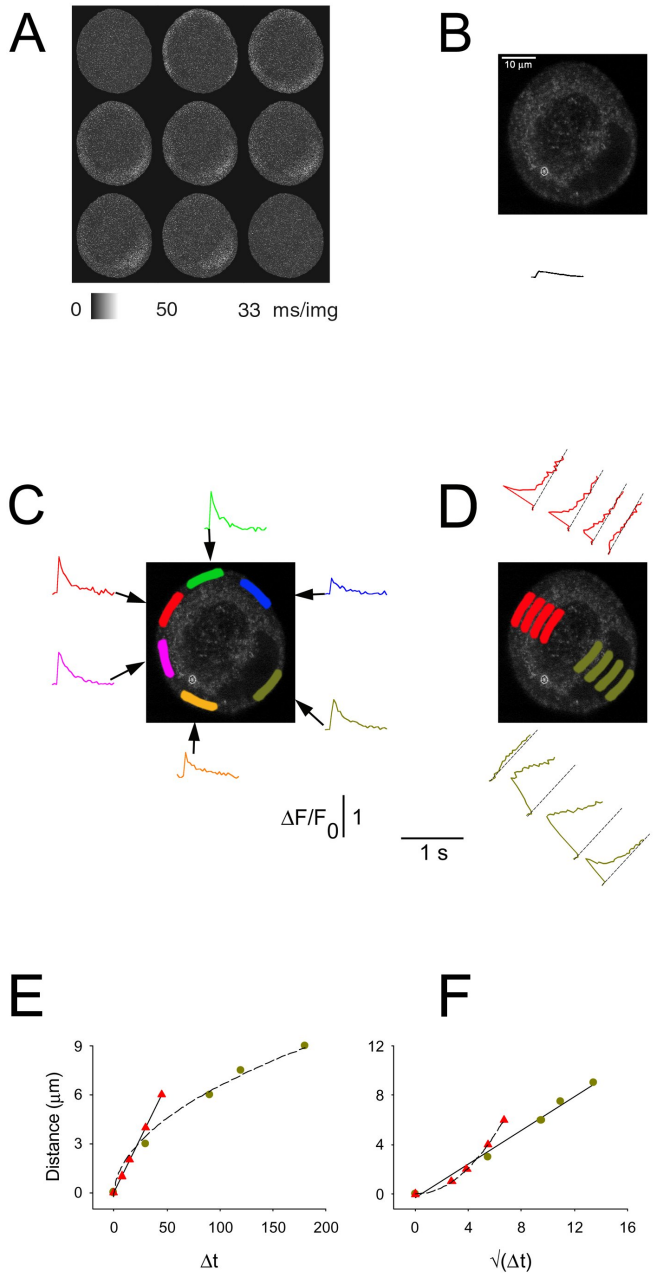

Figure 16. Uniform peripheral Ca^{2+} responses to a single AP in a cultured sympathetic ganglion neuron. A) Video rate confocal images acquired from a SGN cultured for 24 hours show a spatially uniform calcium response. B) shows the

average of 16 fluorescence images of the same neuron. The calcium sensitive fluorescence transient averaged for the entire cell is shown below the image in B. C) and D): average responses to single action potentials at seven peripheral locations (C) and at two locations during radial spread of the signal (D). E) and F): Diffusion plot on linear time scale (E) and on square root time scale (F). The linearity of the olive curve on F) shows free diffusion, whereas the non-linear red curve in F) indicates assisted diffusion.

In experimental conditions very similar to those in Fig.8, cultured SGN were stimulated with single APs and the resulting Ca^{2+} transients were recorded at video rate, as shown in Fig.16. Panel A shows the averaged sequence of video images from one of these cells that responded more uniformly to a single AP than the cells in Figs.11 and 8. Panel B shows the resting fluorescence image, which was recorded with 16 frames/image on-line averaging and which shows raw fluorescence values. The ring-shaped area of elevated fluorescence is likely the result of dye sequestration within intracellular Ca^{2+} stores, especially mitochondria, having higher than cytosolic $[Ca^{2+}]$. The whole-cell average of the single-AP induced $\Delta F/F_0$ signal is plotted under the cell's image. In panel C we show $\Delta F/F_0$ values that were calculated for the six indicated AOIs at the cell periphery, and plotted against time in the same colors as the AOIs. The olive green AOI was drawn in the peripheral perinuclear zone. The records confirm that this cell responded with a uniform Ca^{2+} transient to single APs. Panel D indicates the radial spread of the $\Delta F/F_0$ signal from the red and olive green AOIs in C. The larger signal amplitude in the nuclear area (2^{nd} and 3^{rd} olive green

curves) may in part be caused by different dye characteristics within the nucleus. All AOIs were the same in size and shape (in C and D), and were at a constant distance from the PM (in C) or at constantly increasing distances from the PM (in D). Panel E shows the distance versus time to half peak correlation for this cell, both in the nuclear (olive green circles) and non-nuclear (red triangles) zones. Panel F shows the same data as (E) but on a square root time scale. The data were calculated and plotted as described in Figs.11 and 8.

As we note in the neuron shown in Fig.16, a single AP rapidly and homogenously increased the fluo-4 fluorescence around the entire perimeter of the cell, forming a ring of bright fluorescence that then spread partially towards the center of the cell (Fig.16A). Note that the Ca^{2+} transient in the second frame (in which the stimulus was applied) appeared at a time when the process of image acquisition, which progressed from bottom to top of each image, had already completed scanning of the very bottom of the cell. Thus the bottom of the cell remained dark in the second image in Fig.16A, and only exhibited increased fluorescence in image 3. The resting fluorescence image (Fig.16B) of this cell exhibited a dark region corresponding to the nucleus near the cell periphery (from 3 to 6 o'clock).

Our assay about the uniformity of the fluorescence signals was measured at different points around the periphery of the cell in Fig.16 (see selected peripheral AOIs around the perimeter of the cell). The assay shows that the time courses of both the rising (less than 33 ms) and decaying phases (114 ms $\leq t_{1/2} \leq$ 175 ms;

mean ± SD=137±21 ms, 6 different AOIs) of the fluorescence signals at various AOIs around the periphery of this neuron were all relatively rapid and quite similar, although their amplitude varied somewhat with location. The spread of the fluorescence change from the periphery into the cell interior through the nucleus (bottom, olive; see Fig.16B) and through the cytosolic region across the cell from the nucleus (top, red) are illustrated in Fig.16D. The time course of the fluorescence change became slower with increasing radial distance from both the perinuclear and non-nuclear cell periphery (Fig.16D). It is possible that the increased amplitude signals seen in the nucleus compared to the peripheral AOI just outside the nucleus is an artifact due to different properties of fluo-4 in the nuclear and cytosolic environments (Thomas et al, 2000). The data in panels (E) and (F) of Fig.16 indicate that Ca^{2+} spread mainly via passive diffusion inside the nucleus, whereas Ca^{2+} release from the ER contributed significantly to the spread of the non-nuclear Ca^{2+} signal (red symbols) in this cell with peripherally uniform response, as in the cells exhibiting peripheral hot spots.

The rise and fall of fluorescence was relatively rapid at all regions around the periphery of the uniformly responding cell in Fig.16. In contrast, in the non-uniformly responding neurons the decay of fluorescence was generally slower in the non-nuclear than in the nuclear peripheral primary release sites In a sample of 38 cells selected for uniform peripheral responses, 25 cells exhibited rapid decay of $\Delta F/F_0$ in both the nuclear and non-nuclear regions, having a mean $t_{1/2}$ for decay of 322±109 ms in

the perinuclear periphery and 209±58 in a similar size region roughly across the cell from the nucleus. In 13 other cells with uniform peripheral responses, $t_{1/2}$ was greater than 1.5 s in the perinuclear and/or the non-nuclear peripheral AOI. The $t_{1/2}$ value for the nuclear zone was 121±45 ms (mean±SD) for cells with slow decay only in the non-nuclear AOIs (n=3). The average non-nuclear $t_{1/2}$ was 290±123 ms for the cells with slow decay only in the nuclear AOI (n=3).

	Intact	**Cultured non-uniform**	**Cultured uniform**
# of cells:	7	23	7
Decay half-time at periphery:			
Non-nuclear (ms)	240±26	195±15	113±26
Nuclear (ms)	281±42	330±60	350±110
Radial propagation from periphery:			
Linear velocity into cytoplasm (μm $ms^{-1/2}$)	0.09±0.02	0.12±0.02	0.13±0.01
Square-root velocity into nucleus (μm ms^{-1})	0.9±0.3	0.86±0.03	0.76±0.19

Table 1: Decay- and propagation properties of Ca^{2+} transients in neurons in intact ganglia and in culture.

In order to gain quantitative characterization of our results about Ca^{2+} diffusion, decay times from peak to half maximum at peripheral hot spots were calculated in 7 cells from intact ganglia, as well as in 23 cultured neurons exhibiting non-uniform peripheral Ca^{2+} responses. Decay times at the periphery of cultured cells with uniform peripheral responses were collected from 7 cells in the unbiased sample. In the "cultured uniform"

cells, the decay half times were calculated at one AOI in the peripheral perinuclear zone and in another peripheral AOI of similar size and shape approximately across the cell from the nucleus. These two AOIs corresponded to the perinuclear and non-nuclear hot spots in neurons of intact ganglia and in cultured neurons exhibiting non-uniform Ca^{2+} responses. The 8th uniformly responding cell of the unbiased sample (not included in Table 1) had a half-time decay >1 s in both the nuclear and non-nuclear periphery, which thus could not be estimated using our 1 s sampling interval. Propagation from the nuclear AOI through the nucleoplasm was characterized by the square root velocity, whereas the linear velocities were used to determine the rate of propagation through the non-nuclear ER-rich zone (see Figs.11, 8, 16).

The decay half times at the periphery, and radial propagation properties from the periphery for the nuclear and non-nuclear hot spots are summarized in Table 1. Three categories of cells were considered: neurons in intact ganglia, cultured cells with non-uniform responses and cultured cells with uniform responses. Overall, there seems to be little difference in these properties in each category of these cells. Thus, the newly responding peripheral regions that have appeared in culture in those cultured cells exhibiting uniform peripheral responses may have similar properties as the hot spots in non-uniformly responding cells. A possible basis for the appearance of cells exhibiting uniform peripheral responses in culture might be that the Ca^{2+} transport capability of ER in initially non-responsive

peripheral regions of these cells became more developed during culture. In that case, the ER Ca^{2+} content could increase in the initially non-responsive regions of the ER, thereby potentiating the ER CICR capability such that the entire peripheral ER might release Ca^{2+} in response to the Ca^{2+} influx during an action potential. Alternatively, Ca^{2+} entry could be localized in cells exhibiting hot spots, but be more uniform in cells exhibiting uniform peripheral responses. In any case, Table 1 indicates that the Ca^{2+} handling properties of actively releasing peripheral regions appeared to be very similar in neurons of intact ganglia, and in cultured neurons exhibiting uniform or non-uniform peripheral Ca^{2+} release.

4.1.7. Passive diffusion and active spread of Ca^{2+} in intact and cultured neurons

Calcium spread from the perinuclear hot spot into the nucleus, as well as from the non-nuclear hot spot into the cytosol was carried out by different mechanisms: the spread was passive in the nuclear areas but actively promoted, presumably by Ca^{2+} release from the ER, in the non-nuclear zone (Figs.11F,G; 8E,F and 16E,F). In order to characterize the average behavior of the three main groups of cells (cells in intact ganglia, cultured cells with local peripheral Ca^{2+} responses, and cultured cells with peripherally uniform Ca^{2+} responses), the linear and square-root rates of Ca^{2+} spread were calculated for 3-4 pairs of neighboring AOIs, arranged radially at gradually increasing distances from the PM, and averaged according to the location of the AOIs. The

linear velocity of Ca^{2+} diffusion was calculated by dividing the difference in distance of each AOI from the PM by the difference in time to half peak of the Ca^{2+} signal at that AOI for a set of 3-4 AOIs arranged radially (see Fig.7). The individual velocities were then averaged according to the zone number, where the zone number indicates the relative radial location of the two AOIs. Panel A shows the linear velocities for the nuclear AOIs, whereas panel B contains the data for the non-nuclear AOIs.

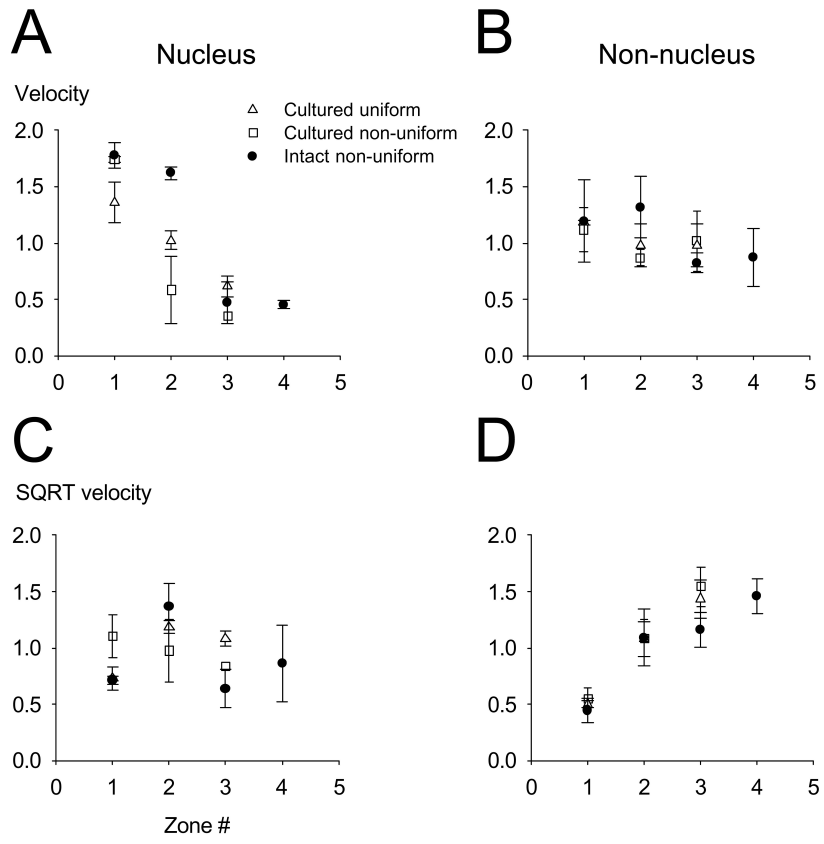

Figure 17. Average velocities of Ca^{2+} diffusion in intact and cultured neurons. Velocity and square-root velocity values for cultured neurons with uniform (open triangles) and non-uniform

(open squares) responses, as well as intact ganglion neurons with non-uniform responses (filled circles).

In order to distinguish between passive diffusion and facilitated spread, the square-root velocities were also calculated for all three cell groups, both in the nuclear **(C)** and non-nuclear **(D)** areas. The square-root velocity was calculated as a ratio of the difference in distance of the two AOIs from the PM (in micrometers) and the difference in the square roots of the time to half peak [in $(\text{milliseconds})^{1/2}$] of the Ca^{2+} signal at those AOIs. Individual square-root velocities were averaged according to the zone number, as described for A and B (above). Data in A through D are plotted as sample mean ± SD for intact cells (filled circles), cultured cells with uniform Ca^{2+} responses (open triangles) and cultured cells with non-uniform Ca^{2+} transients (open squares).

These results demonstrate that the linear velocity of Ca^{2+} spread decreases with distance from the plasma membrane in the nuclear areas, but not in the non-nuclear region for all three groups of cells. These results point out the difference between the passive diffusion and facilitated spread mechanisms characterizing the nuclear and non-nuclear areas, respectively. If the nuclear diffusion mechanism were purely passive, the velocity calculated with the square-root values of the relative half-maximum time (see figure legend) would be constant throughout the radial spread. In Figs.17C and D we show the average square-root velocity values for the nuclear (left) and non-nuclear (right) zones. These data clearly indicate that the main

mechanism of Ca^{2+} spread in the nuclear zone is passive diffusion, whereas the spread of Ca^{2+} in the non-nuclear zone is promoted, probably by CICR via the RyRs of the ER.

The mean rates of "facilitated" spread of Ca^{2+} from the non-nuclear hot spots were 0.09, 0.11, and 0.13 μm/ms in cells in intact ganglia and in cultured cells exhibiting hot spots or uniform peripheral Ca^{2+} release, respectively. These values are similar to the velocities of a Ca^{2+} wave in cardiac myocytes (Cheng et al., 1996). In contrast to the constant velocity of spread across the non-nuclear peripheral ER, the velocity of spread decreased across the nucleus (Figs.11 F, 8E, 16E and 17). Assuming diffusion across the nucleus from an instantaneous point source in the perinuclear ER, the effective diffusion constants were calculated from (Crank, 1975; Yao et al., 1995):

$$C/C_0=\exp(-r^2/4Dt) \qquad (1)$$

Applying Eq.1 at the half-peak concentration and time results in

$$D=(\text{slope})/(4\ln(2)), \qquad (2)$$

where 'slope' is the slope of the distance vs. square root time curve (see Figs.11G, 8F and 16F, olive circles and linear fitted line). The mean effective diffusion constant calculated from the square root velocity of Ca^{2+} spread across the nucleus in the same group of cells was 0.3, 0.24 and 0.20 μm^2/ms.

4.1.8. Rapid rising phase of peripheral calcium transients revealed by high-speed line-scan imaging

Our data from full frame video rate images indicate that the peripheral fluorescence signal jumped from its resting level to a near maximum value from one xy image to the next at the hot spots for Ca^{2+} release (Figs.11, 8 and 15) and around the periphery in uniformly responding cells (Fig.16). Thus, the rise of calcium transients at such locations was actually too fast to be resolved using the full-frame video-rate confocal XY imaging. In order to gain more information about the activation kinetics of the calcium transients, fluo-4 fluorescence data were therefore collected in line-scan mode, which could in principle provide a time resolution of 63 μsec per data point at each pixel location along the scan line. However, due to the noise in the images, in practice we averaged 10 successive lines (at 63 μs/line) to create an image at 630μs/line. In the line-scan experiments, we used cultured cells with uniform peripheral responses so that any line location crossing the cell would pass through two active regions for Ca^{2+} release, one where the scan line crossed each edge of the cell.

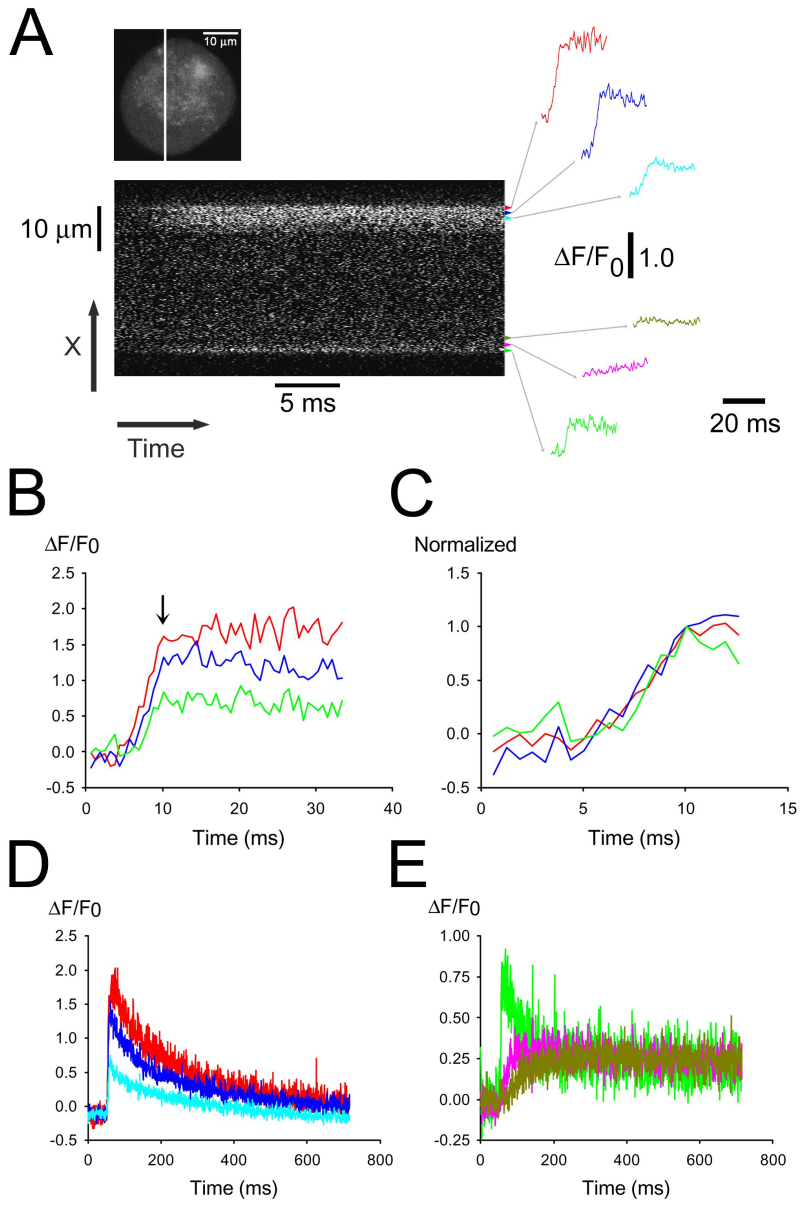

Figure 18. Line-scan confocal recordings of an AP-induced calcium transient. A): High-speed line scan recording of an AP induced calcium transient from a cultured SGN. Inset: XY image of the neuron. Colored curves show the calcium sensitive signal from the corresponding sub-PM areas. B)-E): Time course of the AP-induced calcium transients on absolute (B, D, E) or

normalized (C) fluorescence scales. Note the much longer time scales of D and E.

In Fig.18, calcium transients were induced by 0.5 ms field stimuli and the sequences of line-scan images were collected from a neuron at 63 μs/line. Panel A, top shows the XY image of the resting neuron with the scan line indicated. Panel A, bottom presents the line scan image (480 lines/img) overlapping the time of the field stimulus. The color-coded data curves on the right indicate time- and spatially-averaged relative fluorescence data, corresponding to the areas covered by the base of the color-coded arrowheads. The thin gray lines connect each record to its area-of-interest: the record at the bottom (green) corresponds to the peripheral perinuclear zone, whereas the records directly above it (pink and olive) describe the behavior of intranuclear areas. The top three records (red, blue and cyan) describe the behavior of the non-nuclear periphery. To improve signal/noise, each group of 10 successively acquired lines was averaged to give the 630 μs/point records in A-E. In panels B and C the red, blue and green records are plotted on an expanded time scale. Records in C were normalized to unity; the reference data point is shown by the vertical arrow in B. Data shown in panels D and E show the entire time course of the $\Delta F/F_0$ response in all six areas.

The averaged line-scan (Xt) image collected from this neuron during repeated APs (Fig.18A, bottom), shows that the fast spread of calcium through the non-nuclear ER-rich periphery (top) suddenly comes to a halt at about 6 μm from the PM. This may be due to strong mitochondrial calcium uptake in the

mitochondrial rich zone just inside the peripheral ER rich layer (McDonough et al, 2000; Akita and Kuba, 2000; Fig.14E). In Fig.18B we re-plot data from panel A on an expanded time scale, in order to compare the fluorescence time course in the outermost ER-rich zones in the neuron (red, blue and green). The red and blue records characterize the calcium transient in the non-nuclear periphery (Fig.18A, top), whereas the green record shows similar data from the peripheral perinuclear area (bottom). Comparison of the three records indicates that the activation kinetics of the calcium transients in these three, ER-rich areas were very similar. The initiation time and the rate-of-rise were nearly identical, and the three curves reached their peak essentially simultaneously, as indicated by the arrow in Fig.18B. In order to be able to compare the activation kinetics more directly, we normalized the original $\Delta F/F_0$ values to the peak value measured at the downward arrow in Fig.18B. The normalized curves (Fig.18C) show that any possible difference between the activation rates of these three lines was not resolvable in the present recording.

The full time course of the calcium transients in all six AOIs is shown in Fig.18D and E on a compressed time scale. The successively less peripheral AOIs in the non-nuclear ER-rich periphery (red, blue, cyan; Fig.18D) behaved kinetically similarly, although the amplitudes became gradually lower as areas farther inside the cell were examined. The fluorescence time course in the AOIs within the nucleus (olive and pink in Fig.18E) was very different from that in the peripheral perinuclear ER-rich area (green, in Fig.18E). The peripheral

perinuclear ER-rich zone exhibited a marked initial peak, whereas the fluorescence in the intranuclear regions only gradually increased to the same fluorescence level. These differences are probably due to the lack of ER Ca^{2+} stores and of active Ca^{2+} transporters within the nucleus. The overall conclusion from these line scan data is that fluo-4 fluorescence in the peripheral ER rich zone rises from a resting level to a peak value in less than about 5 ms in response to a single action potential. The radial propagation of elevated Ca^{2+} appears to be extremely rapid within the peripheral ER-rich region, since we see no detectable difference of the time-to-peak within a 4-6 μm thick shell at the cell periphery (Fig.18C).

4.1.9. Addition of cytosolic EGTA reveals "latent" hot spots in cultured SGNs having uniform peripheral responses.

The hot spots for initiation of AP-induced Ca^{2+} transients (Figs.11, 8 and 15) may correspond to regions in the sub-plasma membrane ER with the strongest CICR. In this case, the uniformly responding cells might simply have sufficiently developed CICR mechanism throughout the entire sub-PM ER to locally initiate CICR over the entire cell periphery in response to an AP (Fig.16). However, these cells might still have areas where CICR is stronger than elsewhere, but our experiment would not have revealed them under control conditions. If such "latent" hot spots were indeed present in the uniformly

responding cells, they might be revealed by the addition of an intracellular Ca^{2+} buffer that could silence the less powerful sites, but not totally suppress the more powerful sites of Ca^{2+} release. In 7 cultured cells with uniform peripheral responses, we used a relatively slow Ca^{2+} buffer (EGTA) in an attempt to reveal possible "latent" hot spots.

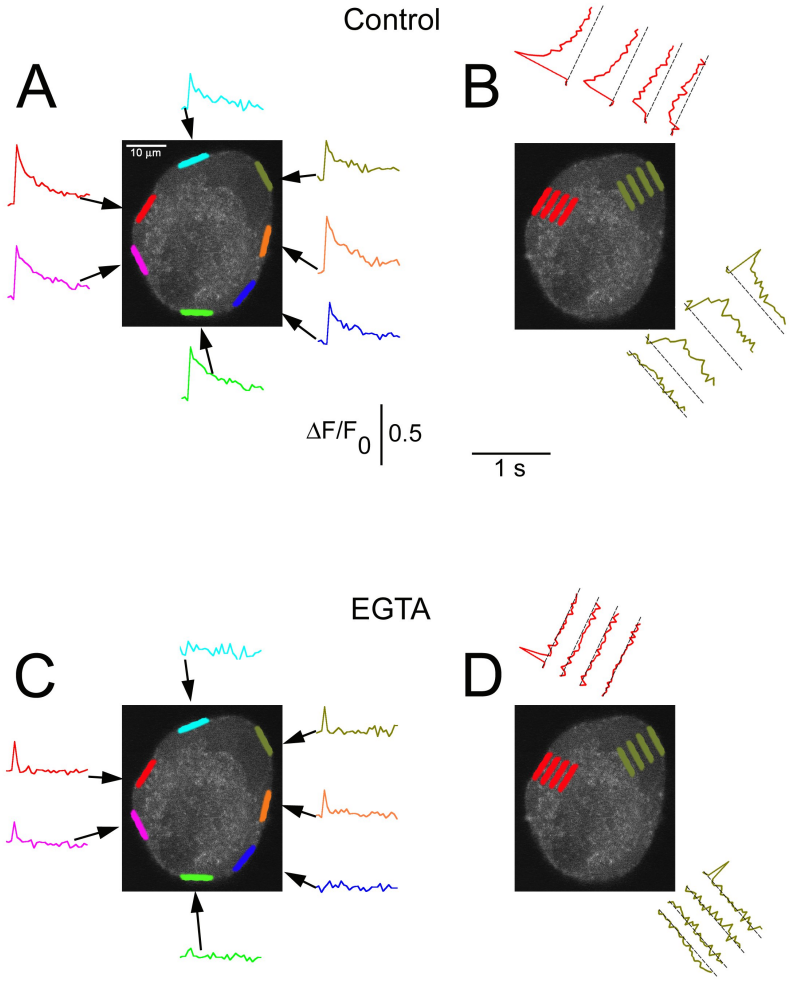

Figure 19. EGTA reveals "latent" hot spots in neurons with uniform peripheral Ca^{2+} transients. A)-B): AP-induced calcium response of a cultured neuron shows spatial uniformity.

C)-D): The slow but robust Ca^{2+} buffer EGTA was added to the bath and the electric stimulus was repeated on the same neuron. The effect of EGTA is to reveal the latent "hot spot" even in this uniform responding cell.

In Fig.19, calcium transients were induced by 0.5 ms field stimuli in a cultured frog SGN and the video sequences for responses to 4 stimuli were averaged. Panel A shows the time course of $\Delta F/F_0$ in the 7 indicated color coded peripheral AOIs. The olive green AOI was drawn in the peripheral perinuclear zone. The calcium transients were uniform in all peripheral AOIs. In panel B the radial spread of the fluorescence signals was characterized inside the nucleus (olive green) and at the site of the largest non-nuclear peripheral response (red). In both regions, the fluorescence signal spread with a slower rise time and decrement in amplitude, but remained detectable throughout. In panels C and D, the same cell was loaded with EGTA AM (20 μM;15 min) in the absence of extracellular Ca^{2+}. The AP protocol was then repeated 15 times in the presence of 2 mM extracellular Ca^{2+} and the calcium transients were recorded from the same AOIs as in A and B.

As Fig.19A shows, control $\Delta F/F_0$ records from the corresponding color coded peripheral AOIs in a neuron exhibited uniform peripheral Ca^{2+} transients in response to a single AP under control conditions. Subsequent loading of the same cell with EGTA AM, the cell's response to APs became non-uniform in the same AOIs around the cell periphery (Fig.19C). A peripheral AOI area within the perinuclear zone (olive green, near 1 o'clock) and several areas in the non-nuclear periphery

now acted as primary sites for Ca^{2+} release, with other peripheral AOIs giving no change in fluorescence. The very fast decay of $\Delta F/F_0$ ($t_{1/2} \leq 30$ ms) in all responsive areas of the EGTA-loaded cells is consistent with Ca^{2+} binding to EGTA, which lowers the free Ca^{2+} much more rapidly after cessation of Ca^{2+} release than in the absence of added Ca^{2+} buffer. Furthermore, the radial spread seen in the AOIs in Fig.19B under control conditions was completely eliminated after loading the cell with EGTA (Fig.19D), even though the peripheral AOI at each of the locations examined in Fig.19D still exhibited a definite, but very brief, fluorescence signal in response to the action potential. This is also consistent with EGTA binding of released Ca^{2+}, thereby restricting the diffusional spread of Ca^{2+} away from the release site

In 2 other cells, application of 10 or 20 μM of the faster Ca^{2+} buffer BAPTA (AM) for 15 min totally eliminated the calcium transient in response to single APs (data not shown). Thus, BAPTA was able to sufficiently limit any local rise in Ca^{2+} so that no detectable CICR response occurred.

4.1.10. Lowered extracellular Ca^{2+} also reveals latent hot spots in cultured SGNs having uniform peripheral responses.

Another way to decrease CICR, and thus possibly reveal latent hot spots in uniformly responding cultured SGNs, was to expose these cells to lowered extracellular Ca^{2+} concentration. This was achieved via a local perfusion system that completely replaced

the extracellular solution around a SGN within two seconds (Cseresnyés et al., 1997; McDonough et al., 2000). In these experiments, a cell was first tested with a single AP in the presence of normal (2 mM) extracellular Ca^{2+} and the resulting Ca^{2+} response was recorded. The cell was then exposed to 0.1 mM extracellular Ca^{2+} Ringer's solution for 6 to 24 seconds, after which a single AP was again applied. The cell was then returned to 2mM extracellular Ca^{2+} Ringer's and an AP-induced Ca^{2+} response was again recorded. The protocol of stimulation in 2mM Ca^{2+} followed by stimulation after 6-24s in low Ca^{2+} Ringer's was repeated 3-4 times. The video sequences for either 2 or 0.1 mM Ca^{2+} were averaged separately. The duration of the low-Ca^{2+} flush was selected by trial and error so that the resulting Ca^{2+} release pattern became inhomogeneous, but was not totally eliminated. In the majority of the cells, 6 seconds was sufficient. The location of the active areas was not sensitive to moderate prolongations of the low-Ca^{2+} flush. However, when the low-Ca^{2+} flush was further prolonged, the Ca^{2+} response to an action potential was totally eliminated, sometimes irreversibly.

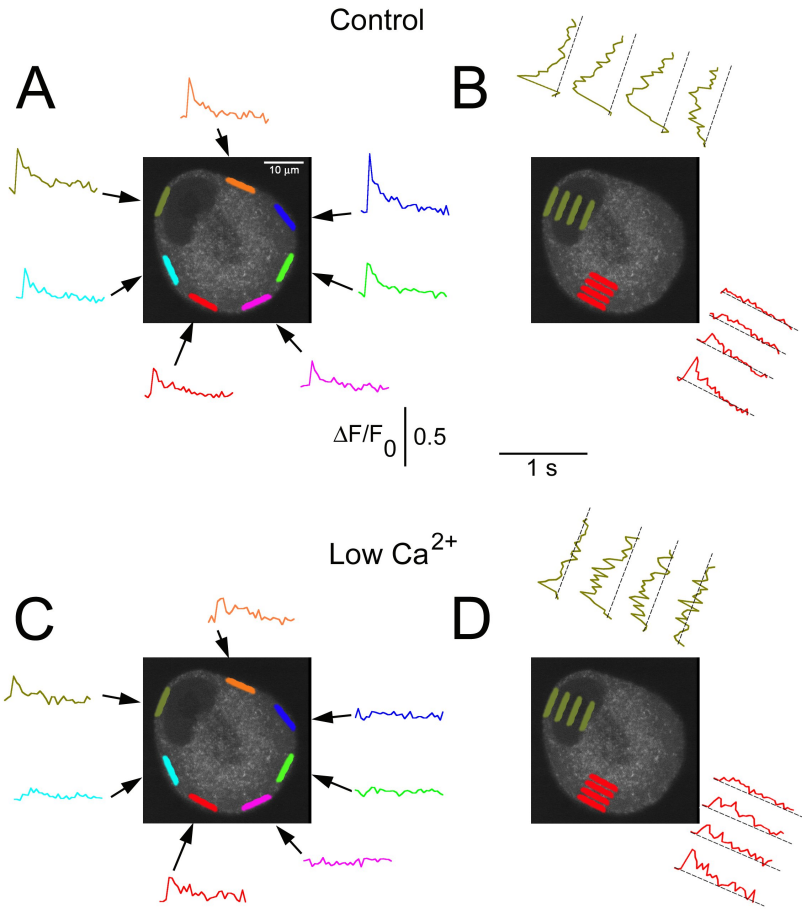

Figure 20. Lowered extracellular Ca^{2+} reveals peripheral hot spots of Ca^{2+} release in cells with uniform Ca^{2+} response. A)-B): AP-induced calcium response of a cultured neuron shows spatial uniformity. C)-D): 0.1 mM Ca^{2+} solution was added to the bath and the electric stimulus was repeated on the same neuron. The effect of low extracellular calcium is to reveal the latent "hot spot" even in this uniform responding cell.

Fig.20A shows the average Ca^{2+} transient of a cultured SGN that responded with a uniform peripheral Ca^{2+} signal to a single AP in the presence of normal (2 mM) extracellular Ca^{2+}. Local spatially averaged fluorescence was calculated in the

small, color-coded peripheral AOIs and plotted in corresponding colors. Fig.20B shows the spread of the Ca^{2+} signal into the cell under control conditions. The Ca^{2+} responses in the peripheral AOIs were nearly identical in this cell in the presence of 2 mM Ca^{2+}. When the cell was exposed to 0.1 mM extracellular Ca^{2+} for 6 seconds between the control (2mM Ca^{2+}) recordings, the single AP-induced Ca^{2+} response became non-uniform (Fig.20C). A peripheral AOI in the perinuclear area (olive green), as well as the extranuclear peripheral AOI located at about 90 degrees relative to the perinuclear zone (red) remained responsive, whereas most of the rest of the peripheral zone became quiescent. The lack of response in many peripheral regions indicates that the reduced Ca^{2+} influx due to lowered extracellular Ca^{2+} was insufficient to initiate CICR in the non-responding regions. It is unlikely that a locally higher extracellular Ca^{2+} concentration could have maintained the responsiveness of the remaining sites, because the perfusion time with lowered extracellular Ca^{2+} solution was 3 times longer than the exchange time of our local perfusion system. It seems more likely that locally higher Ca^{2+} influx, resulting from local clustering of plasma membrane Ca^{2+} channels, or locally concentrated Ca^{2+} release sites of the ER may underlie the locally responsive sites observed after brief perfusion with reduced Ca^{2+} solution. Alternatively, stronger structural or functional coupling between the PM Ca^{2+} channels (Ca^{2+} influx) and the RyRs of the ER (Ca^{2+} release) may also result in sufficient CICR to generate a detectable signal in the responding zones despite a decreased Ca^{2+} influx in low Ca^{2+}

solution. These various possibilities could also explain the local sites induced by EGTA loading of cells previously exhibiting uniform peripheral responses. Interestingly, the propagation into the cell from the remaining hot spots in low Ca^{2+} solution was not drastically suppressed (Fig.20D), even though Ca^{2+} must be much reduced, indicating that intracellular Ca^{2+} release makes a major contribution to the initiation and spread of Ca^{2+} signals at the hot spots.

4.1.11. Single Ca^{2+} transients do not significantly alter ER free Ca^{2+}.

In order to examine the possible effect of brief Ca2+ transients, induced by APs, on the Ca2+ content of the ERA, a double-pulse protocol was applied to SGNs and the resulting Ca^{2+} transient was recorded in line-scan confocal mode.

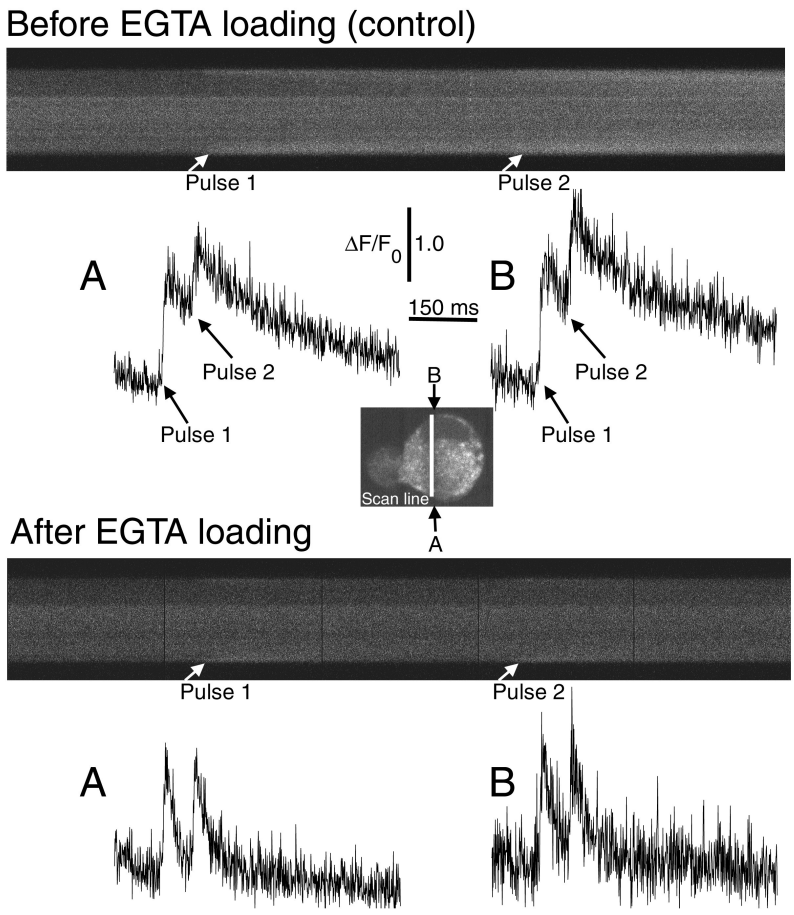

Figure 21. Lack of effect of single Ca^{2+} transients on the Ca^{2+} content of the ER. Line scan confocal recordings of fluorescence transients induced by two consecutive electric stimuli separated by 66 ms in a cultured SGN. A): recordings in control conditions. B): The experiment was repeated after exposing the cell to EGTA AM, which loaded the cytoplasm with the slow Ca^{2+} buffer, thus accelerating the decay phase of the calcium transients.

In Fig.21, the two stimuli were separated by only 66 ms, in order to study the effect of a Ca^{2+} transient on the ER free Ca^{2+} content under conditions where the ER probably has no time to

re-load before the second stimuli arrives (Δt=66 ms). The scan-line was drawn through the nucleus (top of the cell in insert) and two areas were sampled: (**A)** in the non-nuclear periphery and (**B)** in the perinuclear zone. Under control conditions **(top)**, the two Ca^{2+} responses were not directly comparable due to significant overlap. Thus, we loaded the cell with EGTA AM, after which the two Ca^{2+} responses became well separated and thus we were able to directly compare the amplitudes **(bottom)**. Pulse 2 was essentially identical to pulse 1, thus indicating that a single Ca^{2+} transient does not significantly alter CICR and ER free Ca^{2+}.

4.2. Modeling of the spatio-temporal properties of Ca^{2+} signals initiated by action potentials

4.2.1. Model calculations of Ca^{2+} fluxes.

The equations for Ca^{2+} fluxes within each of the 6 domains in the model were modified from our earlier whole-cell 3 compartment model (Cseresnyés et al., 1997, 1999), which was originally based on an earlier model (Friel 1995). Within each domain, the time-course of the cytosolic [Ca^{2+}] (c), the ER [Ca^{2+}] (c_s), the mitochondrial [Ca^{2+}] (c_M) and the "RACT" transport-rate constant for Ca^{2+} uptake by release activated Ca^{2+} transport (k_{RACT}; see Cseresnyés et al., 1997), with RACT and CICR in the ER membrane, were calculated by numerically solving a set of simultaneous differential equations, applying the Euler method (Scarborough, 1966). The equations for c_s and c_M were:

$$dc_s/dt=k_{SERCA}\, c+k_{RACT}\, c-k_{RyR}(c_s-c) \qquad (1)$$

$$dc_M/dt=k_{M,u}(c^2/(K_u+c))-k_{M,x}(c_M/(K_x+c_M)) \qquad (2)$$

where k_{SERCA} and k_{RACT} are the SERCA and RACT rate constants, k_{RyR} is the rate coefficient for Ca^{2+} efflux via the RyRs (see eqn (6)), $k_{M,u}$ and K_u represent the uptake rate constant and the Ca^{2+} sensitivity of the mitochondrial Ca^{2+} uniport, and $k_{M,x}$ and K_x are the corresponding values for the mitochondrial Na^+/Ca^{2+} exchanger. Eqn (2) is an approximation of eqn (21) of

Magnus and Keizer (Magnus and Kaizer, 1997). The cytosolic $[Ca^{2+}]$ is described by:

$$dc/dt=\delta k_{PM}(c_0-c)-\delta k_{PMCA}c+\alpha k_{RyR}(c_s-c)\alpha 3-\alpha k_{SERCA}c\alpha 2-\alpha k_{RACT}c\alpha 2-\omega k_{M,u}(c^2/(K_u+c))+\omega k_{M,x}(c_M/(K_x+c_M)) \quad (3)$$

where k_{PM} and k_{PMCA} are flux constants for influx via plasma membrane Ca^{2+} channels or efflux via the plasma membrane Ca^{2+} pump, respectively, and are non-zero only in domains 1 and 2; c_0 is the extracellular $[Ca^{2+}]$, and α and ω are the ratios of the respective domain volumes occupied by the ER and the mitochondria lumen relative to the entire volume of the cytosol in that domain. An additional linear instantaneous cytosolic Ca^{2+} buffer is also included.

The RACT rate coefficient (k_{RACT}) is controlled by both local and global cytosolic $[Ca^{2+}]$:

$$dk_{RACT}/dt=k_{ON,R}(k_{RACT,max}-k_{RACT})c_{lR}-k_{OFF,R}k_{RACT} \quad (4)$$

where $k_{ON,R}$ and $k_{OFF,R}$ are the ON and OFF rate constants of the RACT regulatory sites, and $k_{RACT,max}$ is the maximum value for the flux coefficient of RACT. In eqn (4), the local concentration of $[Ca^{2+}]$ (c_{lR}) around the RACT regulatory sites is given by:

$$c_{lR}=c+\beta(c_s-c)k_{RyR} \quad (5)$$

where β is the transformation constant between the ER Ca^{2+} flux and the local increment of extraluminal [Ca^{2+}], and k_{RyR} is an instantaneous function of cytosolic [Ca^{2+}]:

$$k_{RyR}=k_{RyR,0}+k_{RyR,1}/(1+(K_D/c)^n) \quad (6)$$

where $k_{RyR,0}$ and $(k_{RyR,0}+k_{RyR,1})$ are the flux coefficients for the RyR at zero and full activation of CICR, and K_D and n are the Ca^{2+} dissociation constant and the Hill coefficient of the RyR regulatory sites for CICR. Within all domains the concentration of ER and mitochondria are constant, but these concentrations can vary between domains.

4.2.2. Ca^{2+} fluxes between domains and model calculation of Ca^{2+} time course.

Equations (1) – (6) are used simultaneously to calculate the changes Δc, Δc_s and Δc_m in each domain for a small time increment Δt, as $\Delta c = (\Delta t)\, dc/dt$. Δt was 1 ms. Calculated values of c, c_m, and c_s were stored every 10ms.

To simulate Ca^{2+} diffusion, an additional inter-domain flux to c is added in each domain, corresponding to the Ca^{2+} flux into each domain from its neighboring domains:

$$\Delta_C(i) = \Sigma\, Vf(i)*F_{ji}(c(i)-c(j)) \; ; \; j = 1 \text{ to } 6,\; i \neq j \quad (7)$$

The flux coefficients were set up manually in an Excel spreadsheet, taking the real morphology of the typical SCG

neuron into account (Table 1). E.g., the inter domain flux coefficients for D 1 (F_{12} through F_{16}) were zeros for all domains except D 3, whereas the flux coefficients for D 3 (F_{31} through F_{36}, $F_{33} = 0$) were non-zero for D 1 and D 5. The time courses of c_s, c, k_{RACT} and c_M were then calculated for each domain by incrementing c, c_s, k_{RACT} and c_m by Δc, Δc_s, Δk_{RACT} and Δc_m, calculated with the Euler method. The starting values of the parameters were as in our previous papers (Cseresnyés et al., 1997, 1999) and were then adjusted for rat SCG neurons to produce simulated curves similar to the experimental data. Ca^{2+} influx during an action potential was simulated by a time course similar to that observed in action-potential command V clamp measurements, or by a single point elevation of k_{PM}.

4.2.3. Scale conversion of simulated data from $[Ca^{2+}]$ to $\Delta F/F_0$

In order to be able to compare the experimental and simulated data directly, we needed to convert the simulated results onto a $\Delta F/F_0$ scale. This was necessary because the simulations were done in $[Ca^{2+}]$ and we didn't attempt to convert the experimentally determined non-ratiometric fluo-4 fluorescence values into $[Ca^{2+}]$. Instead, we used an iterative method that provided $\Delta F/F_0$ values calculated from simulated $[Ca^{2+}]$ independently of the steady state fluorescence. Assuming that the dye-Ca^{2+} binding is described by a first-order linear binding equation, it is possible to use the following iterative formula to

calculate the fluorescence values F_i at time point "i", assuming an arbitrary value for F_0:

$$F_{i+1} = F_i + k_{ON} F_0 [Ca^{2+}]_{i+1} - k_{OFF} F_i \quad (8)$$

where $k_{ON} = 1.3\ \mu M^{-1}$ and $k_{OFF} = 0.75$ for all simulations.

The iteration formula in eqn.(8) converges very quickly in the beginning (after approximately 5-10 iterations), and can then be used to calculate $\Delta F/F_0$ in an F_0-independent manner. The formula could be used either in parallel with the model calculations of $[Ca^{2+}]$, or could be done afterwards by any programmable spreadsheet program. Here we used a custom written macro in Sigmaplot 8.0 (SPSS, Inc. Chicago, IL, USA) to convert simulated $[Ca^{2+}]$ values that were calculated before we implemented the $[Ca^{2+}]$ to $\Delta F/F_0$ conversion.

4.2.4. Main characteristics of simulated Ca^{2+} transients

The plasma membrane (PM) Ca^{2+} influx was calculated by multiplying the Ca^{2+} gradient between the extracellular and intracellular space by an influx coefficient, which was part of the input parameter set. When simulating the effect of increased PM Ca^{2+} influx, e.g. during a simulated AP, value of this coefficient in the resting cell was multiplied by 500-3000.

The base value and the multiplier of the PM influx coefficient in resting cells was set such that model matched the experimentally determined steady state (StSt) value of $[Ca^{2+}]$ in an SCG neuron, as well as the peak value of a single AP-induced $[Ca^{2+}]$ transient. Based on ratiometric studies, steady state $[Ca^{2+}]$ is expected to be in the range of 60 to 100 nM in a cultured SGN of the rat (Thayer et al., 1988; Trouslard et al., 1993; Wanaverbecq et al., 2003). In our model, the simulated StSt value of free Ca^{2+} was uniform throughout the six domains, and its value was solely determined by the ratio of the PM Ca^{2+} influx and efflux rates (V-gated Ca^{2+} channels and PMCA, respectively).

The rising phase of the simulated Ca^{2+} signal in domains 1 and 2 was very steep when using a one-point step function for the simulated stimulus. A more gradual rise of simulated Ca^{2+} was easily achieved by applying a triangular waveform as input for the simulated influx. The triangular waveform also provided a more realistic representation of the actual AP time course (see Fig.24A). However, for all practical purposes the single-point simulated stimulation was a satisfactory estimation, because even with the high temporal resolution of the Zeiss LSM 5 LIVE system, we usually were unable to resolve the time course of the rising phase of the $\Delta F/F_0$ transients in the peripheral domains (D 1 and D 2).

The spread of the simulated signal from peripheral domains D 1 and D 2 to the neighboring domains (D 3 and D 4, respectively) via instantaneous diffusion was determined by a set

of flux coefficients (F_{ij}, i, j = 1 to 6, i≠j). These coefficients could theoretically connect any pair of domains, their values thus forming a diagonally symmetrical matrix with zeros at the main diagonal. The actual values of these coefficients were set based on the morphology of the typical SCG neuron, revealed by antibody staining (see Fig.23; Fig.22, neuron with peripherally located nucleus; Fig.30, neuron with centrally located nucleus). In rat SCG neurons, the amplitude of the $\Delta F/F_0$ signal observed along the D1 → D3 → D5 pathway decreased only slightly. In order to simulate this behavior, we had to set the flux coefficients relatively high for the D1 → D3 → D5 pathway, and we also had to assume that the ER and mitochondria don't absorb much Ca^{2+}. This was achieved by lowering the K_D of the RyRs/IP3Rs throughout the four domains that are rich in these receptors (D 1, D 2, D 3, D 6), as well as increasing the Ca^{2+} sensitive rate coefficient ($K_{RyR,1}$) of the receptors. The distribution of the RyRs and IP3Rs was assumed to be non-uniform between the domains, based on antibody staining (see Fig.23A).

The rate of decay for domains 1 and 2 was mainly affected by the rate of Ca^{2+} removal by PMCA (see Fig.25). Because this parameter also affected steady state $[Ca^{2+}]$, any alteration had to be compensated for by adjusting the resting level of Ca^{2+} influx across the PM. The stimulus strength also had to be adjusted accordingly, in order to keep the simulated signal amplitude close to the observed values. The decay rate of $[Ca^{2+}]$ in more centrally located domains was somewhat affected

by SERCA and RACT, as well as by the flux coefficients in and out of that domain.

4.2.5. The effect of CICR-related model parameters on simulated Ca^{2+} transients

In order to be able to fine-tune the CICR-related behavior of the model system, we introduced two separate parameters to describe the relative density of the RyRs (α_3) and of the Ca^{2+} pumps (α_2) in the ER membrane. Relatively low values of α_3 had to be set in D 1 and D 2 when simulating rat SCG data where the radial spread of the Ca^{2+} signal showed very little decrement. In the more centrally located cytosolic domains (D 3 and D 5), α_3 was set 2-2.5 times higher than in the two peripheral domains (D 1 and D 2), resulting in a smaller net Ca^{2+} uptake by the ER in the more centrally located domains, thus compensating for the dilution of Ca^{2+} that occur naturally during the radial spread of Ca^{2+}. This compensation effect was further enhanced by the lower overall density of ER in the more centrally located domains, in accordance with the results of our antibody staining (Fig.23A).

The Ca^{2+} sensitive rate of Ca^{2+} release of RyRs (K_{RyR1}) was described by the following equations:

Ca^{2+} release from ER via RyRs = $\alpha * \alpha_3 *$ Kryr * (CaS - CaI), (9)

where $\alpha = V_{ER\ lumen}/V_{cytosol}$, the ER volume-ratio; α_3=relative density of RyRs;

$$K_{ryr} = K_{ryr0} + K_{ryr1}/(1 + K_D/CaI)^n, \quad (10)$$

where K_{ryr0} and K_{ryr1} are the Ca^{2+} independent and Ca^{2+} sensitive RyR leak coefficients, respectively

Based on our result, in rat SCG neurons the ER Ca^{2+} store behaves as a Ca^{2+} sink, rather than a Ca^{2+} source, during single and multiple AP stimuli.

4.2.6. Local Ca^{2+} transients induced by single APs in a phasic neuron with peripherally located nucleus.

As we have recently shown, cells that were cultured for 24-48 hours were likely to produce a single AP and corresponding single Ca^{2+} transient when stimulated with a single depolarizing pulse via either field stimulation or direct current injection from a patch-clamp electrode (Hernandez-Ochoa et al., 2006).

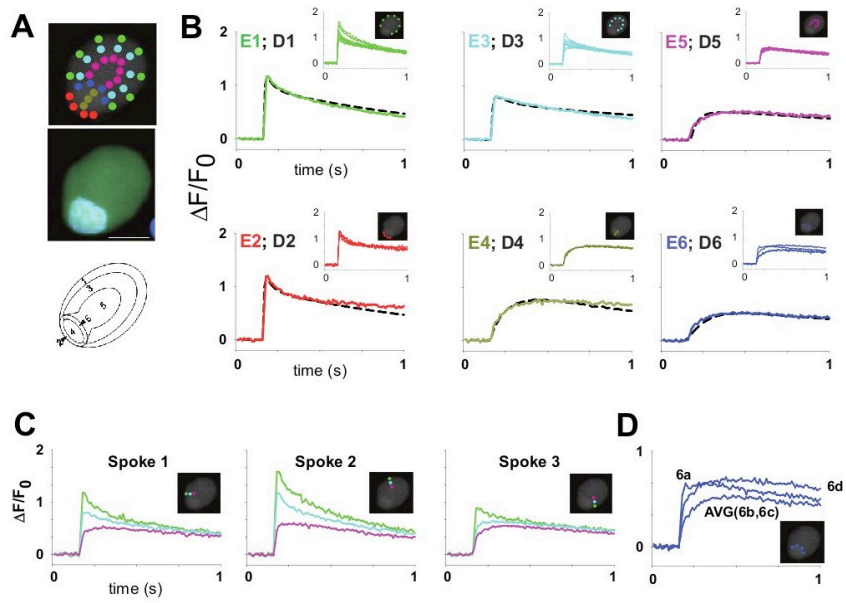

Figure 22. Spatial distribution of local Ca^{2+} transients in a cultured SCG neuron. Measured and simulated calcium-sensitive fluorescence transients are plotted at the locations shown in A), top panel, colored dots. Functionally separated cell compartments are shown in the cartoon, bottom panel of A). B): measured average time courses are shown as color lines, labeled with Ex, where "x" indicates the region where the signal comes from (see cartoon in A). The corresponding simulated curves are plotted as black dashed lines. Individual measured time courses are shown in the insets, using the same color as the averaged time course. C): Measured time courses of the calcium signal along the cell radius. D): $\Delta F/F_0$ transients from the 4 sub-domains of E6 on an expanded scale.

Fig.22 presents the subcellular spatio-temporal evolution of a single Ca^{2+} transient initiated by a single field stimulus in a 24-h cultured SCG neuron. This cytosolic Ca^{2+} transient is characterized in Fig.22 by the $\Delta F/F_0$ time courses calculated at 35 small locations throughout the cell, as represented by the small colored circles (5-10 μm^2) in Fig.22A, top. The precise location

of the nucleus was determined by DAPI staining, shown in light blue in Fig.22A, middle panel. Morphologically, a typical SCG neuron with peripherally located nucleus can be sub-divided into 6 domains, as shown by the cartoon in the bottom panel of Fig.22A (see also Methods). Comparing the cartoon with the results of antibody staining (Fig.23A) indicates that domain 1 corresponds to the IP3R rich non-nuclear peripheral zone; domain 2 is the peripheral perinuclear area; domain 3 is rich in RyRs; domain 4 is the nucleus; domain 5 is the mitochondria-rich central region, and domain 6 is the central perinuclear zone.

The 8 small green circles in Fig.22A top were selected from domain 1 and the $\Delta F/F_0$ transients were plotted individually in the insert of panel E1 of Fig.22B. The locations of the green circles can also be observed in the image at the top right corner of the E1 insert. Note that "En" is used to denote a record experimentally recorded from domain n, and is used in distinction to record "Dn", which denotes a simulated record calculated for domain n using our numerical simulation program (see below). The 8 individual $\Delta F/F_0$ time courses recorded from different locations in the sub-PM non-nuclear area (green-colored lines in the E1 insert), all exhibited a rapid rise, followed by a relatively rapid and then a slower decline in the signal. The mean $\Delta F/F_0$ response obtained by averaging the responses recorded from the 8 individual sub-areas of the domain 1 are shown in Fig.22B, panel E1 (green line). Similar characterization of average $\Delta F/F_0$ responses for domains 2 through 6 are shown in

panels E2 through E6, plotted as colored lines for the experimental data.

	Domain 1	**Domain 2**	**Domain 3**	**Domain 4**	**Domain 5**	**Domain 6**
Domain 1	0	0	10	0	0	0
Domain 2	0	0	0	0.05	0	0
Domain 3	10	0	0	0	4	0
Domain 4	0	2	0	0	0	0.5
Domain 5	0	0	4	0	0	1
Domain 6	0	0	0	0.2	1	0

Table 2. Model parameters for simulations in Figure 22: Inter-domain Ca^{2+} flux coefficients (F_{ij}, i,j = 1 to 6, F_{ii}=0).

	α	**ω**	**δ**	**Vf**	**α2**	**α3**
Domain 1	0.6	0.2	74	0.21	2	10
Domain 2	0.6	0.2	24	0.07	2	10
Domain 3	0.6	0.01	0.005	0.21	2	20
Domain 4	0	0	0.005	0.2	0.001	0.001
Domain 5	0.4	0.5	0.005	0.22	8	24
Domain 6	0.6	0.1	0.005	0.09	6	24

Table 3. Model parameters for simulations in Figure 22: Intra-domain density of organelles and Ca^{2+} transport mechanisms.

$k_{SERCA}(s^{-1})$	$k_{RACT,max}(s^{-1})$	$k_{OFF,R}$ (s^{-1})	$k_{ON,R}$ $(\mu M^{-1}s^{-1})$	$k_{RyR,0}$ (s^{-1})	$k_{RyR,1}$ (s^{-1})	K_D (μM)	n	β (s)
0.1	0.02	20	1.5	0.02	0.2	2	2	6

$k_{M,u}$ (s^{-1})	K_u (μM)	$k_{M,x}$ (s^{-1})	K_x (μM)	k_{PM} (s^{-1})	k_{PMCA} (s^{-1})
0.06	0.2	0.01	0.2	$5.00*10^{-8}$	0.32

Table 4. Model parameters for simulations in Figure 22: Numerical values of model parameters for Ca^{2+} transport mechanisms in all domains.

Even though the local Ca^{2+} signals selected from the peripherally located domains showed fairly uniform kinetics, the peak amplitude of $\Delta F/F_0$ in domain 1 varied between 0.8 and 1.6. As expected, the sub-areas with the highest amplitude in domains 1 and 3 were nearest neighbors (i.e., located along the same radial "spoke"), thus confirming the idea of diffusional coupling between radially arranged domains and sub-domains. In order to further characterize the radial spread of the Ca^{2+} signal, we plotted the experimental $\Delta F/F_0$ time courses at three radially arranged sub-areas of domains 1, 3 and 5 at three different circumferential locations (Fig.22C, Spokes 1, 2 and 3, colored lines). Spoke 2 corresponded to the location with the largest local Ca^{2+} transient, whereas the Ca^{2+} signal at Spoke 1 was kinetically very similar to that of Spoke 2, but smaller. The third circumferential location (Spoke 3) was characterized by smaller Ca^{2+} diffusion between domains 1 and 3, as indicated by the lack of the initial spike in the E3 signal, given rise to variable responses in E3 (inset in Fig.22B).

Records from the 4 sub-areas of domain 6 (Fig.22B, blue circles and records in E6) showed appreciable non-uniformity. Fig.22D shows the individual records from the two most peripheral sub-areas (6a and 6d; blue lines), as well as the average from the two sub-areas in the middle (AVG(6b,6c); blue line), 6b and 6c being very similar. The sub-area at the left (6a) showed the fastest kinetic properties, due probably to its proximity to the fast-responding domain 3. Note that the

observed Ca^{2+} transient for domain 6 in Fig.22B is the average of the middle two sub-domains only.

4.2.7. Simulation of spatio-temporal distribution of elevated Ca^{2+} in response to a single action potential.

In order to simulate the $\Delta F/F_0$ confocal fluorescence signals from E1 we had to account for the extremely fast raising phase, and the subsequent mono- or biphasic decay of Ca^{2+}. The increase in fluorescence from the pre-stimulus baseline to the post-stimulus maximum $\Delta F/F_0$ value usually occurred in a time period shorter than the time from one image frame to the next (<10 ms) even when using the fastest XY recording rate during our experiments (108 f/s). Our simulation was able to reproduce the fast elevation by assuming that 1) the two peripheral domains (D1 and D2) were directly connected to the PM Ca^{2+} influx (parameter 'δ' in eqn.(3) and table 3), and 2) the time course of the simulated influx was described by a step-function. The more centrally located domains, being spatially separated from the PM, did not directly receive any PM influx, and thus their rate of rise of simulated $\Delta F/F_0$ was determined by the Ca^{2+} flux from their more peripherally located neighbors, as well as by their simulated Ca^{2+} sinks and sources (ER and mitochondrial Ca^{2+} uptake and release pathways). In several cells, the E3 signal was very similar to E1, including a very sharp rise at the beginning. The simulation of this type of response required that we set the D 1 to D 3 flux coefficient (F_{13}) relatively high in our model parameter array (see Table 3).

In Fig.22 we show the spatial distribution of local Ca^{2+} transients in a cultured SCG neuron. A single Ca^{2+} transient was initiated by 2-ms long field stimulus and was monitored by using fluo-4 fluorescence recorded at 108 f/s. The $\Delta F/F_0$ time courses were calculated in small circular areas selected at 35 various positions within the neuron as indicated by the color circles in **(A)**, top. The green circles were selected at the periphery of the non-nuclear sub-PM area of the cell, and were chosen to characterize the IP3R-rich zone (see Fig.23Ab) corresponding to domain 1 of the cartoon in (A), bottom. Similarly, the cyan colored circles characterize the behavior of the RyR-rich zone (see. Fig.23Aa), corresponding to domain 3 in the cartoon (A, bottom), whereas the pink circles are in the mitochondria-dominated zone (see Fig.23Ac), labeled as domain 5 in the cartoon. The three domains selected at or near the cell's nucleus (domains 2, 4 and 6 in the cartoon) were characterized by the red, dark yellow and blue circles. The precise location of the nucleus is indicated by DAPI staining in (A), middle panel. In Fig.22B we show the individual $\Delta F/F_0$ transients recorded from the 8 peripherally located green circles are plotted in the insert of the E1. The insert also shows the exact locations of the green circles, superimposed onto the cell's image (top right corner of E1 insert). The solid green line in the main panel (E1) was calculated by averaging these 8 individual transients, whereas the black dashed line shows the simulated result of the 6-domain model (D1). Identical arrangements are shown for the other five domains (E2 and D2 through E6 and D6), with 4 small circles

selected in E2, 8 in E3, 3 in E4, 8 in E5 and 4 in E6 (numerical values of the model parameters are provided in Appendix 3, Tables 2-4). In panel D we show the $\Delta F/F_0$ transients from the 4 sub-domains of E6 on an expanded scale. The most "spiky" curve (6a) corresponds to the first sub-domain on the left; the lowest running transient is the average of the two sub-domains in the middle ("AVG(6b,6c)"), whereas the "6d" curve is calculated from the blue circle on the right. The inserted image shows the locations of the 4 sub-domains, "6a" through "6d", arranged clockwise. Panel D shows the radial spread of the $\Delta F/F_0$ transient from E1 to E3 to E5 along 3 "spokes" formed by radially arranged sub-domains of E1, E3 and E5. The circumferential locations of the three spokes were selected approximately 90° and 180° apart, as indicated by the three small circles in the inserted images shown above the three sets of records. The three lines corresponding to the E1, E3 and E5 sub-domains were colored as in (B).

In order to produce the dashed black lines in Fig.22B, showing the simulated responses calculated for domains D1 to D6 by our 6-domain computer model superimposed on the corresponding averaged responses from experimental records E1 to E6, the model parameters were adjusted by eye until the simulated and experimental curves matched in all domains (see Tables 2-4 for all model parameter values used in Fig.22B). In these calculations, we reproduced the *average* responses from E1, E3 and E5, but using alternative parameters we could have also reproduced the spread of Ca^{2+} signals along the radial spokes

in Fig.22C. The simulated Ca^{2+} transients were initiated by elevation of the PM Ca^{2+} influx coefficient (k_{PM}, see Eqn.(3)) during a single simulation time point (10 ms). The initial values of k_{PM} and k_{PMCA} were set so that the steady state cytosolic Ca^{2+} of the model was around 100 nM, a widely accepted value in these neurons based on earlier observations (Thayer et al., 1988; Trouslard et al., 1993; Wanaverbecq et al., 2003). The value of k_{PMCA} was chosen to agree with our observations indicating that PMCA provided the main Ca^{2+} removal mechanism during periods of elevated cytosolic Ca^{2+} (see Fig.25 below). Because of this restriction, the simulated contribution of PMCA to cytosolic Ca^{2+} removal was much larger that those of Ca^{2+} uptake by the ER and mitochondria. This restriction agreed well with previous observations, confirmed by our data (see Fig.26 below), regarding the relatively small contribution of ER Ca^{2+} uptake via SERCA pumps, following modest Ca^{2+} elevations (e.g. brief depolarizations or a single AP) in these neurons (Wanaverbecq et al., 2003).

The step-like elevation of k_{PM} naturally resulted in the sharp rise of Ca^{2+} at the beginning of simulated transients in domains 1 and 2, in agreement with the experimental data. The relatively fast rise of simulated Ca^{2+} in domain 3 was reproduced by setting the F_{13} ($=F_{31}$) flux coefficient high. The relative amounts of ER in domains 1 through 3 were set to identical values, in accordance with the results of our antibody staining for ER markers (see Fig.23A). The slower rising phase of the domain 5 signal was simulated by setting the F_{35} ($=F_{53}$) coefficient 2.5

times smaller than F_{13}. The slow decay of the domain 5 signal was a consequence of the 1) low ER content; 2) low rate of mitochondrial Ca^{2+} uptake; and 3) slow Ca^{2+} flux between domains 5 and 6 (F_{56} = 0.25 * F_{35}). The fast rise of Ca^{2+} in domain 2 was due to the direct contribution from PM Ca^{2+} influx, similar to domain 1. Here, the relative density of PM influx and efflux in domain 2 was set to 1/3 of that in domain 1, corresponding to the approximate volume ratio of the two domains (see 'δ' and 'Vf' values in Table 3), estimated from antibody staining (see Fig.23A). This ratio reproduced the relative $\Delta F/F_0$ amplitudes of the observed domain 1 and 2 signals very well (Fig.22B, compare E1 and D1, as well as E2 and D2). The relatively slow rate of rise of the domain 4 and 6 signals was reproduced by setting F_{24} and F_{46} relatively low. Domain 4, the nucleus, was not assigned any ER or mitochondria. Thus, the only pathway of Ca^{2+} efflux from domain 4 was via Ca^{2+} diffusion into domains 2 and 6.

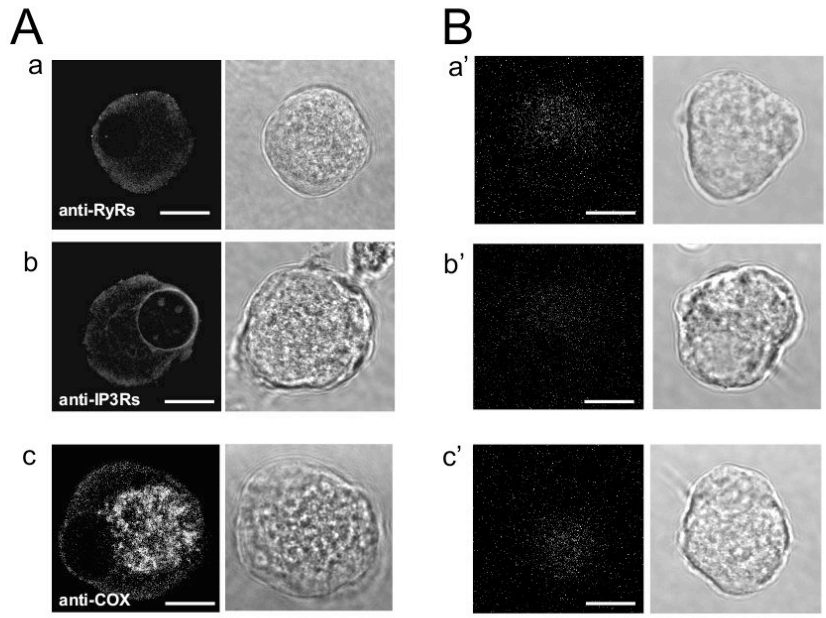

Figure 23. Distribution of Ca^{2+} release channels in cultured SCG neurons. Antibody staining of cultured SCG neurons for ryanodine receptors (Aa), IP3 receptors (Ab) and mitochondria (Ac). Corresponding controls (secondary antibody only) are shown in B).

In Fig.23 we show the distribution of Ca^{2+} release channels in cultured SCG neurons. Panel A contains confocal images of fluorescence patterns for RyRs (*a*), IP3R isoform type 1 (*b*), or cytochrome c oxidase (COX) complex IV subunit Vb (*c*). These cells were labeled with mouse RyR antibody that detects RyRs isoforms 1 and 2; mouse monoclonal COX antibody; and rabbit IP3Rs1 antibodies. Note that the RyRs staining was non-uniform, indicating receptor localization mainly in the sub-plasma membrane area, whereas the Mit-compIV (COX) staining was more evident at the center of the neuron. IP3Rs staining exhibited a regular pattern in the sub-plasma

membrane and perinuclear areas. In panel B we show transmitted light images and fluorescence patterns of cultured SCG neurons treated with the secondary antibody only (*a'* and *c'*) or with the IP3Rs inhibitory peptide (*b'*), and used as controls. The scale bars correspond to 10μm.

4.2.8. Action potentials and Ca^{2+} currents via VGCCs of the plasma membrane in cultured SCG neurons.

In Fig.24. we compare action potential-induced and caffeine-induced Ca^{2+} signals in rat SCG neurons. First, action potentials were recorded in fast current-clamp mode (inset). The bold trace shows the spike used in panel A as voltage command. The amplifier was then switched to whole-cell voltage-clamp mode. The ionic current was elicited by this voltage command (red trace) in the presence of 155 mM TEA^{+} to block potassium currents and TTX to block sodium currents.

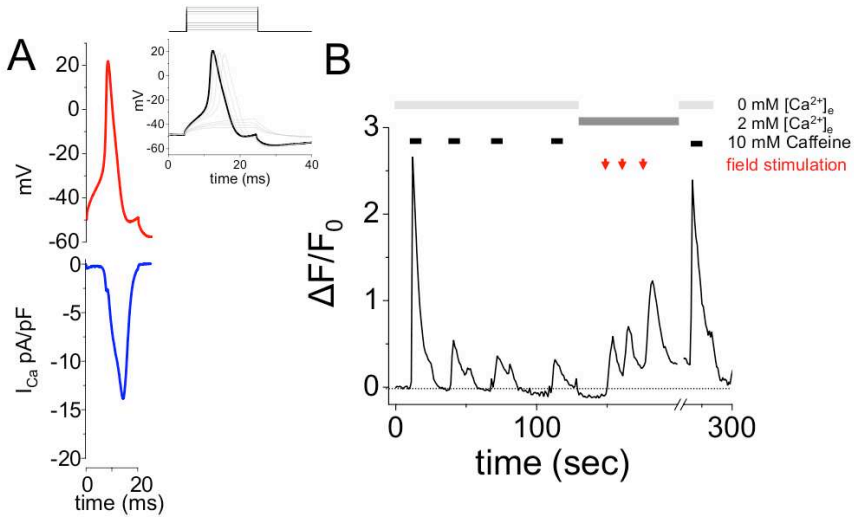

Figure 24. Action potential-induced and caffeine-induced Ca^{2+} signals in rat SCG neurons. A): membrane potential (top, red curve) and total membrane current (bottom, blue curve) time courses of a cultured SCG neuron. The voltage curve was recorded during an AP using current clamp, and was then used to induce the current curve in blue. B): caffeine induced calcium sensitive fluorescence transients in a similar neuron. 0, 2 and 10 mM caffeine was applied in the bath solution.

Incomplete compensated linear capacitive transients were subtracted using the remaining current recorded in a similar solution, except with Ca^{2+} replaced by Mg^{2+}. In panel A the calcium current (blue trace) was signal averaged based on the subtraction of currents recorded with and without Ca^{2+} (replaced by Mg^{2+}). In panel B the caffeine-induced Ca^{2+} transients and the effect of repetitive caffeine application are shown. Ca^{2+} transients were recorded from a fluo4-loaded sympathetic neuron in response to four consecutive applications (10 sec each; black

bars) of a solution containing 10 mM caffeine or in response to brief (2 ms) extracellular field stimuli (red vertical arrows). Horizontal gray-colored bars of two different shades are used to indicate resting [Ca^{2+}] (0 or 2 mM). Note that caffeine was applied under conditions where the extracellular Ca^{2+} was removed and that the repetitive caffeine application elicited Ca^{2+} transients of decreasing amplitude and only the first caffeine application showed a maximal effect. With these observations we are able to confirm that each AP was followed by Ca^{2+} entry via voltage-dependent Ca^{2+} channels. Namely, when the 2 day cultured SCG neuron in Fig.24 was stimulated with a depolarizing current pulse using the current clamp mode of the whole-cell clamp technique (i.e., by injecting suprathreshold current stimuli), the neuron responded with a membrane action potential spike as shown in Fig.24A (red trace). The AP waveforms that were recorded during increasingly larger depolarizing current pulses were characterized by a gradually faster rising phase and shorter time-to-peak (Fig.24A, gray traces). In order to measure the total PM Ca^{2+} current during an AP, we used an AP waveform previously recorded from the same cell as command potential (Fig.24A, black trace) whilst we recorded the resulting membrane current in voltage-clamp mode (Fig.24A, blue trace). These data indicate that the typical AP of such cells lasts for about 20 ms, and the underlying Ca^{2+} current that depolarizes the PM is about 13 pA/pF at its peak. We modeled this Ca^{2+} entry using a 10ms Ca^{2+} influx.

4.2.9. Ca^{2+} induced Ca^{2+} release

The Ca^{2+} influx via plasma membrane Ca^{2+} channels can be amplified when Ca^{2+} induced Ca^{2+} release via Ca^{2+} release channels enhances the intracellular rise in Ca^{2+} primary initiated by the Ca^{2+} entry (Endo, 1970; Berridge 1998). In order to demonstrate the existence of the Ca^{2+} induced Ca^{2+} release (CICR) mechanism under appropriate experimental conditions, as well as to examine the effect of APs on ER Ca^{2+} content, we applied 10 mM extracellular caffeine repeatedly to an SCG neuron, in the absence of extracellular Ca^{2+} (Fig.24B). The existence of caffeine-induced intracellular Ca^{2+} transients clearly indicated that these neurons were sensitive to caffeine-induced Ca^{2+} release, presumably due to the presence of RyRs that were sensitive to Ca^{2+} and caffeine. Four consecutive applications of caffeine severely lowered the amount of releasable ER Ca^{2+}, as shown by the quickly diminishing amplitude of consecutive caffeine-induced Ca^{2+} transients (Fig.24B). However, the amount of releasable ER Ca^{2+} was quickly restored when the same neuron was subjected to three single field stimuli in the presence of 2 mM e.c. Ca^{2+} (Fig.24B, red arrows), resulting in three single transients of cytosolic Ca^{2+}. When caffeine was applied shortly after the third field stimulus, the resulting Ca^{2+} transient was almost of the same amplitude as the first caffeine response, indicating the recovery of releasable ER Ca^{2+}. Thus, single AP induced Ca^{2+} transients are capable of providing a significant refilling of the ER Ca^{2+} store in these neurons.

4.2.10. Observed and simulated effects of PMCA and SERCA inhibitors on single Ca^{2+} transients in phasic neurons.

Numerous observations have been published regarding the relative importance of plasma membrane and Ca^{2+} store-related Ca^{2+} transport mechanisms that contribute to single and multiple cytosolic Ca^{2+} responses in mammalian and amphibian sympathetic neurons (Thayer et al., 1988; Trouslard et al., 1993; Hua et al., 1993; Hua et al., 2000; Wanaverbecq et al., 2003; Friel and Tsien, 1992; Friel 1995; Pivovarova et al., 1999; Albrecht et al., 2001 and 2002; Patterson et al., 2007; for a review see Verkhratsky, 2005). It has been shown that in frog sympathetic ganglion neurons both the PM Ca^{2+} ATPase (PMCA) and the SERCA pump contribute significantly to the removal of excess cytosolic Ca^{2+} following Ca^{2+} influx (Cseresnyés et al., 1997; Patterson et al., 2007). However, in rodent SCG neurons the SERCA contribution has been shown to be negligible compared to that of by PMCA (Wanaverbecq et al., 2003). In order to confirm these results and to extend them to subcellular resolution, as well as to verify that our model could simulate the results of PMCA inhibition simply by decreasing the PMCA contribution to the model, we performed experiments where we selectively blocked either the PMCA or the SERCA pump whilst we recorded single AP-induced Ca^{2+} transients in rat SCG neurons after 24-48 hours in culture.

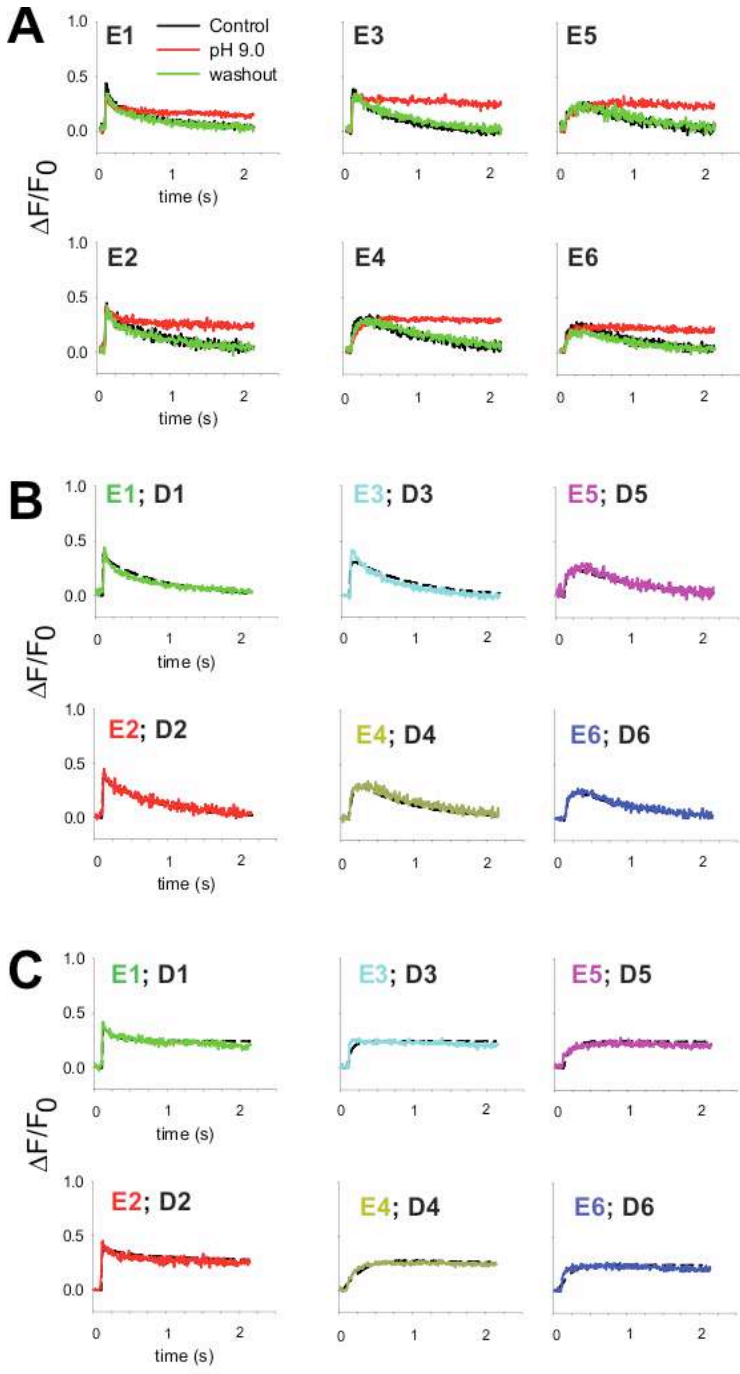

Figure 25. Observed and simulated effects of alkalic pH on single AP-induced Ca^{2+} transients. A): Measured calcium

sensitive fluorescence transients under control conditions (black curves), in the presence of high pH (an inhibitor of the plasma membrane calcium ATPase PMCA; red curves), and after washout (green curves). B): The measured (colored curves) and simulated (black dashed lines) calcium transients under control conditions. C): Measured and simulated calcium transients in the presence of high pH (pH 9.0). Colored lines show the measured data, whereas the black lines indicate the simulated results.

Several publications have shown that high pH effectively eliminates the Ca^{2+}/H^{+} transport provided by PMCA (Benham et a., 1992; Park et al., 1996; Cseresnyés et al., 1997; Wanaverbecq et al., 2003). Here we used a mammalian Ringers's solution with pH 9.0 in order to accomplish this inhibition. In Fig.25A, we show the results of such an experiment. In Fig.25 we show observed and simulated effects of alkalic pH on single AP-induced Ca^{2+} transients. In panel A we show the experimental data from 6 sub-cellular domains (E1 through E6, see cartoon in Fig.22A, bottom) illustrating the effect of pH 9.0, applied here to inhibit PMCA, in a cell of 24-h in culture. The cell was subjected to a 2-ms long field stimulus, which resulted in a single AP and the corresponding cytosolic Ca^{2+} transient. The solid black curves indicate the control results, the red lines correspond to the data collected in the presence of pH 9.0, whereas the green solid lines show the effect of 5 min washout in pH 7.4 mammalian Ringer's solution. The reversible slowdown of the decay phase in high pH is clearly observable in all 6 domains. In panel B we re-plot the control data from all 6 domains (E1 through E6), using the same color coding as in Fig.22B, as well as the simulated $\Delta F/F_0$ transients for those same domains (D1

through D6, plotted as black dashed curves). The model parameters different from those in Tables 2 through 4 were: $F_{1,3}$=15, $F_{2,4}$=4, $F_{3,5}$=8, $F_{5,6}$=4; α(D3)=4, α2(D3)=20, α3(D3)=20; k_{PMCA}=0.45. The simulated data agree well with the experimental observations. The results in panel C repeat the experimental data in the presence of high pH for E1 through E6, in a similar arrangement to (B). Simulations for these data were executed by setting k_{PMCA} to 5% of the control value (see eqn.(3)) and are plotted as black dashed lines (D1 through D6). Even though only the k_{PMCA} value was changed between the simulations in (C) and (B), the resulting fit of the model to the experimental data in (C) was satisfactory, confirming the dominance of PMCA in controlling the removal of elevated cytosolic Ca^{2+}.

These six sub-cellular domains were selected according to the map in Fig.22A, bottom, and the corresponding experimental Ca^{2+} transients were labeled E1 through E6. As shown here, the strongly alkaline pH slowed the decay of Ca^{2+} following the single AP-induced Ca^{2+} influx (red curves), with the effect especially impressive in the non-peripheral domains (E3 through E6), where the decay was almost completely halted by extracellular pH 9.0. In the peripheral domains (E1 and E2), the decay phase of the cytosolic Ca^{2+} transient still contained a small but relatively rapidly decaying component, which was followed by a very slow component. During the rapid component of decay of Ca^{2+} in E1 and E2, some of the Ca^{2+} that entered these peripheral domains was leaving by radial diffusion into more

central regions, which increased Ca^{2+} with a similar time course. In contrast, during the slow component of decay in E1 and E2, changes in Ca^{2+} were sufficiently slow that Ca^{2+} concentration was apparently at equilibrium between all regions of the cell, as evidenced by the similar slow decay time courses (E1 - E6) observed in all regions.

In order to examine the reversibility of the high pH effect, and thus exclude general run-down as a contributor to the slow decay, we repeated the experiments after a 5 min washout, which was achieved by replacing the high pH solution with pH 7.4. The green curves in Fig.25A clearly indicate that the high pH effect was indeed reversible, and that short-term inhibition of the main PM Ca^{2+} removal mechanism did not cause permanent damage to the Ca^{2+} handling mechanisms of the cell. Even more importantly, Fig.25A shows that PMCA alone is responsible for about 90-95% of the Ca^{2+} removal capacity after AP-induced elevations of cytosolic Ca^{2+} in rat SCG neurons. These results are in good agreement with observations by others in mammalian neurons (Benham et a., 1992; Wanaverbecq et al., 2003).

We also simulated the effect of PMCA inhibition on single Ca^{2+} transients using the 6-domain model. The control experimental records and the corresponding simulations are shown in Fig.25B using the same color coding for the 6 domains as in Fig.22, and with the simulated results presented by black dashed lines (see Fig.22 for details about setting the model parameters). Under the control conditions, the Ca^{2+} signals in all six domains were well reproduced by the simulations, as shown

by the close overlap between the colored lines (E1 through E6) and their simulations (D1 through D6, black dashed curves). In order to simulate the effect of high pH, we set the k_{PMCA} parameter to 5% of its control value and ran the model simulation again without changing any of the other parameter values. The good agreement of the experimental and simulated results in high pH for all 6 domains is clearly indicated by Fig.25C, where we re-plotted the experimental data from Fig.25A, and overlaid the simulated results, using the same color coding again as in Fig.25B. The close match between the observed and simulated results of the high pH effect when only the rate constant for the PMCA was changed in the simulation further confirms the dominance of PMCA in removing excess cytosolic Ca^{2+} following single AP-induced Ca^{2+} influx in rat SCG neurons.

There has been a long-standing disagreement in the literature regarding the importance of ER Ca^{2+} influx and efflux in shaping the cytosolic Ca^{2+} response during AP-induced Ca^{2+} transients in rodent sympathetic neurons. Several publications agree on the lack of high-amplification CICR and of strong Ca^{2+} uptake into the ER via SERCA pumps in SCG neurons (Thayer et al., 1988; Hernández-Cruz et al., 1997; Wanaverbecq et al., 2003). Our results in Fig.25 indicate that the SERCA contribution to Ca^{2+} removal should indeed be very small since inhibition of PMCA almost completely halted the removal of cytosolic Ca^{2+} following single AP-induced Ca^{2+} transients. In order to directly investigate the contribution of SERCA to the removal of elevated cytosolic Ca^{2+}, we compared single AP-

induced Ca^{2+} transients before and during the application of 5 μM cyclopiazonic acid (CPA), a specific SERCA pump inhibitor (Inesi and Sagara, 1994). The comparison between the control results in all six sub-cellular domains (Fig.26, E1 through E6, black lines) and those in the presence of CPA (Fig.26, red curves) confirm earlier results. Our computer simulations were also able to reproduce these results (not shown), as a trivial consequence of the overwhelming influence of PMCA on the rate of Ca^{2+} removal, as shown in Fig.25.

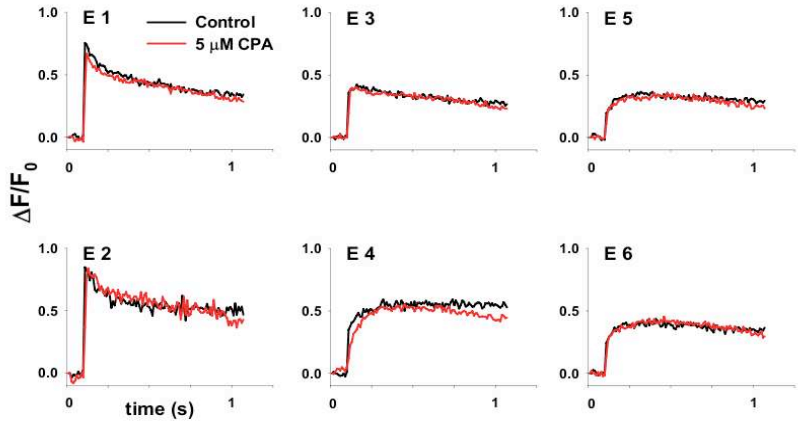

Figure 26. Inhibition of SERCA pumps by CPA during single AP-induced Ca^{2+} transients. The measured effect of the sarco/endoplasmic reticulum ATPase (SERCA) pump inhibitor cyclopiezonic acid (CPA). Control responses in black, CPA effect in red.

4.2.11. Experimental studies and model simulations of Ca^{2+} transients during 1 Hz and 10 Hz periodic stimuli

We recently examined the effect of low and high frequency periodic electrical stimuli on cytosolic Ca^{2+} and NFATc1 nuclear translocation in rat SCG neurons (Hernandez-Ochoa et al, 2006). In cells that were cultured for a relatively long time (2-5 days), each brief field stimulus resulted in a single AP and the consequent Ca^{2+} influx and cytosolic Ca^{2+} transient.

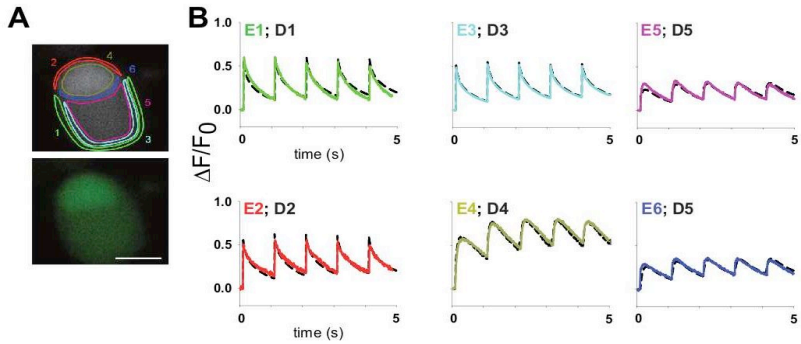

Figure 27. Observed and simulated Ca^{2+} transients in six cytosolic domains during 1-Hz periodic field stimuli. A): Fluorescence image of a cultured SCG neuron (top) with the "E" zones labeled as colored areas; A) bottom: DAPI staining shows the location of the nucleus. B): measured and simulated effects of periodic 1-Hz stimuli at the 6 areas marked in A).

Here in Fig.15 we show the observed and simulated Ca^{2+} transients in six cytosolic domains during *1-Hz* periodic field stimuli. Panel A shows data from an SCG neuron, cultured for 24-h and loaded with fluo-4 AM and imaged in xy mode at 108 ms/frame. The location of the six domains is shown in **(A)**, top, superimposed onto a fluorescence image of the cell and

color-coded similarly to Fig.22. Here the nucleus was peripherally located as revealed by the bean-shaped area of above-average fluorescence in (A), bottom. The neuron was stimulated for 5 seconds at 1 Hz with 2-ms long field stimuli of constant polarity. In panel B we show simulated data as dashed black curves, superimposed onto the experimental records, revealing a fairly close fit between the data and the model. The model parameters different from those in Tables 2 through 4 were: $F_{1,3}$=4 $F_{2,4}$=0.6, $F_{3,5}$=6, $F_{3,6}$=0.7; k_{PMCA}=1.2, $k_{RyR,0}$=0.017. In Fig.28 we show observed and simulated records of Ca^{2+} transients that were induced by *10-Hz* periodic field stimuli. The conditions were similar to those in Fig.22: the cell was field-stimulated for 5 seconds, applying 2-ms long electrical pulses at 10 Hz frequency. The fluo-4 fluorescence responses were imaged in xy mode at 108 ms/frame and the $\Delta F/F_0$ records were calculated from the six intracellular domains depicted in **(A)**, top. The colored domains in panel A top appear superimposed onto a fluorescence image of the cell, recorded near to the highest level of fluorescence during the 5-sec stimulus (bottom). Similarly, panel B shows the experimental data of $\Delta F/F_0$ transients recorded from the 6 domains, using the same color coding as in panel A, top. Results of the model simulations are plotted as thin black lines, superimposed onto the experimental records. The inserts show the first second of the experimental and simulated results on an extended time scale. The model parameters different from those in Tables 2 through 4 were: $F_{1,3}$=4, $F_{2,4}$=0.6, $F_{3,2}$=4, $F_{3,5}$=6; k_{PMCA}=1.2.

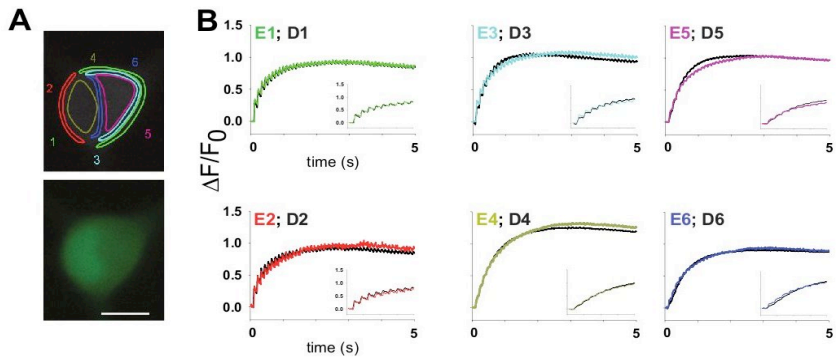

Figure 28. Ca^{2+} transients induced by 10-Hz periodic field stimuli: observed and simulated records. A): Fluorescence image of a cultured SCG neuron (top) with the "Ex" zones labeled as colored areas (x from 1 to 6); A) bottom: DAPI staining shows the location of the nucleus. B): measured and simulated effects of periodic 10-Hz stimuli at the 6 areas marked in A).

As indicated by these results, when such cells were stimulated repeatedly for 5-s at 1 Hz (Fig.27) or 10 Hz (Fig.28), the cells responded with a train of cytosolic Ca^{2+} transients of the corresponding frequency (Figs.27 and 28, colored lines). The 1 Hz train of responses showed little summation (Fig.27), whereas the 10 Hz stimulation produced a much more robust summation effect (Fig.28).

In order to better understand the cellular mechanisms that affect the periodic Ca^{2+} responses during low- and high-frequency stimuli, we used our 6-domain Ca^{2+} signaling model to reproduce the cytosolic Ca^{2+} responses shown in Figs.27 and 28. In case of the 10 Hz stimulations, our experimental data showed that the amplitude of the individual $\Delta F/F_0$ steps, caused by individual APs, was decreasing with time during continuous stimulation (Fig.28). The decrease of the individual $\Delta F/F_0$ step

size was observed not only during the initial few transients of cytosolic Ca^{2+}, but also during the slow, plateau-like phase that appeared after about 1-1.5 seconds into the train of stimuli. The model with constant Ca^{2+} increments for each AP predicted the declining step size during the initial rising phase of accumulating Ca^{2+} but not the continued decrease during the plateau. This gradual decrease of transients that appeared later in the experiment required that we introduce a gradual inactivation of the Ca^{2+} influx into our model. In support of this inactivation mechanism, several groups had reported that N type Ca^{2+} channels, the channel population that carries much of the Ca^{2+} current in cultured rat SCG neurons (Plummer et al., 1989; Regan et al., 1991; Garcia-Ferreiro et al., 2001; Hernandez-Ochoa et al., 2006), undergo cumulative inactivation during AP trains at frequencies ranging from 2.5 Hz to 50 Hz (see Patil et al., McDavid and Currie 2006). In our model, this inactivation was introduced by calculating the influx amplitude assuming a constant percentage of inactivation upon the arrival of each simulated AP, followed by a recovery from this inactivation along a single exponential time course. The recovery time constant was set to 200 ms in order to fit the time course in Fig.28. This value indicates that in a 10 Hz train of stimuli, there is only a partial recovery of Ca^{2+} influx in the 100 ms between two consecutive APs. On the other hand, in a 1 Hz train (Fig.27) the recovery is almost complete before the arrival of the next AP when using these parameters. In our model calculations, only 50% of the influx was subject to inactivation, and the inactivated

portion per AP of that 50% was set to between 2 and 5% in order to account for the observed gradual decrease of Ca^{2+} transient amplitude.

Attempting to match the observed and simulated spatial distributions of the $\Delta F/F_0$ transients during single and repeated APs further restricts the possible range of values of the model parameters. When examining the spatial distribution of the $\Delta F/F_0$ signal in rat SCG neurons during periodic stimuli (Figs.27 and 28), we noticed that in order to simulate the relatively small decrement of the $\Delta F/F_0$ signal between domains, we had to set the inter-domain flux coefficients relatively large between D 1 and D 3, as well as between D 3 and D 5. This restriction on the flux coefficients was similar to that applied during simulations of single AP-induced Ca^{2+} transients (see Fig.22). Another set of modeling restrictions arises from our results in Figs.25 and 26 regarding the relative contributions of PMCA and SERCA to the removal of excess cytosolic Ca^{2+}. Based on those results, here we also assumed that k_{SERCA} was much smaller than k_{PMCA}, and thus Ca^{2+} uptake via SERCA, and Ca^{2+} release via CICR did not contribute significantly to the kinetics of cytosolic Ca^{2+} signals during periodic stimuli.

4.2.12. Ca^{2+} transients recorded at various focal planes in a neuron with peripherally located nucleus.

A major advantage of using confocal microscopy in studies of intracellular Ca^{2+} signaling is the shallow depth-of-field, which results in axially specific experimental data. The limited depth of

field not only improves image contrast and resolution, but also helps to isolate Ca^{2+} signaling events in the current focal plane from those occurring in XY planes of different axial position. At the same time, our six-domain model is also implicitly limited to a 2-D section of an SCG neuron, where the domains are well separated not only in the XY plane but also axially, corresponding to ideal confocal settings, i.e. without any crosstalk between domains of XY planes at slightly different axial positions. In practice, however, the depth of field is not always shallow enough to completely exclude out-of-focus information. For example, when the selected XY plane of focus is located near the top or the bottom of the cell, fluorescence signals experimentally recorded from the more centrally located domains of the cell in the image XY plane may contain a mixture of fluorescence signals from the central domains (E5 or E6) of the focal plane as well as from the peripheral domains (E1, 2 or 3) of the out of focus plane(s). When the selected XY focal plane is near the vertical center of the cell, signals recorded from the central domains (E5, E6) may still contain a similar contamination from peripheral domains above and/or below the focal plane, although probably to a lesser extent. We thus distinguish signals experimentally recorded from a particular region (n) in the XY plane z μm above or below the vertical center of the cell (denoted by En,z) from the theoretically pure signal (Dn) generated by the model for domain n. As described below, we account for out of focus fluorescence from theoretical domains above and below the focal plane by reproducing En by a

linear combination, $\sum f_i D_i$, (i = 1 to 6) of pure signals Di generated by the model for different domains in and/or above and below the plane of focus.

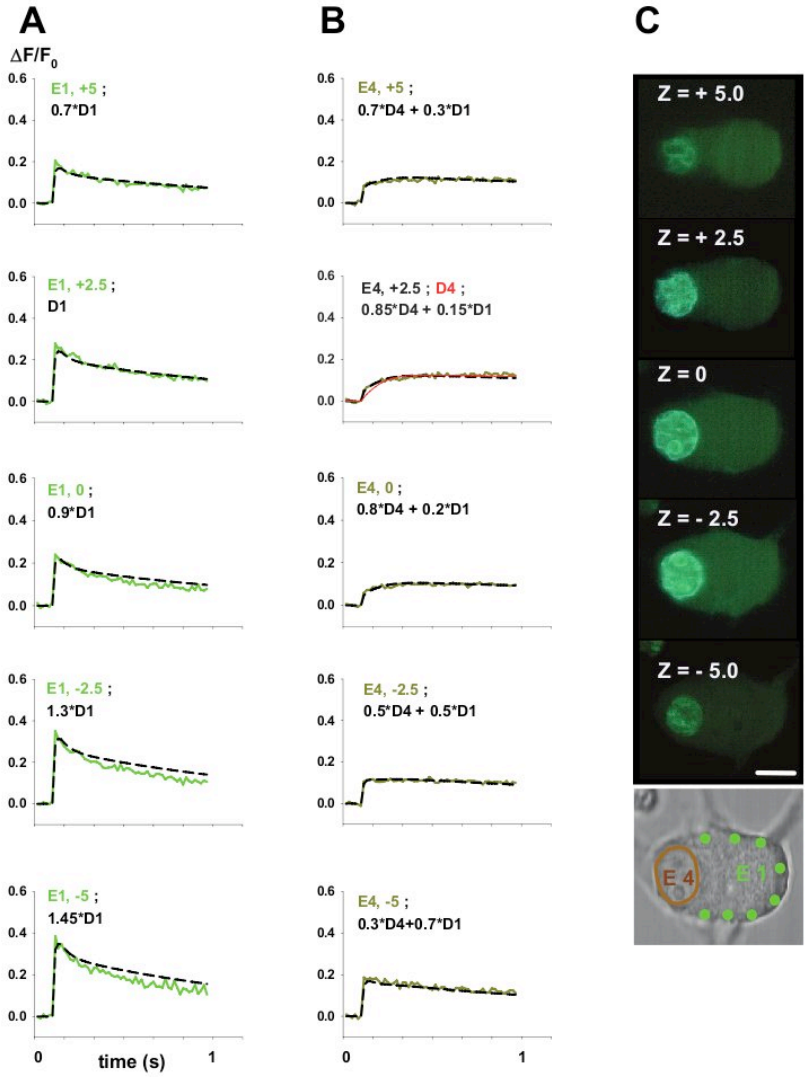

Figure 29. The effect of focal plane selection on the apparent kinetic properties of single Ca^{2+} transients recorded with a confocal microscope system. A): Sub-plasma membrane calcium transients measured (green) and simulated (black dashed line) at the focal plane (middle row), at 2.5 μm below and above

the focal plane (row 4 and 2, respectively), and at 5.0 μm below and above the focal plane (row 5 and 1, respectively). B): Intra-nuclear calcium transients measured (green) and simulated (black dashed line) at the focal plane (middle row), at 2.5 μm below and above the focal plane (row 4 and 2, respectively), and at 5.0 μm below and above the focal plane (row 5 and 1, respectively). C): Fluorescence images of the neuron at the 5 axial locations, with DAPI marking the exact location of the nucleus. B Bottom): the location of E4 (nucleus) and E1 (sub-PM areas in green, fluorescence signal was averaged from areas to provide the E1 values).

We characterized the axial position-dependence of the experimental confocal fluorescence signals by recording single AP induced Ca^{2+} transients from several axially separated focal planes in 6 neurons and characterizing the resulting experimentally observed single Ca^{2+} transients by the time course of fluo-4 $\Delta F/F_0$ in different regions of the cell in each focal plane. Fig.29 presents experimental results from a peripherally located domain (E1), and from the nucleus (E 4) in each of the focal planes (i.e., E1,5 thru E1,-5 and E4,5 thru E4,-5). Here an SCG neuron of 24 hours in culture was loaded with fluo-4 and DAPI, and $\Delta F/F_0$ transients of fluo-4 fluorescence were recorded at 60 frames per second during single AP-induced Ca^{2+} transients. The APs were initiated by single, 2-ms long field stimuli. The $\Delta F/F_0$ values were calculated at two intracellular domains: data from E1 are shown in **(A),** whereas data from E4 are plotted in **(B)**. Experimental data are shown as color lines, green corresponding to E1 and dark yellow to E4. The color circles shown at the bottom of panel **(C)** indicate the locations of the AOIs used to calculate the E1 signal, whereas the bean-shaped dark yellow

area in (C), bottom panel depicts the location of the E4 domain. The $\Delta F/F_0$ transients recorded at the vertical center of the cell's nucleus (Z=0) are shown in the middle of panels A and B. The total recording time was 1 sec. The experiments were performed at 5 different focal planes, where the distance between two neighboring locations was 2.5 μm. The vertical position of the focal plane relative to the center of the nucleus (Z=0) is shown above each panel in Aa and Ab (Z=+5 μm to -5 μm). The nomenclature of the E 1 and E 4 curves (E1, +5 through E1, -5; E4, +5 through E4, -5) indicates the vertical position of the focal plane relative to the z=0 location (+5 through -5 μm). The black dashed lines in (A) and (B) show the results of the model simulations. The model parameters different from those in Appendix 3, Tables 2 through 4 were: $F_{1,3}$=15, $F_{2,4}$=4, $F_{3,5}$=8, $F_{5,6}$=4; α(D3)=4, α2(D3)=20, α3(D3)=20; k_{PMCA}=0.45. In (A), the E1 data recorded at the z=+2.5 μm position was simulated first, and then this simulated transient was scaled up or down in order to fit the rest of the E1 curves in (A). In (B), all E4 records were fitted by a linear combination of the "ideal" D4 transient, plotted in red at the z=+2.5 μm position, and the "ideal" D1 transient, shown at the z=+2.5 μm position in (A). The weight factors describing the D4 and D1 contributions are plotted above each curve in (A) and (B).

As these results show, the kinetic behavior of the E 1 signals remains fairly constant throughout (Fig.29A). In contrast, the rising phase of the E 4 signal was slowest when recording slightly above the vertical center of the nucleus (z=+2.5 μm,

Fig.29B, E4,0) whereas the E4 signal was definitely “spikier” when the focal plane was selected close to the bottom of the cell (Fig.29B, E 4,-5), presumably due to contamination with a component of the E1 or E3 signal from the more peripheral region below the nucleus.

4.2.13. Simulating pure and mixed domain Ca^{2+} signals in various focal planes arising from different regions of a cell.

The observed relative time courses in region E1 were similar in all focal planes in Fig.29, so a simple scaling of the theoretical D1 signal was used to provide fairly good description of these experimental records (Fig.29Ba, black dashed lines). In contrast, because the time course of the E4 signals changed with the vertical position, becoming more rapid at the -5 μm focal plane, we used a linear combination of the D1 and D4 signals to reproduce the E4 experimental records (Fig.29Bb, black dashed lines). For the focal plane at the z = 2.5 μm position the relative fast contribution was small (15 %), whereas at the bottom of the cell (E4, -5) the fast contribution became significant (70 %) in the simulated records.

4.2.14. Observations and simulations of single Ca^{2+} transients in neurons with a centrally located nucleus.

Whereas a large percentage of cultured neurons exhibited a peripherally located nucleus (~87 %), especially during the first 24-48 hours in culture, there were also many cells in which the nucleus was located near the center. Similarly, varied localization of the nucleus was also observed in freshly dissociated neurons as well as neurons inside intact ganglia (unpublished observations). The neuron in Fig.30 is an example of a cell with centrally located nucleus.

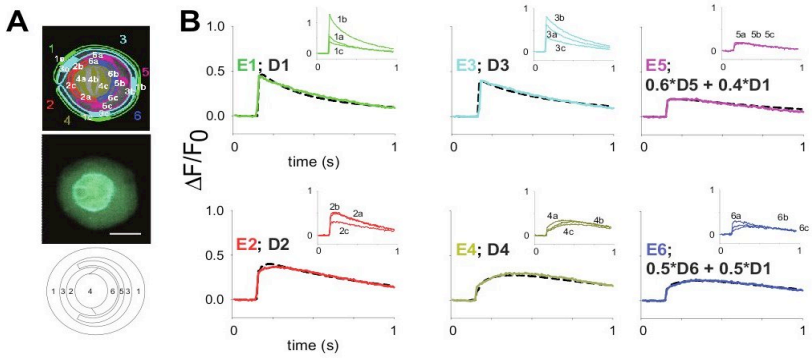

Figure 30. Cytosolic Ca^{2+} transients induced by a single field stimulus in a 24-h cultured SCG neuron with a centrally located nucleus: experimental and simulated data. Measured and simulated calcium-sensitive fluorescence transients are plotted at the locations shown in A), top panel, colored areas. Functionally separated cell compartments are shown in the cartoon, bottom panel of A). The central location of the nucleus is shown by the DAPI staining in A) middle panel. B): measured average time courses are shown as color lines, labeled with Ex, where "x" indicates the region where the signal comes from (see cartoon in A). The corresponding simulated curves are plotted as black dashed lines. Individual measured time courses are shown in the insets, using the same color as the averaged time course.

Here, cytosolic Ca^{2+} transients were induced by a single field stimulus in a 24-h cultured SCG neuron with a centrally located nucleus. This SCG neuron was loaded with fluo-4 AM and imaged in xy mode at 108 ms/frame. The nucleus was located near the cell's geometrical center as revealed by DAPI staining, **(A)**, middle panel, nucleus pseudo-colored in light blue. The 6 main domains were drawn according to the chart in panel A, top, and the color coding was maintained for the experimental records in panel B. The six main domains were divided into 3 sub-domains each and their experimental $\Delta F/F_0$ values were plotted as inserts of the segments of **(B)**. The neuron was stimulated with a 2-ms long single field stimulus applied via parallel field electrodes. The resulting cytosolic Ca^{2+} transients were characterized in all domains and sub-domains by calculating the time course of the $\Delta F/F_0$ values, which are shown here in the same colors as the corresponding areas in the map of panel A, top. In addition to the experimental records for each main domain (E1 through E6, color coded according to panel A, top) and sub-domains (#a, #b, #c, # = 1 to 6, in the same color as the corresponding main domain), panel B also shows the results of the computer simulations using our 6-domain model (D1 through D6, in cartoon at Fig.30A, bottom), plotted in black dashed lines superimposed onto the corresponding main domains' experimental records. The model parameters different from those in Tables 2 through 4 were: $F_{1,3}$=16, $F_{2,4}$=8, $F_{3,2}$=4, $F_{3,5}$=0.5, $F_{3,6}$=0.7, $F_{6,4}$=5, $F_{5,6}$=7; δ(D1)=0.54, δ(D2)=0, α(D2)=0,

α2(D1)=1, α2(D2)=0.2, α2(D3)=1, α2(D5)=2, α2(D6)=0.5. Please note that $F_{3,2}$ was set to a non-zero value in order to account for the Ca^{2+} flux between domains 3 and 2, due to the central location of the nucleus.

The model simulation consisted of adjusting the simulated results until the experimental data from the peripherally located domains were well reproduced. At the same time, an independent routine of the simulations software suite calculated linear combinations of the simulated signals from D 5 and D 3 (or D 1), as well as from D 6 and D 3 (or D 1). The weight coefficient of the linear combination was varied until the mixed D 5&D 3 signal fitted the measured E 5 transient, and the mixed D 6&D 3 signal overlapped the measured E 6 data. The method also resulted in the "pure" D 5 and D 6 simulated transients. The simulated time courses that most closely fit the E5 and E6 data were the result of a linear combination of the simulated D5 and D6 data with weight factors of 0.4 and 0.5, calculated according to the expressions printed above the E5 and E6 records.

Domains 1 and 3 were characterized by kinetically similar $\Delta F/F_0$ transients (E1 and E3), whereas domain 5 exhibited a smaller and slower transient (E5). In contrast to Ca^{2+} transients observed in the outer perinuclear domain around peripherally located nuclei, (e.g., Figs.22 and 24), the experimental records for the domains at or near the centrally located nucleus (E2, E4, E6) were all characterized by a more gradual rising phase and

slower decays as opposed to the "spiky" appearance in the non-nuclear domains (E1, E3, E5).

The central localization of the nucleus in the neuron in Fig.30 had to be taken into account when generating the simulated $\Delta F/F_0$ records using our 6-domain model. As shown in the map of AOIs in Fig.30A, top, the peripherally located perinuclear domain 2 was now not at the cell periphery, but instead was neighboring domain 3 in this neuron, whereas in cells with peripheral nuclei it was directly connected to the PM (see Fig.22). Consequently, the $\Delta F/F_0$ signal in domain 2 was the result of Ca^{2+} diffusion from domain 3, simulated via the inter-domain Ca^{2+} flux coefficient F_{32} (see map of domains in Fig.30A bottom). In those cells where the nucleus was at the periphery, the peripheral perinuclear domain 2 was assigned approximately 25% of the PM, thus resulting in a sharp rise of the $\Delta F/F_0$ transient followed by a fairly fast decay, similar to the transient in domain 1 (compare with Fig.22). In Fig.30, however, the model had to account for the sharp rise at the beginning of the D 2 transient, which was accomplished by assuming a robust Ca^{2+} flux between D 3 and D 2. The flexibility provided by the unrestricted array of model parameters allowed us to take the new domain arrangement into account by assigning a non–zero value to the F_{32} flux coefficient (please note that F_{32} would be set to zero if the nucleus were located peripherally). As shown by the close fit between the experimental results and the simulated data in D 1, D 3, D 2 and D 4, these model parameters were able to reproduce the observed behavior of the cell.

4.2.15. Using the 6-domain model to un-mix optical signals that have arisen from domains above or below the focal plane of observation.

As we have seen above, Fig.30 presents data recorded at a focal plane selected at the vertical center of the cell's nucleus. The existence of a very fast component of the rising phase of the Ca^{2+} signals recorded experimentally from centrally located regions E 5 and E 6 indicates that these signals consist of an optical mix of a "pure" D 5/D 6 signal, which would rise slowly, with a more peripheral D 1/D 3 signal, which would rise more abruptly. This situation is similar to that in Fig.29, where the recorded $\Delta F/F_0$ signal from the nucleus showed an unexpected sharp rise at the beginning of the transient at certain focal positions. Based on our model (see Fig.30A bottom), the main route of Ca^{2+} into domains D 5 and D 6 would ideally be via diffusion from the neighboring domains D 3 and D 4. In simulating the experimental observation (E5 and E6) in Fig.30, the relatively slow component of the rising phase that characterizes a pure D 5 or D 6 signal had to be mixed with a scaled version of the sharply rising signal from D 1 or D 3. This was achieved by calculating a linear combination of the simulated optical signals from D 5 and D 3 (Fig.30B, top right) or D 6 and D 3 (Fig.30B, bottom right), according to the expressions printed above the colored and black curves. The weight factors had to be set to 0.4 and 0.5, in order to provide the best fit.

5. DISCUSSION

5.1. Non-uniform calcium responses to action potentials in frog SGNs

In our earlier studies, we showed that caffeine-induced Ca^{2+} release from the ER of cultured frog SGNs is a spatially inhomogeneous event (McDonough et al., 2000). In our current studies, we used neurons in intact ganglia as well as cultured cells, and applied electrical field stimulation instead of caffeine. The electrical stimuli generated somatic APs, which in turn resulted in Ca^{2+} influx via voltage-activated Ca^{2+} channels of the plasma membrane. The resulting Ca^{2+} influx then activated CICR via RyRs of the sub-plasma membrane ER. These AP-induced Ca^{2+} transients exhibited clear spatial and temporal non-uniformity around the periphery of all cells studied in intact ganglia, as well as in the large majority of cultured cells. Such non-uniform responses were characterized by local peripheral sites (1-3 per neuron) exhibiting rapidly rising Ca^{2+} transients (termed "hot spots"), whereas extensive intervening peripheral regions showed little or no Ca^{2+} transient. In contrast, other cultured neurons exhibited peripherally uniform Ca^{2+} transients. Although peripheral non-uniformity was not directly observable in such neurons, it was clearly revealed by addition of cytosolic EGTA or by lowering extracellular Ca^{2+} concentration. These results thus indicate that spatial non-uniformity of Ca^{2+} responses is an inherent property of frog SGNs, and that the non-uniformity is maintained in primary cell cultures, even though the hot spots

may not always be directly observable in all cultured SGNs. The localized peripheral signals observed in response to single APs were not due to non-responsive dye since trains of APs or ionomycin elevated fluorescence throughout the same neurons. The hot spot locations appear to be structurally determined. Ca^{2+} store depletion eliminated the hot spots. Store refilling caused the hot spots to reappear at their original locations, but no hot spots appeared at any new locations.

5.2. Advantages of high-speed 2D confocal imaging

Akita and Kuba (2000) previously demonstrated that single action potentials produce rapid Ca^{2+} transients at the periphery of patch clamped cultured frog sympathetic ganglion neurons using line scan imaging (2 ms/line). They could thus detect elevation of calcium at the cell periphery, but only at the single spatial location at which their scan line was located. In contrast, we now obtained xy images of the entire cell (at 63 μs/line). Thus, we could distinguish a uniform peripheral response from a localized peripheral response. Although both response types 1 and 2 are localized at the cell periphery, type 1 is uniform around the cell periphery whereas type 2 occurs only at a few distinct hot spots around the cell periphery. Akita and Kuba (2000) did not distinguish 1 from 2. However, if they used random placement of the line location (not specified in their paper) and if they detected rapid peripheral Ca^{2+} transients at all locations tested, then the cells that they selected for study after 1 week in culture must have exhibited response type 1. In contrast, we now show

that cells in fresh ganglia give the localized (type 2) response, as do the majority of cells in culture. We also show that a minority of cultured cells gives the peripherally uniform (type 1) response, but that this uniform response can be transformed into a local (type 2) response by intracellular EGTA or by reduced extracellular [Ca^{2+}]. It should also be noted that uniform peripheral Ca^{2+} responses are more noticeable during live observation or live imaging than non-uniform, local peripheral responses. Thus, in seeking a "responsive cell" it is more likely to select a uniformly responding cell than a non-uniform one.

5.3. Functional significance of non-uniform Ca^{2+} signaling in SGNs and SCG neurons

The functional significance of the non-uniform Ca^{2+} responses has yet to be established. We speculate that the hot spot in the peripheral perinuclear ER signals the arrival of an external stimulus directly to the nucleus, thus enabling the cell to reliably decode this message. The other hot spot was typically situated roughly across the cell from the nucleus. This site might thus be related to the axonal hillock, which is often located opposite to the nucleus in intact neurons within the ganglion (Fig.6; see also Pick, 1963). These autonomic neurons do not have dendrites. The axons of presynaptic neurons end directly on the soma of the postsynaptic SGN, forming axosomatic synapses. The axon of the postsynaptic neuron is usually situated across the cell from the nucleus, and the presynaptic axon(s) wrap around the postsynaptic axon before forming the axosomatic synapses.

These axonal and synaptic structures are likely to be intact in our whole-ganglia preparation (Fig.6). The close proximity of the non-nuclear hot spots and the axonal hillock in a neuron in an intact ganglion (Figs.6, 7) points toward a possible functional relationship between the non-nuclear hot spot and the initiation of axonal Ca^{2+} transients. The molecular basis for the observed hot spots may be i) clusters of N- or P-type Ca^{2+} channels in the plasma membrane, ii) local ER specialization, or iii) local concentration of cross-links between PM Ca^{2+} channels and ER Ca^{2+} release channels, possibly mediated by cross linking Homer proteins (Tu et al., 1998; Kammermeier et al., 2000; for review, see Xiao et al., 2000).

Although we do not have a definitive explanation for why some cultured SGNs exhibit uniform peripheral AP-induced Ca^{2+} signals (Fig.16), the experimental data with EGTA-loaded cells (Fig.19) and with low-Ca^{2+} flushes (Fig.20) provide some unity to our findings. Based on these results, it appears that every frog sympathetic neuron may have potential hot spots for initiation of Ca^{2+} release, but that these spots may not always be apparent. In the case of cells exhibiting uniform peripheral Ca^{2+} transients under control conditions, the cell may exhibit sufficient CICR around the entire periphery that the Ca^{2+} transient occurs over the entire surface. However, such cells still have "latent" hot spots, as evidenced by the existence of areas that remain responsive to APs even in EGTA-loaded cells or under conditions of lowered extracellular Ca^{2+}.

5.4. Non-uniform Ca^{2+} signaling in non-neuronal cell types

It is interesting to compare the localized Ca^{2+} signals observed here at peripheral hot spots in frog sympathetic ganglion neurons with the localized Ca^{2+} sparks observed at triad junctions in frog skeletal muscle fibers (Lacampagne et al, 1999; Schneider, 1999) since both signals are believed to be generated by Ca^{2+} release via RyR Ca^{2+} release channels in the ER or SR, respectively. The peak amplitude of the local Ca^{2+} signals observed here is roughly in the range of 0.5 to 1.0 in $\Delta F/F_0$, whereas the largest frog muscle Ca^{2+} sparks have peak amplitudes several fold larger. However, the local $\Delta F/F_0$ records presented here were averaged over relatively larger peripheral AOIs, and would presumably be somewhat larger in amplitude if monitored in smaller areas centered at the peak of the response as is commonly done for the muscle Ca^{2+} sparks. The rise time of the muscle Ca^{2+} sparks is about 4 to 5 ms (Lacampagne et al, 1999), which is remarkably close to the rise time of somewhat under 5 ms obtained here from line scan image of the peripherally uniform Ca^{2+} signals in frog neurons. Although line scan imaging has not yet been carried out on localized peripheral responses due to the difficulty of centering the scan line on an active location, it seems likely that the localized signal may exhibit similar kinetics as seen for the uniform peripheral response, and thus also be similar in rise time to a muscle Ca^{2+} spark. However, in contrast to this similarity of rise times, the decay time course of 100s of ms for both the localized and the uniform peripheral Ca^{2+} signals in neurons is

much slower than the 10 to 20 ms decay time course of Ca^{2+} sparks in muscle.

From the preceding comparisons, it seems possible that the amount and the time course of Ca^{2+} release might be rather similar for muscle Ca^{2+} sparks and neuronal local Ca^{2+} signals, consistent with the similar amplitudes and rise times. However, to account for the much slower decay of Ca^{2+} in the neuronal signals compared to the muscle Ca^{2+} sparks, either the Ca^{2+} uptake system must be much less efficient in the neurons or release must be much more prolonged. Another difference between these two types of local Ca^{2+} signals is that muscle Ca^{2+} sparks are stochastic events that do not occur reproducibly at the same time and location during repeated stimuli, whereas the local Ca^{2+} signals observed here in neurons occur reproducibly with each electrical stimulus (Figs.7 and 8). A final difference is that individual Ca^{2+} sparks in frog skeletal muscle do not propagate from the triad at which they are initiated to the next set of RyRs at the neighboring triad, whereas the more continuous distribution of RyR channels within the peripheral ER rich zone of the neurons provides for the very rapid propagation of the Ca^{2+} signal across the entire ER rich shell as observed here.

5.5. Computer simulations and mathematical modeling of calcium signaling in neurons: basic considerations

In part 4.2 of this work, we provide not only an experimental characterization of the dynamics of the intracellular local Ca^{2+}

signals initiated by AP-induced Ca^{2+} entry, but also a multi-compartmental computer simulation to account for these observations. The computer model is based on morphological and functional studies, and it provides a characterization of the system in terms of Ca^{2+} fluxes underlying the spatio-temporal properties of local Ca^{2+} signals during and after single AP induced by electrical field stimulation in mammalian sympathetic neurons.

The results presented here constitute some of the first records of the complete distribution of the local intracellular Ca^{2+} signal initiated by AP-induced Ca^{2+} entry in SCG neurons as a function of time at any intracellular location in the selected image plane of the imaged cell. Our results show that Ca^{2+} rises rapidly (within 10 ms) at all locations around the periphery of the neuron. The rise of Ca^{2+} is slower and less marked in the more interior cytosolic regions and often slowest in rise and fall within the nucleus, even when the nucleus is peripherally located. The slower responses in the cell interior presumably reflect the gradual diffusion into the cell interior of the Ca^{2+} that entered across the plasma membrane, with the diffusional equilibration being perhaps slowest in the nucleus. Overall, our results show that during single action potentials, local Ca^{2+} responses in sympathetic neurons are spatially heterogeneous. Our results also confirm previous observations by others (Thayer et al., 1988; Hernández-Cruz et al., 1997; Wanaverbecq et al., 2003) that Ca^{2+} entry, via voltage-activated Ca^{2+} channels, is the main Ca^{2+} flux mechanism responsible for the increase in intracellular

Ca^{2+}, with little or no contribution from CICR. We also confirmed that the plasma membrane Ca^{2+} ATPase (PMCA) constitute the main Ca^{2+} efflux mechanism during the decline of intracellular Ca^{2+}. following Ca^{2+} influx-induced transient elevations. The majority of the decline of the Ca^{2+} transient thus seems to be provided by PMCA, since blocking PMCA by high extracellular pH (pH 9.0) essentially halts further Ca^{2+} removal. The intracellular amplification of Ca^{2+} signals relies mostly on the intrinsic plasma membrane properties, above all on repetitive firing.

Ca^{2+} signaling in sympathetic neurons represent a typical example of a complex system. In such complex systems, any prediction of Ca^{2+} signaling related behavior would be very difficult without the use of a quantitative model. Models replace intuitive guesswork with the quantitative results a mathematical system, composed usually of a series of differential equations that describe the time-dependent changes of the functionally and/or morphologically identifiable cellular compartments. These equations combine the mathematical expressions describing the main transport mechanisms related to the Ca^{2+} reaction/diffusion kinetics of the cellular system. The complexity of such model systems also depends on the required spatio-temporal resolution of the numerical solution. It is usually impractical, an often impossible, to solve the equations analytically. Thus, the majority of the model systems are solved numerically, using a computer-based approximation for solving differential equations. The numerical solutions of model systems

found in the Ca^{2+} signaling-related literature vary from the simplest case of one-domain studies of time dependence only to high spatial and time-resolution studies of 3-D (Loew and Schaff, 2001) and 1-D systems (Sala and Hernandez-Cruz, 1990; Yamada et al., 1998; McHugh and Kenyon, 2004; Patterson et al., 2007). Here we apply the Euler method due to its simplicity and relatively low demand for computing power (Scarborough, 1966.). We also limited our calculations to 6 spatial domains, instead of attempting to provide a continuous solution for two or three spatial dimensions, partly because that would have required much more computing power (compare with Loew's Virtual Cell; Loew and Schaff, 2001).

5.6. Simulations of complex Ca^{2+} signaling systems: are the results unique?

In complex systems of Ca^{2+} signaling, including mammalian and amphibian sympathetic ganglion neurons, model simulations provide an invaluable tool to investigate the possible relative contributions of various intracellular and plasma membrane Ca^{2+} transport mechanisms to the observed cytosolic Ca^{2+} signal (Sala and Hernandez-Cruz 1990; Friel 1995; Cseresnyés et al., 1997, 1999; Patterson et al, 2007). However, such complexity of the simulated system in turn requires that the model consist of numerous components, including Ca^{2+} pools of intracellular organelles (ER, mitochondria, Golgi apparatus), voltage-and ligand sensitive Ca^{2+} fluxes, and Ca^{2+} transporters. Working with such large numbers of components and parameters provides

many degrees of freedom to work with when adjusting the model to reproduce the experimental data. Such freedom also comes with a severe drawback. Due to the large number of variables, it may be difficult to argue that the simulated results are unique. One possible approach to increase the uniqueness of the simulated results is to use the model to reproduce more complex temporal and/or spatial patterns of the experimentally observed parameter, e.g. in our case the cytosolic Ca^{2+}. In our studies, we examined the effect of single and multiple AP-like stimuli in SCG neurons, and using our high-speed confocal microscope system we were able to retrieve both temporal and spatial information at high resolution. We then applied our model to reproduce not only single Ca^{2+} transients (Figs.22, 25, 26, 29 and 30) but more complex temporal patterns of cytosolic Ca^{2+} generated by periodic stimuli of phasic neurons (Figs.27 and 28). Moreover, we simulated not only the temporal properties of both the simple and complex Ca^{2+} responses, but also included a characterization of the spatial distribution of the observed signals. Our analysis of more complex temporal and spatial patterns confirmed that the parameter set that successfully described the complex patterns, also automatically reproduced the single Ca^{2+} transients, recorded from the same cell.

5.7. The importance of CICR in phasic and adapting neurons during single and train stimuli

The involvement of CICR in Ca^{2+} signaling may simply be interpreted as Ca^{2+} dependence of the RyR Ca^{2+} conductance. In

model systems, the RyR conductance is usually expressed as a sum of two terms, corresponding to the Ca^{2+} independent and Ca^{2+} dependent components. The net contribution of the ER Ca^{2+} store to the cytosolic Ca^{2+} signal is determined by the relative amplitudes of the Ca^{2+} influx into the ER via the SERCA pumps, and the Ca^{2+} efflux from the ER via the RyRs and IP3Rs. In this matter of speaking, we may say that CICR is contributing to the cytosolic Ca^{2+} transients even when the net ER Ca^{2+} flux is directed into the ER. By increasing or decreasing the sensitivity of the RyRs' Ca^{2+} conductance to cytosolic Ca^{2+}, we may increase or decrease the ER efflux component, which will in turn increase or decrease cytosolic Ca^{2+}. The detailed results of our model simulations indicated that the ER Ca^{2+} store(s) always behaved as net Ca^{2+} sinks during simulated Ca^{2+} transients evoked by single or multiple APs. These results agree well with existing data in mammalian sympathetic neurons (Hernández-Cruz et al., 1997; Wanaverbecq et al., 2003), but disagrees with earlier findings by ourselves and others in frog sympathetic ganglion neurons, where CICR was shown to produce a net increase of cytosolic Ca^{2+}, both in experimental studies (Akita and Kuba, 2000; Cseresnyés and Schneider, 2004) and, more recently, in a model system as well (Patterson et al, 2007). This disagreement may simply be caused by species differences. This may include the lack of dendrites in frog SGNs as opposed to an extensive dendritic arbor in rat and mouse SCG neurons. Moreover, in vivo recordings performed in mammalian SCG neurons confirmed that these neurons receive trains of APs at

frequencies between 0.01 and 20 Hz due to ongoing and reflex periodic presynaptic events (Skok and Ivanov 1983; Ivanov and Purves, 1989; McLachlan 1974 and1997). Periodic AP-like stimuli may be able to amplify the input signal by generating supralinear responses via large elevations of cytosolic Ca^{2+}, thus providing a cytosolic amplifying mechanism for small external stimuli. This mechanism may be also present in amphibian sympathetic neurons, and thus it may provide another powerful intracellular Ca^{2+} signal-amplifying mechanism in addition to CICR.

5.8. Indirect inclusion of an instantaneous buffer in our model

In numerical models described in the literature, a diffusible or fixed Ca^{2+} buffer was often included in the system. The inclusion of the buffer in those models was justified by experimental findings indicating that in sympathetic neurons the free Ca^{2+} vs. bound Ca^{2+} ratio was rather low, in the range of ~0.15% due to a large endogenous Ca^{2+} buffering capacity (Wanaverbecq et al., 2003). Antibody staining of sympathetic neurons also revealed a dense distribution of cytosolic buffers, including Calbindin D28K (Grkovic and Anderson, 1997). In a model system, the main role of an instantaneous fixed buffer is to limit the elevation of cytosolic Ca^{2+} in a spatially non-uniform manner, thus increasing the radial Ca^{2+} gradient in the cytosol (Sala and Hernandez-Cruz, 1990; Stern, 1992; Roberts, 1994; Patterson et al, 2007). Thus, in a non-compartmental model, the addition of a buffer will make the radial Ca^{2+} gradient tunable,

providing an invaluable tool for the user of the model to fit the simulated data onto the experimental values. Without a buffer, the concentration drop during the radial spread of free Ca^{2+} would only be the result of increasing volume (i.e. dilution of Ca^{2+}) and Ca^{2+} uptake into intracellular compartments (e.g., the ER and mitochondria). However, in our multi-domain model, where the Ca^{2+} transport between domains is described by adjustable flux coefficients, the inclusion of an instantaneous buffer would be redundant. Thus, no buffer was included in our model calculations. Instead, we adjusted the F_{ij} parameters (i, j = 1 to 6, $i \neq j$) according to the observed decay of the $\Delta F/F_0$ signal between peripheral and central domains.

5.9. The 6-domain model contains information about inter-domain Ca^{2+} fluxes.

Even though our model in its current form does not explicitly calculate the spatial diffusion of cytosolic Ca^{2+}, the flux coefficients between the six spatial domains do provide implicit information about intracellular Ca^{2+} fluxes. These parameters would be very hard to measure experimentally, whereas a real 2-D or 3-D diffusion-reaction model would require much more robust software and hardware, and would thus limit the availability of the technique (Loew and Schaff, 2001). The following few examples attempt to point out this potentially useful aspect of our relatively simple 6-domain model.

In several neurons (data not shown), the experimental data recorded from the nucleus (D4) showed a biphasic rise, and

sometimes a biphasic decay as well. Using our 6-domain model, the biphasic rise could simply be accounted for by assuming a strong flux of Ca^{2+} from D2 to D4, followed by a delayed influx from D6 into D4. At the same time, D6 was able to provide the delayed rise of the D4 Ca^{2+} transient because it had received significant Ca^{2+} influx from D5 via the D1→D3→D5 pathway. As we have shown earlier, the D1→D3→D5 pathway already had to be set fast in order to account for the relatively small decay of the $\Delta F/F_0$ signal along that pathway.

As another example, in the peripheral perinuclear area (D2) of several cells we observed a biphasic decay (data not shown), consisting of a fast initial drop of $[Ca^{2+}]$, followed by a long tail. The decay rate of the fast component was determined by the flux coefficient from D2 to D4, as well as the SERCA and RACT density in D2. The long tail was accounted for by a buildup of Ca^{2+} in neighboring D4, which was coupled to D2 via a relatively high flux coefficient. Thus, this coefficient proved to be a very useful tool that had to be set higher when simulating the biphasic decay of D2, and lower when accounting for a monophasic type of decay in D2.

5.10. Application of the 6-domain model to un-mix contaminated optical signals

The results in Figs.29 and 30 indicate that the fluorescence signal recorded from the central regions of a cell (D 5 and 6) in any XY plane could be a combination of "pure" signals from more than one theoretical domain: the domain sampled in the focal plane

and one or more domains above or below the focal plane. The actual mixing ratio of the fluorescence signals from these domains will depend on the vertical position of the focal plane and the depth of field characterizing the axial location. Our examinations show that it is possible, using confocal data and applying our 6-domain model, to un-mix the contaminated optical signals and thus to estimate what the "pure" signals would be in an ideal confocal section.

6. SUMMARY

In this dissertation, we examined neurons in intact ganglia and in cell cultures. We applied electrical field stimuli to generate somatic action potentials (APs). AP-induced plasma membrane (PM) depolarisations were found to activate voltage gated calcium channels (VGCC), which in turn resulted in Ca^{2+} influx from the calcium-rich extracellular space into the cytosol of the neuron.

We have shown that the Ca^{2+} influx also activated calcium induced calcium release (CICR) via ryanodine receptors (RyRs) of the sub-plasma membrane endoplasmic reticulum (ER).

We observed that the AP-induced Ca^{2+} transients were spatial and temporally non-uniform around the periphery of all cells studied in intact ganglia, as well as in the large majority of cultured neurons. We have shown that these non-uniform responses consisted of 1 to 3 local "hot spots", i.e. small sub-PM areas with rapidly rising and falling Ca^{2+} transients.

We found that a sub-group of cultured neurons produced peripherally uniform Ca^{2+} transients when stimulated with single or multiple APs. However, even in these uniformly responding cells, it was possible to reveal "hot spots" by loading the cells' cytosol with the slow Ca^{2+} buffer EGTA, as well as by lowering the extracellular Ca^{2+} concentration to 0.1 mM, i.e. approximately $1/20^{th}$ of the normal extracellular calcium level.

We have also studied the possibility of artificial origins behind the observation of hot spots. Firstly, we found that the localized peripheral signals observed in response to single APs were not due to non-responsive dye. Here we observed that trains of APs or extracellular application of the calcium ionophor ionomycin successfully elevated Ca^{2+} sensitive cytosolic fluorescence throughout the entire cell when applied to the same neurons where APs only induced Ca^{2+} responses at hot spots beforehand.

We also observed that the hot spot locations were likely to be structurally determined: one hot spot was nearly always at the location of the axon hillock, whereas another one existed in the peripheral perinuclear area of the cytoplasm.

The importance of CICR in the generation of these AP-induced calcium transients was proven by using various tools to deplete the ER Ca^{2+} store, which then eliminated the hot spots. Here we used the sarco-endoplasmic reticulum calcium ATPase (SERCA) inhibitor cyclopiezonic acid (CPA) to block the refilling of the ER Ca^{2+} store, or the RyR receptor activator ryanodine (Ry) to empty the ER calcium store by locking the RyR Ca^{2+} channels in a fully open state. With either method we succeeded in eliminating or massively decreasing the AP-induced Ca^{2+} transients.

At the same time, ER Ca^{2+} store refilling was shown to restore the ability of the neuron to respond with Ca^{2+} transients to APs. Here we used large cytosolic Ca^{2+} transients, induced by the extracellular application of 50 mM K^{+}, to reload the ER Ca^{2+}

stores with Ca^{2+} after the SERCA pump activity and/or RyR gating were properly restored. In these cases, the hot spots always reappeared at their original locations, but no hot spots appeared at any new locations.

As for the possible functional significance of these hot spots, we speculate that the peripheral perinuclear hot spot may serve as a very efficient beacon that signals the arrival of an external stimulus directly to the nucleus, thus enabling the cell to reliably decode this message. The efficiency of this hot spot as a signal transmitter is due partly to its closeness to both the VGCCs of the PM and the nucleus, and partly to the high density of functional ER in the narrow gap between the PM and the nuclear envelope in the perinuclear area. This arrangement may allow the AP-induced Ca^{2+} influx to elevate the cytosolic Ca^{2+} level to a high value in the narrow perinuclear space, thus activating massive CICR from the abundant nearby ER Ca^{2+} stores. The short distance to the nuclear envelope allows the diffusion of all this Ca^{2+} to be fast and with little loss.

The other hot spot that was typically found near the axonal hillock may also serve a beacon, transmitting AP-induced Ca^{2+} signals directly to the axon.

The second half or our work describes a multi-compartmental computer simulation to account for the observed dynamics of the intracellular local Ca^{2+} signals initiated by AP-induced Ca^{2+} entry. The computer model was built based upon the morphological and functional findings that were described in the first half of our results. The model describes the Ca^{2+} fluxes

between the extracellular space, the cytoplasm, the Ca^{2+} stores of the ER and of the mitochondria

We also confirmed that the plasma membrane Ca^{2+} ATPase (PMCA) constitute the main Ca^{2+} efflux mechanism during the decline of intracellular Ca^{2+} following Ca^{2+} influx-induced transient elevations. The majority of the decline of the Ca^{2+} transient thus seems to be provided by PMCA, since blocking PMCA by high extracellular pH (pH 9.0) essentially halts further Ca^{2+} removal.

We composed a series of differential equations to describe the behaviour of sub-cellular compartments. These equations combine the mathematical expressions describing the main transport mechanisms related to the Ca^{2+} reaction/diffusion kinetics of the cellular system. We solved our model system's differential equations numerically, using a computer-based approximation for solving differential equations. We limited our calculations to 6 spatial domains, instead of attempting to provide a continuous solution for two or three spatial dimensions, thus providing a toolkit that can be easily run on any modern PC.

Here we examined the effect of single and multiple AP-like stimuli in SCG neurons. We applied our model to reproduce single Ca^{2+} transients as well as more complex temporal patterns of cytosolic Ca^{2+} generated by periodic stimuli of phasic neurons. Our analysis of more complex temporal and spatial patterns confirmed that the parameter set that successfully described the complex patterns, also automatically reproduced the single Ca^{2+} transients, recorded from the same cell.

In our model systems, the RyR conductance was expressed as a sum a Ca^{2+} independent and a Ca^{2+} dependent component. Even when we varied the relative contributions of these components, as well as increased or decreased the sensitivity of the RyRs' Ca^{2+} conductance to cytosolic Ca^{2+}, our model simulations always indicated that the ER Ca^{2+} stores behaved as net Ca^{2+} sinks during simulated Ca^{2+} transients evoked by single or multiple APs. These results agree well with existing data in mammalian sympathetic neurons (Hernández-Cruz et al., 1997; Wanaverbecq et al., 2003), but disagrees with earlier findings by ourselves and others in frog sympathetic ganglion neurons, where CICR was shown to produce a net increase of cytosolic Ca^{2+}, both in experimental studies (Akita and Kuba, 2000; Cseresnyés and Schneider, 2004) and, more recently, in a model system as well (Patterson et al, 2007). This disagreement may simply be caused by species differences.

Our results indicate that the fluorescence signal recorded from the central regions of a cell in any XY plane could be a combination of "pure" signals from more than one theoretical domain: the domain sampled in the focal plane and one or more domains above or below the focal plane. Our examinations show that it is possible, using confocal data and applying our 6-domain model, to un-mix the contaminated optical signals and thus to estimate what the "pure" signals would be in an ideal confocal section.

Conclusions:

From these results we concluded that spatial non-uniformity of Ca^{2+} responses to APs is an inherent property of frog SGNs and rat SCG neurons, and that the non-uniformity is maintained in primary cell cultures, even though the hot spots may not always be directly observable in all cultured SGNs. The hot spots possibly serve as information transmitters that signal the arrival of the AP-induced calcium signals to the cell nucleus and the axon.

Our computer simulations proved to be successful in reproducing our experimental characterization of the dynamics of the intracellular local Ca^{2+} signals initiated by AP-induced Ca^{2+} entry in a multi-compartmental model. The model provided a characterization of the SCG and SGN neuronal systems in terms of Ca^{2+} fluxes underlying the spatio-temporal properties of local Ca^{2+} signals during and after single AP induced by electrical field stimulation.

7. ÖSSZEFOGLALÁS

Jelen dolgozatban az idegsejtek viselkedését vizsgáltuk részint teljes ganglionokban, részint pedig tenyésztett sejtekben. Az akciós potenciálok (AP) előállítása végett elektromos téringerlést alkalmaztunk. Megállapítottuk, hogy az AP-ok hatására létrejövő membrán depolarizáció aktiválja a feszültség vezérelte kalcium csatornákat, amelyeken keresztül aztán kalcium áramlik a kalciumban gazdag sejtközötti térből a neuron belsejébe.

Ugyancsak megmutattuk hogy a Ca^{2+} beáramlás hatására kalcium ionok lépnek ki a plazma membrán (PM) alatti endoplazmatikus retikulumból (ER). Az áramlás a ryanodine receptorok csatornáin keresztül történik (calcium induced calcium release, CICR).

Megfigyeltük hogy az AP-ok hatásásra létrejött Ca^{2+} tranziensek inhomogén módon jelentkeztek mind térben mind pedig időben. Ez az inhomogenitás jellemezte az összes intakt ganglionbéli neuront, s ugyancsak a tenyésztett sejtek nagy részét. Az inhomogén kalcium válaszok együtt jártak 1-3 ú.n. "forró pont" (FP) megjelenésével. A FP egy, a PM alatti régióban megjelenő gyorsan emelkedő és ereszkedő Ca^{2+} tranziens.

Megállapítottuk, hogy a tenyésztett sejtek egy része homogén Ca^{2+} tranzienst produkált amikor egyszeri vagy ismételt AP-lal stimuláltuk őket. Ugyanakkor még ezen sejtekben is megtaláltuk a FP-kat, ha a sejteket EGTA-val töltöttük meg, vagy

pedig a fürdő kalcium tartalmát 0.1 mM-ra (azaz a normal érték 1/20-ra) csökkentettük.

Ugyancsak megvizsgáltuk hogy a megfigyelt FP-ok nem műtermékek-e. Azt találtuk, hogy a FP-ok megjelenése nem az inhomogén festék-eloszlás következménye: nagyszámú AP kiváltása, illetve a Ca^{2+} ionofór ionomycin alkalmazása a teljes sejtben hozott létre Ca^{2+} választ, még akkor is ha előzőleg az AP-ok hatására FP-okban jelentkezett a kalcium válasz ugyanazon sejtben.

Megfigyeltük továbbá hogy a FP-ok sejten belüli helye a sejt szerkezetéhez kötődik. Az egyik FP ugyanis csaknem minden sejtben az axon-domb területén jelent meg, míg a második FP a sejtmag és a PM közötti keskeny résben volt megfigyelhető.

A kalcium-indukálta kalcium kivalasztás (CICR) szerepe az AP-ok által kiváltott Ca^{2+} tranziensek létrehozásában igen jelentős. Itt azt találtuk, hogy az ER kalcium tartályainak kiűrítése a Ca^{2+} tranziensek eltűnését eredményezte. Ezt egyrészt úgy érhettük el, hogy az ER kalcium pumpáit (SERCA) CPA-vel (cyclopiezonic acid) gátoltuk. Másrészt az ER ryanodine receptorainak nyitott állapotban való rögzítése (amit ryanodine hozzáadásával értünk el) is az ER kalcium tartályainak kiürüléséhez vezetett. Mindkét módszer alkalmazása a kalcium tranzeinsek eltűnéséhez, vagy legalábbis nagyon jelentős csökkenéséhez vezetett.

Ugyanakkor az ER kalcium tartályainak gyors újratöltése teljesen helyreállította az AP-ok által kiváltott kalcium

tranzienseket. Erre a célra a sejt jelentős depolarizációjával együttjáró Ca^{2+} beáramlást használtuk fel. A nagymértékű depolarizációt 50 mM kálium sejten kívülre történő hozzáadásával idéztük elő, miután a SERCA pumpa ill. a ryanodine receptorok normál működését előzőleg helyreállítottuk (a SERCA blokkolók illetve a ryanodine alapos kimosásával). A helyreállított FP-k ugyanott jelentek meg a sejten belül ahol az ER kiürítése előtt voltak, u.a. új FP-k megjelenését egyszer sem figyeltük meg a kimosás után.

Ami a FP-ok lehetséges élettani funkcióját illeti, a jelátadó szerepe látszik valószínűnek. A sejtmag közelében elhelyezkedő FP gyorsan és hatékonyan jelezheti a sejtmagnak a külső elektromos inger ill. az AP megérkezését, ezzel lehetővé téve hogy a sejt gyorsan dekódolhassa a beérkezett információt. Ezen FP részint annak köszönheti hatékonyságát, hogy mind a PM kalcium csatornái, mind pedig a sejtmag nagyon közel vannak ehhez a FP-hoz, részint pedig annak hogy ebben a PM és sejtmag közötti keskeny tartományban az ER nagyon sűrűn helyezkedik el. Mindezek következményeként az AP-ok által kiváltott Ca^{2+} beáramlás igen magas lokális Ca^{2+} koncentrációt idézhet elő ebben a keskeny tartományban, ami jelentős CICR megjelenését is eredményezi. A PM és a sejthártya közelsége miatt a diffúziós Ca^{2+} veszetség sem jelentős.

A második FP amely általában az axon-domb közelében helyezkedik el, valószínűleg hasonló szerepet tölt be, amikor is az AP-ok által indukált Ca^{2+} jelet közvetlenül az axon felé továbbítja.

A dolgozat második felében egy számítógépes modellt mutattunk be, melynek segítségével sikeresen reprodukáltuk és jósoltuk a sejtek 6 tartományában megfigyelhető, AP-ok keltette Ca^{2+} jeleket. A model alapjául szolgáló szerkezeti és funkcionális megfigyelések a dolgozat első felében leírt eredményekből származtak. A model segítségével leírtuk a Ca^{2+} ionok mozgását a sejten kívüli tér, a citoplazma, az ER és a mitokondriumok Ca^{2+} tartályai, valamint a sejtmag között.

Eredményeink megerősítették azt a korábbi megfigyelést miszerint az AP érkezése által megemelt sejten belüli Ca^{2+} eltávolításáért elsősorban a PM Ca^{2+} ATP-áz (PMCA) a felelős. Megmutattuk ugyanis, hogy a sejten kívüli tartomány pH-jának megemelése (pH 9.0) jelentősen lelassította ill. megszüntette a Ca^{2+} eltávolítást az AP-ok által előidézett Ca^{2+} tranziensek után.

A kalcium ionok sejten belüli viselkedését differenciál egyenletek segítségével irtuk le. Ezen egyenletekben összefoglaltuk mindazon Ca^{2+} transzport folyamatokat amelyek ezen neuronokban már ismertek (többek között az általunk 1997-ben leírt Release Activated Calcium Transport, RACT, Cseresnyés et. al., 1997). Az egyenleteket numerikusan oldottuk meg, számítógépes algoritmusok segítségével. Számításainkat csupán 6 sejt-tartományra terjesztettük ki, u.i. a térben folyamatos megoldás jóval nagyobb számítógépes kapacitást igenyelt volna, ami egyúttal a model széleskörű felhasználhatóságát is veszélyeztetné.

A model segítségével megvizsgáltuk az egyedi és ismételt AP-ok hatását. Sikeresen leírtuk nemcsak az egyszerű Ca^{2+}

tranzienseket, hanem a fázisos neuronokban megfigyelhető bonyolultabb jelenségeket is. Megfigyeltük, hogy a bonyolult jelenségeket jól leíró paraméterek automatikusan visszaadták az egyszerű Ca^{2+} tranzienseket is ugyanazon sejtekben.

Modellünkben a ryanodine receptorok leírására egy kalcium függő és egy kalcium független kifejezés összegét használtuk. Azt tapasztaltuk, hogy ezen két kifejezés relativ súlyának változtatása, amely a model illesztése során szükséges volt, nem befolyásolta azt a tényt, hogy az ER Ca^{2+} tartálya minden esetben Ca^{2+} felvevőként szerepelt. Ez az eredmény megegyezik a korábban emlős neuronokon mértekkel (Hernández-Cruz et al., 1997; Wanaverbecq et al., 2003), de ellenkezik a béka szimpatikus ganglion sejteken mértekkel, ahol a CICR szerepét jelentősnek találták mind kísérletes (Akita and Kuba, 2000; Cseresnyés and Schneider, 2004), mind pedig szimulációs vizsgálatokban (Patterson et al, 2007). Az ellentmondás oka valószínűleg a fajok közötti különbségben rejlik.

Eredményeink azt is megmutatták, hogy a sejtek közepéhez közel felvett fluoreszcens jelek különböző, egymáshoz közeli sejt-tartományokból származó ”tiszta” jelek keverékei. Megmutattuk, hogy modellünk segítségével el tudjuk különíteni ezeket az összetevőket, és így ki tudjuk számítani a ”tiszta” jeleket.

Összefoglalás:

Eredményeinkből arra a következtetünk, hogy a Ca^{2+} tranziensek inhomogén volta szerves része a béka és patkány szimpatikus neuronok viselkedésének. Ez a viselkedés tenyésztett sejtekben is megmarad, még ha a tenyésztett sejtek egy részében a FP-ok létezése nem látható azonnal. A FP-ok nagy valószínűséggel mint jelátadók szerepelnek, melyek a sejtmag és az axon felé továbbítják az AP indukálta Ca^{2+} tranzienseket.

Számítógépes modellünk igen hasznosnak bizonyult a AP indukálta Ca^{2+} jelek leírásában ill. azok jóslásában. A modell jól leírja mind a béka SGN, mind pedig a patkány SCG neuronok viselkedését az AP-k által gerjesztett Ca^{2+} tranziensek során, figyelembe véve az időbeli és térbeli jellemzőket**.**

8. ACKNOWLEDGEMENTS

My most heartfelt Thank You goes to my Mother, who passed away in 2008 and couldn't witness the final stages of my preparation of this PhD dissertation. Without her encouragement I would have never even had the slimmest chance to work through the whole PhD procedure at such a late stage of my career. She was also the one who helped me the most throughout the whole process by taking care of the official issues that come with such complicated procedure.

My deepest Thank You and sympathy goes to my partner, Marian Angela Ryan, who encouraged me throughout, and who put up with my many days of working late into the night, and not seeing much of me during these busy periods.

Professionally and personally I owe so much to my supervisor, Prof. Gáspár Bánfalvi, that I will never be able to thank him enough. His patience with my slow progress when I was going through a rough time during my Mother's illness and passing away, as well as changing jobs, made it possible for me to finish this stage of my PhD preparation at all.

Without my friend and the Head of Department, Dr. István Pócsi I wouldn't even have had this late chance of applying for a PhD. It was his idea originally to try to get this degree, and if I succeed at all, it will be in large part due to him.

Many-many thanks go to those whom I worked with in Baltimore, Maryland when I collected the results and wrote the papers that now serve as a basis for this dissertation. Most of all, to Prof. Martin F. Schneider, group leader, and to Ben Busby, a great friend who encouraged me throughout.

9. REFERENCES

Abrenica, B., and J.S. Gilchrist. 2000. Nucleoplasmic Ca^{2+} loading is regulated by mobilization of perinuclear Ca^{2+}. *Cell Calcium* 28:127-136

Akita, T., and K. Kuba. 2000. Functional triads consisting of ryanodine receptors, Ca^{2+} channels, and Ca^{2+}-activated K^{+} channels in bullfrog sympathetic neurons. Plastic modulation of action potential. *J Gen Physiol* 116:697-720

Albrecht M.A., S.T. Collegrove, D.D. Friel. 2002 Differential regulation of ER Ca^{2+} uptake and release rates accounts for multiple modes of Ca^{2+}-induced Ca^{2+} release*, J Gen Physiol.* 119:211-233.

Albrecht, M.A., S.L. Colegrove, J. Hongpaisan, N.B. Pivovarova, S.B. Andrews, and D.D. Friel. 2001. Multiple Modes of Calcium-induced Calcium Release in Sympathetic Neurons I. Attenuation of endoplasmic reticulum Ca^{2+} accumulation at low. *J Gen Physiol* 118:83-100

Augustine GJ, F. Santamaria, K. Tanaka. 2003. Local calcium signaling in neurons, *Neuron* 40:331-46

Benham C.D., M.L. Evans, C.J McBain. 1992. Ca^{2+} efflux mechanisms following depolarization evoked calcium transients in cultured rat sensory neurons, *J Physiol.* 455:567-83.

Berridge, MJ 1998. Neuronal calcium signaling, *Neuron.* 21:13-26

Bezprozvanny, I., J. Watras, and B.E. Ehrlich. 1991. Bell-shaped calcium response curves of Ins(1,4,5)P3- and calcium-gated channels from endoplasmic reticulum of cerebellum. *Nature* 351:751-754

Boehm S., H. Kubista. 2002. Fine tuning of sympathetic transmitter release via ionotropic and metabotropic presynaptic receptors, *Pharmacol. Rev.* 54:43-99.

Carafoli E. 2005. Calcium-a universal carrier of biological signals*, FEBS J.* 272:1073-89.

Cheng, H., M.R. Lederer, W.J. Lederer, and M.B. Cannell. 1996. Calcium sparks and $[Ca^{2+}]_i$ waves in cardiac myocytes. *American Journal of Physiology* 270, C148-159

Clapham, D.E. 1995. Calcium signaling. *Cell* 80:259-268

Cohen, A.S., K.A. Moore, R. Bangalore, M.S. Jafri, D. Weinreich, and J.P. Kao. 1997. Ca^{2+}-induced Ca^{2+} release mediates Ca^{2+} transients evoked by single action potentials in rabbit vagal afferent neurones. *J Physiol* 499:315-328

Cong Y.L., S. Takeuchi, H. Tokuno, K. Kuba. 2004. Long-term potentiation of transmitter exocytosis expressed by Ca2+-induced Ca2+ release from thapsigargin-sensitive Ca2+ stores in preganglionic nerve terminals, *Eur. J. Neurosci.* 20:419-26.

Crank, J. 1975. *The Mathematics of Diffusion*. Clarendon Press, London: 28-29

Cseresnyés Z., A.I. Bustamante, M.G. Klein, M.F. Schneider. 1997. Release-activated Ca^{2+} transport in neurons of frog sympathetic ganglia, *Neuron* Aug;19(2):403-19.

Cseresnyés, Z., A.I. Bustamante, and M.F. Schneider. 1991. Caffeine-induced [Ca^{2+}] oscillations in neurones of frog sympathetic ganglia. *J Physiol* 514 (Pt 1):83-99

Cseresnyés Z., M.F. Schneider. 2004. Peripheral hot spots for local Ca^{2+} release after single action potentials in sympathetic ganglion neurons, *Biophys J* 86:163-81.

Cyert, M.S. 2001. Regulation of nuclear localization during signaling. *J Biol Chem* 276:20805-20808

Endo M. 1977. Calcium release from the sarcoplasmic reticulum, *Physiol Rev.* 57:71-108.

Friel, D.D. 1995. [Ca^{2+}]i oscillations in sympathetic neurons: an experimental test of a theoretical model. *Biophys J* 68:1752-1766

Friel D.D., R.W. Tsien. 1992. A caffeine- and ryanodine-sensitive Ca2+ store in bullfrog sympathetic neurons modulates effects of Ca2+ entry on [Ca2+]i, *J Physiol.* 450:217-46.

Garcia-Ferreiro R.E., E.O. Hernandez-Ochoa, D.E. Garcia. 2001. Modulation of N-type Ca^{2+} channel current kinetics by PMA in rat sympathetic neurons, *Pflugers Arch.* 442:848-58.

Ghosh, A., and M.E. Greenberg. 1995. Calcium signaling in neurons: molecular mechanisms and cellular consequences. *Science* 268:239-47

Grkovic I., C.R. Anderson. 1997. Calbindin D28K-immunoreactivity identifies distinct subpopulations of

sympathetic pre- and postganglionic neurons in the rat, *J Comp Neurol.* 386:245-59.

Hamill O.P., A. Marty, E. Neher, B. Sakmann, F.J. Sigworth. 1981. Improved patch-clamp techniques for high-resolution current recording from cells and cell-free membrane patches*, Pflugers Arch.* 391:85-100.

Hardingham, G.E., S. Chawla, and C.M. Johnson. 1997. Distinct functions of nuclear and cytoplasmic calcium in the control of gene expression. *Nature* 385:260-265

Hernandez-Cruz, A., A.L. Escobar, and N. Jimenez. 1997. Ca^{2+}-induced Ca^{2+} release phenomena in mammalian sympathetic neurons are critically dependent on the rate of rise of trigger Ca^{2+}. *J Gen Physiol* 109:147-67

Hernandez-Ochoa E.O., M. Contreras, Z. Cseresnyés, M.F. Schneider. 2007. Ca(2+) signal summation and NFATc1 nuclear translocation in sympathetic ganglion neurons during repetitive action potentials, *Cell Calcium* Jun; 41(6):559-71. Epub 2006 Nov 27.

Hongpaisan, J., N.B. Pivovarova, S.L. Colegrove, R.D. Leapman, D.D. Friel, and S.B. Andrews. 2001. Multiple modes of calcium-induced calcium release in sympathetic neurons. *J Gen Physiol* 118:101-112,

Hua, S.Y., C. Liu, F.M. Lu, M. Nohmi, and K. Kuba. 2000. Modes of propagation of Ca^{2+}-induced Ca^{2+} release in bullfrog sympathetic ganglion cells. C*ell Calcium* 27:195-204

Hua, S.Y., M. Nohmi, and K. Kuba. 1993. Characteristics of Ca^{2+} release induced by Ca^{2+} influx in cultured bullfrog sympathetic neurones. *J Physiol* 464:245-272

Inesi G, Y. Sagara, Specific inhibitors of intracellular Ca^{2+} transport ATPases, *J Membr Biol.* 141 (1994) 1-6.

Ivanov A., D. Purves. 1989. Ongoing electrical activity of superior cervical ganglion cells in mammals of different size, *J Comp Neurol.* 284:398-404.

Kammermeier, P.J., B. Xiao, J.C. Tu, P.F. Worley, and S.R. Ikeda. 2000. Homer proteins regulate coupling of Group I metabotropic glutamate receptors to N-type calcium and M-type potassium channels. *J Neurosci* 20:7238-7245

Kawai Y., E. Senba 2000. Spontaneous synaptogenesis in ex vivo sympathetic ganglion and the blockade by serum treatment.

J Comp Neurol. Sep 4;424(4):670-8.

Koopman, W.J., W.J. Scheenen,. R.J. Errington, P.H. Willems, R.J. Bindels, E.W. Roubos, and B.G. Jenks. 2001. Membrane-initiated Ca^{2+} signals are reshaped during propagation to subcellular regions. *Biophys J* 81:57-65

Kuba, K. 1994. Ca^{2+}-induced Ca^{2+} release in neurones. *Jpn J Physiol* 44:613-650

Kuba, K., M. Nohmi, and S.Y. Hua 1992. Intracellular Ca^{2+} dynamics in response to Ca^{2+} influx and Ca^{2+} release in autonomic neurones. *Can J Physiol Pharmacol* 70 Suppl:S64-S72

Kues, T., R. Peters, and U. Kubitscheck. 2001. Visualization and tracking of single protein molecules in the cell nucleus. *Biophys J* 80:2954-2967

Lacampagne, A., C.W. Ward, M.G. Klein, and M.F. Schneider. 1999. Time course of individual Ca^{2+} sparks in frog skeletal muscle recorded at high time resolution. *J Gen Physiol* 113:187-98

Lamond, A.I., and W.C. Earnshaw. 1998. Structure and function in the nucleus. *Science* 280:547-553

Linden, D.J. 1999. The return of the spike: postsynaptic action potentials and the induction of LTP and LTD. *Neuron* 22:661-666

Lipp, P., D. Thomas, M.J. Berridge, and M.D. Bootman. 1997. Nuclear calcium signalling by individual cytoplasmic calcium puffs. *EMBO J.* 16:7166-7173

Lipscombe, D., D.V. Madison, M. Poenie, H. Reuter, R.W. Tsien, and R.Y. Tsien. 1988. Imaging of cytosolic Ca^{2+} transients arising from Ca^{2+} stores and Ca^{2+} channels in sympathetic neurons. *Neuron* 1:355-365

Loew L.M., J.C. Schaff. 2001. The Virtual Cell: a software environment for computational cell biology, *Trends Biotechnol.* 19:401-6.

Magnus G., J Keizer. 1997. Minimal model of beta-cell mitochondrial Ca2+ handling, *Am J Physiol.* 273:C717-33.

Malviya, A.N., and P.J. Rogue. 1998. "Tell me where is calcium bred": clarifying the roles of nuclear calcium. *Cell* 92:17-23

Marchant, J.S., and I. Parker. 2000. Functional interactions in Ca^{2+} signaling over different time and distance scales. *J Gen Physiol* 116:691-696

Marrion, N.V., and P.R. Adams. 1992. Release of intracellular calcium and modulation of membrane currents by caffeine in bullfrog sympathetic neurones. *J Physiol* 445:515-535

Marsh S.J., N. Wanaverbecq, A.A. Selyanko, D.A. Brown. 2000. Calcium signalling in neurones exemplified by rat sympathetic ganglion cells. In: R. Pochet (Ed.), Calcium: The Molecular Basis of Calcium Action in Biology and Medicine, The Netherlands, Kluwer Academic Publishers, pp. 27-44.

Martinez-Pinna J., E.M. McLachlan, R. Gallego. 2000. Distinct mechanisms for activation of Cl- and K+ currents by Ca2+ from different sources in mouse sympathetic neurons, *J. Physiol.* 527:249-64.

Mazzanti, M., J.O. Bustamante, and H. Oberleithner. 2001. Electrical dimension of the nuclear envelope. *Physiol Rev* 81:1-19

McDavid S., K.P. Currie. 2006. G-proteins modulate cumulative inactivation of N-type (Cav2.2) calcium channels, *J Neurosci.* 26:13373-83.

McDonough, S.I., L.M. Boland, I.M. Mintz, and B.P. Bean. 2002 Interactions among toxins that inhibit N-type and P-type calcium channels. *J Gen Physiol* 119:313-328

McDonough, S.I., Z. Cseresnyés, and M.F. Schneider. 2000. Origin sites of calcium release and calcium oscillations in frog sympathetic neurons. *J Neurosci* 20: 9059-9070

McHugh J.M., J.L. Kenyon. 2004 An excel-based model of Ca^{2+} diffusion and fura 2 measurements in a spherical cell, *Am J Physiol Cell Physiol.* 286:c342-348.

McLachlan E.M., P.J. Davies, H.J. Habler, J Jamieson. 1997. On-going and reflex synaptic events in rat superior cervical ganglion cells, *J Physiol.* 501:165-182.

McLachlan E.M. 1974. The formation of synapses in mammalian sympathetic ganglia reinnervated with preganglionic or somatic nerves. *J Physiol* 237:217-42.

McPherson, P.S., Y.K. Kim, H. Valdivia, C.M. Knudson, H. Takekura, C. Franzini-Armstrong, R. Coronado, and K.P.

Campbell. 1991 The brain ryanodine receptor: a caffeine-sensitive calcium release channel. *Neuron* 7:17-25

Park Y.B., J. Herrington, D.F. Babcock, B. Hille. 1996. Ca2+ clearance mechanisms in isolated rat adrenal chromaffin cells, *J Physiol.* 492:329-46.

Patil P.G., D.L. Brody, D.T. Yue. 1998. Preferential closed-state inactivation of neuronal calcium channels, *Neuron* 20:1027-1038.

Patterson M., J. Snead, D.D. Friel. 2007. Depolarization-induced calcium responses in sympathetic neurons: Relative contributions from Ca^{2+} entry, extrusion, ER/mitochondrial Ca^{2+} uptake and release, and Ca^{2+} buffering*, J Gen Physiol.* 129:29-56.

Pick, J. 1963. The submicroscopic organization of the sympathetic ganglion in the frog (Rana Pipiens.) *J Comp Neurol* 120: 409-462

Pivovarova N.B., J Hongpaisan, S.B Andrews, D.D. Friel. 1999. Depolarization-induced mitochondrial Ca accumulation in sympathetic neurons: spatial and temporal characteristics, *J Neurosci.* 19:6372-84.

Plummer M.R., D.E. Logothetis, P. Hess. 1989. Elementary properties and pharmacological sensitivities of calcium channels in mammalian peripheral neurons, *Neuron* 2:1453-63.

Pozzo-Miller, L.D., J.A. Connor, S.B. Andrews. 2000. Microheterogeneity of calcium signalling in dendrites. *J Physiol* 525: 53-61

Regan L.J., D.W. Sah, B.P. Bean. 1991. Ca^{2+} channels in rat central and peripheral neurons: high-threshold current resistant to dihydropyridine blockers and ω-Conotoxin, *Neuron* 6:269-80.

Roberts W.M. 1994. Localization of calcium signals by a mobile calcium buffer in frog saccular hair cells*, J Neurosci.* 5:3246-62.

Sala F., A. Hernandez-Cruz. 1990. Calcium diffusion modeling in a spherical neuron: Relevance of buffering properties, *Biophys J.* 57:313-324.

Scarborough J.B. 1966. Numerical mathematical analysis. Baltimore, The Johns Hopkins Press, pp 310-316.

Schneider, M.F. 1999. Ca^{2+} sparks in frog skeletal muscle: Generation by one, some, or many release channels? *J. Gen. Physiol.* 113:365-371

Skok V.I., A.Y. Ivanov. 1983. What is the ongoing activity of sympathetic neurons? *J Auton Nerv Syst.* 7:263-70.

Smith, P.A. 1994. Amphibian sympathetic ganglia: an owner's and operator's manual. *Progress in Neurobiology* 43:439-510

Stehno-Bittel, L., C. Perez-Terzic, and D.E. Clapham. 1995. Diffusion across the nuclear envelope inhibited by depletion of the nuclear Ca^{2+} store. *Science* 270:1835-1838

Stern M.D. 1992. Buffering of calcium in the vicinity of a channel pore, *Cell Calcium*. 3:183-92.

Thayer S.A., L.D. Hirning, R.J. Miller. 1988. The role of caffeine-sensitive calcium stores in the regulation of the intracellular free calcium concentration in rat sympathetic neurons in vitro, *Molecular Pharmacology* 31:664-673.

Thomas, D., S.C. Torey, T.J. Collins, M.D. Bootman, M.J. Berridge, and P.A. Lipp. 2000. comparison of fluorescent Ca^{2+} indicator properties and their use in measuring elementary and global signals. *Cell Calcium* 28:213-223

Trouslard J., S.J. Marsh, D.A. Brown. 1993. Calcium entry through nicotinic receptor channels and calcium channels in cultured rat superior cervical ganglion cells, *J Physiol.* 468:53-71.

Tu, J.C., B. Xiao, J.P. Yuan, A.A. Lanahan, K. Leoffert, M. Li, D.J. Linden, and P.F. Worley 1998. Homer binds a novel proline-rich motif and links group 1 metabotropic glutamate receptors with IP3 receptors. *Neuron* 21:717-726

Usachev, Y.M., and S.A. Thayer. 1997. All-or-none Ca^{2+} release from intracellular stores triggered by Ca^{2+} influx through voltage-gated Ca^{2+} channels in rat sensory neurons. *J. Neurosci.* 17:7404-7414

Usachev, Y.M., and S.A. Thayer. 1999a. Ca^{2+} influx in resting rat sensory neurons that regulates and is regulated by ryanodine-sensitive Ca^{2+} stores. *J Physiol* 519 Pt 1:115-130

Usachev, Y.M., and S.A. Thayer. 1999b Controlling the urge for a Ca^{2+} surge: all-or-none Ca^{2+} release in neurons. *Bioessays* 21:743-750

Verkhratsky A. 2005. Physiology and pathophysiology of the calcium store in the endoplasmic reticulum of neurons, *Physiol. Rev.* 85:201-279.

Verkhratsky, A.J., and O.H. Petersen. 1998. Neuronal calcium stores. *Cell Calcium* 24:333-343

Wanaverbecq N., S.J. Marsh, M Al-Qatari, D.A. Brown DA. 2003. The plasma membrane calcium-ATPase as a major mechanism for intracellular calcium regulation in neurones from the rat superior cervical ganglion, *J Physiol.* 550:83-101.

Wheeler D.G., C.F. Barrett, T.W. Tsien. 2006. L-type calcium channel ligands block nicotine-induced signaling to CREB by inhibiting nicotinic receptors, *Neuropharmacology*. 51:27-36.

Xiao, B., Tu, J.C., and P.F. Worley. 2000. Homer: a link between neural activity and glutamate receptor function. *Current Opinion in Neurobiology* 10:370-374

Yamada W.M., C. Koch, P. R. Adams. Multiple Channels and Ca^{2+} Dynamics, In: C. Koch, I. Segev, (Ed.), Methods in neuronal modeling: from ions to networks, Massachusetts, MIT Press, 1998: pp. 137-170.

Yao, Y., J. Choi, and I. Parker. 1995. Quantal puffs of intracellular Ca^{2+} evoked by inositol trisphosphate in Xenopus oocytes. *J Physiol* 482 Pt 3:533-553

Young, R.C., R. Schumann, and P. Zhang . 2001. Intracellular calcium gradients in cultured human uterine smooth muscle: a functionally important subplasmalemmal space. *Cell Calcium* 29:183-189.

10. RESUME

Publications used directly for this dissertation:

1. Hernández-Ochoa, E.O., **Cseresnyés, Z.**, and Schneider, M.F. (2007) Ca^{2+} signal summation and NFATc1 nuclear translocation in sympathetic ganglion neurons during repetitive action potentials induced by M-channel inhibition. Cell Calcium 41(6), 559-571.

2. **Cseresnyés, Z.,** and Schneider, M.F. (2004). Peripheral hot spots for local Ca^{2+} release after single action potentials in sympathetic ganglion neurons. Biophysical Journal *86(1)*, 163-81.

3. McDonough, S.I., **Cseresnyés, Z.**, and Schneider, M.F. (2000). Origin sites of calcium release and calcium oscillations in frog sympathetic neurons. Journal of Neuroscience 20.24, 9059-9070.

4. **Cseresnyés, Z.,** Bustamante, A.I., and Schneider, M.F. (1999). Caffeine-induced [Ca^{2+}] oscillations in neurones of frog sympathetic ganglia. Journal of Physiology *514.1*, 83-99.

Σ IF: 22.02

Other publications:

1. **Cseresnyés, Z.**, Schwarz, U., and Green, C.M. (2009): Analysis of replication factories in human cells by super-resolution light microscopy BMC Cell Biology **10:**88

2. Bischoff, M. and **Cseresnyés, Z.** (2009) Cell rearrangements, cell divisions and cell death in a migrating epithelial sheet in the abdomen of Drosophila. Development 136(14), 2403-2411.

3. Shen, T., **Cseresnyés, Z.**, Liu, Y., Randall, W.R., and Schneider, M.F. (2007) Regulation of NFATc1 nuclear export by protein kinases after slow fiber type electrical stimulation of adult mouse skeletal muscle fibers. Journal of Physiology 579(Pt2), 535-551.

4. Shen, T, Liu, Y, **Cseresnyés, Z**, Hawkins, A, Randall, WR, and Schneider, M.F. (2006) Activity- and Calcineurin-independent Nuclear Shuttling of NFATc1, but Not NFATc3, in Adult Skeletal Muscle Fibers. Molec. Biol. Cell 17(4), 1570-1582.

5. Thomas, S, Zinter, R**., Cseresnyés, Z.**, Hutter-Paier, B., and Hofmeister, A. (2003). Structured Light Imaging: An Accessible Alternative to Confocal Imaging. American Biotechnology Laboratory 21(11), 14-16.

6. Liu, Y., **Cseresnyés, Z.**, Randall, W.R., and Schneider, M.F. (2001). Activity-dependent nuclear translocation and intranuclear distribution of NFATc in adult skeletal muscle fibres. Journal of Cell Biology 155(1), 27-39.

7. **Cseresnyés, Z.,** Bustamante, A.I., Klein, M.G., and Schneider, M.F. (1997). Release-activated Ca^{2+} transport in neurons of frog sympathetic ganglia. Neuron *19*, 403-419.

Σ IF: 45.36

Selected conferences with presentations:

- Annual Meeting of European Working Group of Cardiac Physiology, 1992, Ferrara, IT
- Word Conference of Biophysics, 1993, Budapest, Hungary
- Annual Meeting of the European Working Group of Cardiac Physiology, 1993, Graz, Austria
- "Fluorescent Techniques" Summer School, 1993, Milan, Italy
- 39th Annual Meeting of the Biophysical Society, Febr. 12-16, 1995, San Francisco, CA

- 40th Annual Meeting of the Biophysical Society, Febr. 17-21, 1996, Baltimore, MD
- 41st Annual Meeting of the Biophysical Society, March -6, 1997, New Orleans, LA
- 42nd Annual Meeting of the Biophysical Society, Febr. 22-26, 1998, Kansas City, MO
- Federation of American Societies of Experimental Biology (FASEB) Summer Conference, July 4-9, 1998, Snowmass, CO
- 43rd Annual Meeting of the Biophysical Society, February 13-17, 1999, Baltimore, MD
- "Calcium Signaling" Gordon Research Conference, August 8-13, 1999, Henniker, NH
- 44th Annual Meeting of the Biophysical Society, Febr. 12-16, 2000, New Orleans, LA
- Federation of American Societies of Experimental Biology (FASEB) Summer Conference, "Calcium and Cell Function", July 9-14, 2000, Copper Mountain, CO
- 45th Annual Meeting of the Biophysical Society, February 17-21, 2001, Boston, MA
- "Calcium Signaling" Gordon Research Conference, September 2-7, 2001, Oxford, UK
- 46th Annual Meeting of the Biophysical Society, Febr. 22-26, 2002, San Francisco, CA
- 47th Annual Meeting of the Biophysical Society, March 2-5, 2003, San Antonio, TX
- "Calcium Signaling" Gordon Research Conference, July 6-11, 2003, Mt. Holyoke, MA
- International Workshop on Calcium Release and Cellular Calcium Signaling Domains, September 28-October 2., 2003, Marbella, Chile
- 48th Annual Meeting of the Biophysical Society, February 14-18, 2004, Baltimore, MD
- Experimental Biology 2004, April 17-21, 2004, Washington, DC
- Society for Neuroscience Annual Meeting, November 2005, San Diego, CA

Mentoring:

1985-1991 Supervisor of undergraduate students, Debrecen University, Hungary

1992-1994 Supervisor of undergraduate and graduate students, Debrecen University School of Medicine, Hungary

1995-2007 Supervisor of **undergraduate students**, University of Maryland Baltimore School of Medicine

Alex Bustamante, UMBC undergraduate student, 1994-1995. Photometric recordings of calcium signals in neurons; supervision of research work on a daily basis.

Naima Carter, UMBC undergraduate student, 1994-1997. Neuron and smooth muscle cell culture.

Benjamin Busby, UMBC undergraduate student, then UMB graduate student, 1998-2007. Culturing cerebellar Purkinje neurons and studying cytosolic and intra-compartmental calcium transients in these neurons; supervision of research work on a daily basis.

1996-2007 Training **graduate students**, University of Maryland Baltimore School of Medicine

Macrae Williams, UMB graduate student in Physiology, 1996-1997. Rotation student and lab assistant, training in avian dorsal root ganglia cell culture and intracellular calcium recording.

Ashish Bagal, UMB MD/PhD student 1998. Rotation student; training in nerve cell culture and intracellular calcium recording; supervision of research work on a daily basis.

Lois Chun, UMB graduate student in Biochemistry and Molecular Biology, 1999-2005. Fura-2 recording techniques for whole-cell calcium measurements.

1998-2007 Training **postdoctoral fellows**, University of Maryland Baltimore School of Medicine

Stefan McDonough PhD, UMB postdoctoral fellow in Biochemistry and Molecular Biology, 1998-2000. Initial training in whole-cell neuronal calcium signalling and high-speed confocal imaging of neuronal cells; supervision of research work on a daily basis.

Yewei Liu MD/PhD, UMB postdoctoral fellow in Biochemistry and Molecular Biology, 1999-2003. Training in use of custom computer image analysis program for tracking intracellular distribution and concentration of Green Fluorescent Protein-tagged proteins in confocal images of muscle cells.

Teaching:

Physical Sciences

1984-1985 Teaching Assistant, Optics and Mechanics, Debrecen University, Hungary

1985-1991 Course Master, Optics and Mechanics Practical Course, Debrecen University, Hungary

1987-1990 Course Master, Electrodynamics Theoretical Course, Debrecen University, Hungary

1988-1989 Lecturer, Physics Practical and Theoretical Course, Debrecen University, Hungary

Medical Sciences

1992-1994	Lecturer, Clinical Physiology Practical Course, University of Debrecen School of Medicine, Hungary
1993-1994	Lecturer, Clinical Physiology, University of Debrecen School of Medicine, Hungary